The growth of wind waves in finite water depth

PLEASE TYPE

UNIVERSITY OF NEW SOUTH WALES

Thesis/Project Report Sheet

Surname or Family name: VERHAGEN

First name: Louis Other name/s: ANDRE

Abbreviation for degree as given in the University calendar:

School: Civil Engineering Faculty:

Title: THE GROWTH OF WIND WAVES IN FINITE WATER DEPTH

Abstract 350 words maximum: (PLEASE TYPE)

See Attached Sheet.

Abstract

Wind wave growth in deep water has been studied extensively. However, most interaction of humanity and the sea is in shallow water. In this area knowledge is lacking. Although there have been many measurements of wave growth in deep water, there was a need for an extensive data set in shallow water. Therefore an experiment was setup to measure differential one-dimensional wave growth at eight stations in a shallow water lake. The lake where the experiment was held is called Lake George, Canberra Australia. The lake is 24 km long by 12 km wide. At a single station near the middle of the lake, two-dimensional directional measurements were also made.

The data set which resulted from the experiment was large and of high quality. Amongst the measured quantities, were one-dimensional spectra, two-dimensional spectra and wind speed and direction. During the three year duration of the experiment, a total of 67,225 individual time series were measured.

In finite water depth (dimensionless depth, δ) there are two limits to the growth of the waves. First, there is fetch (dimensionless fetch, χ) limited growth where it was found that the maximum dimensionless energy $\epsilon = 1.6 \times 10^{-7}\ \chi$ and the lowest dimensionless frequency $\nu = 2.18\ \chi^{-0.27}$. If the fetch is long enough there is a depth limit to growth where it was found that the maximum dimensionless wave height $\Lambda = 0.13\ \delta^{0.65}$ or dimensionless energy $\epsilon = 1.06 \times 10^{-3}\ \delta^{1.3}$ and the lowest dimensionless frequency $\nu = 0.20\ \delta^{-0.375}$. Also, support for the Pierson-Moskowitz limit at long fetch was found. From these limits the following growth curves for waves in shallow water were developed

$$\epsilon = 3.64\times10^{-3}\left\{\tanh\left(0.493\ \delta^{3/4}\right)\tanh\left(\frac{3.13\times10^{-3}\ \chi^{0.57}}{\tanh\left(0.493\ \delta^{3/4}\right)}\right)\right\}^{1.74}$$

$$\nu = 0.133\left\{\tanh\left(0.331\ \delta^{1.01}\right)\tanh\left(\frac{5.215\times10^{-4}\ \chi^{0.73}}{\tanh\left(0.331\ \delta^{1.01}\right)}\right)\right\}^{-0.37}$$

The shape of the one-dimensional spectra fitted the TMA spectral from better than the JONSWAP spectrum. The relation between the TMA coefficient α and the non-dimensional wave number (κ) for the Lake George data is

$$\alpha_{TMA} = 0.0078\ \kappa^{0.49}$$
$$\alpha_{JONSWAP} = 0.01\ \kappa^{0.33}$$

The data suggest a dependency of the peak enhancement factor on the non-dimensional fetch and/or non-dimensional depth. No relationship was found between the peak enhancement factor and the non-dimensional wave number.

In general, the two-dimensional directional spread of the waves in finite water has similar characteristics to deep water. The spectra are, however, directionally broader in finite depth conditions.

A $\cos^{2s}\theta/2$ function was found appropriate for the directional spread with the directional spreading factor (s) being dependent on f/f_p.

No dependence on either the inverse wave age (U_{10}/C_p) or the dimensionless depth parameter ($k_p d$) was established although a dependence on the dimensionless depth parameter is not ruled out. Nonlinear interactions may play an important role in determining the directional spreading.

It was observed that for $f > 2f_p$ the spreading becomes bi-modal. This feature cannot be fully explained, although it is very likely that nonlinear interactions control this process.

Declaration relating to disposition of project report/thesis

I am fully aware of the policy of the University relating to the retention and use of higher degree project reports and theses, namely that the University retains the copies submitted for examination and is free to allow them to be consulted or borrowed. Subject to the provisions of the Copyright Act 1968, the University may issue a project report or thesis in whole or in part, in photostate or microfilm or other copying medium.

I also authorise the publication by University Microfilms of a 350 word abstract in Dissertation Abstracts International (applicable to doctorates only).

The University recognises that there may be exceptional circumstances requiring restrictions on copying or conditions on use. Requests for restriction for a period of up to 2 years must be made in writing to the Registrar. Requests for a longer period of restriction may be considered in exceptional circumstances if accompanied by a letter of support from the Supervisor or Head of School. Such requests must be submitted with the thesis/project report.

FOR OFFICE USE ONLY Date of completion of requirements for Award:

Registrar and Deputy Principal

THIS SHEET IS TO BE GLUED TO THE INSIDE FRONT COVER OF THE THESIS

The University of New South Wales

The Growth of Wind Waves in Finite Water Depth

a Thesis submitted in candidature for
Doctor of Philosophy

by **Louis Verhagen**

Department of Civil Engineering
University College
University of New South Wales
Australian Defence Force Academy
1999

Dedication

This thesis is dedicated to my wife Mirjam who patiently waited for me to come back from Australia and encouraged me all the way into finishing this.

I also dedicated this thesis to my joyful children who give me pleasure every day.

Declaration of Originality

I herby declare that this submission is my own work and that, to the best of my knowledge and belief, it contains no material previously published or written by another person nor material which to a substantial extent has been accepted for the award of any other degree or diploma of a university or other institute of higher learning, except where due acknowledgement is made in the text of the thesis.

Louis Verhagen

20 March, 1999

Zoetermeer, The Netherlands

Abstract

Wind wave growth in deep water has been studied extensively. However, most interaction of humanity and the sea is in shallow water. In this area knowledge is lacking. Although there have been many measurements of wave growth in deep water, there was a need for an extensive data set in shallow water. Therefore an experiment was setup to measure differential one-dimensional wave growth at eight stations in a shallow water lake. The lake where the experiment was held is called Lake George, Canberra Australia. The lake is 24 km long by 12 km wide. At a single station near the middle of the lake, two-dimensional directional measurements were also made.

The data set which resulted from the experiment was large and of high quality. Amongst the measured quantities, were one-dimensional spectra, two-dimensional spectra and wind speed and direction. During the three year duration of the experiment, a total of 67,225 individual time series were measured.

In finite water depth (dimensionless depth, δ) there are two limits to the growth of the waves. First, there is fetch (dimensionless fetch, χ) limited growth where it was found that the maximum dimensionless energy $\varepsilon = 1.6 \times 10^{-7} \chi$ and the lowest dimensionless frequency $\nu = 2.18 \chi^{-0.27}$. If the fetch is long enough there is a depth limit to growth where it was found that the maximum dimensionless wave height $\Lambda = 0.13 \delta^{0.65}$ or dimensionless energy $\varepsilon = 1.06 \times 10^{-3} \delta^{1.3}$ and the lowest dimensionless frequency $\nu = 0.20 \delta^{-0.375}$. Also, support for the Pierson-Moskowitz limit at long fetch was found. From these limits the following growth curves for waves in shallow water were developed

$$\varepsilon = 3.64 \times 10^{-3} \left[\tanh\left(0.493\ \delta^{3/4}\right) \tanh\left(\frac{3.13 \times 10^{-3}\ \chi^{0.57}}{\tanh\left(0.493\ \delta^{3/4}\right)} \right) \right]^{1.74}$$

$$\nu = 0.133 \left[\tanh\left(0.331\ \delta^{1.01}\right) \tanh\left(\frac{5.215\times10^{-4}\ \chi^{0.73}}{\tanh\left(0.331\ \delta^{1.01}\right)} \right) \right]^{-0.37}$$

The shape of the one-dimensional spectra fitted the TMA spectral from better than the JONSWAP spectrum. The relation between the TMA coefficient α and the non-dimensional wave number (κ) for the Lake George data is

$$\alpha_{TMA} = 0.0078\ \kappa^{0.49}$$
$$\alpha_{JONSWAP} = 0.01\ \kappa^{0.33}$$

The data suggest a dependency of the peak enhancement factor on the non-dimensional fetch and/or non-dimensional depth. No relationship was found between the peak enhancement factor and the non-dimensional wave number.

In general, the two-dimensional directional spread of the waves in finite water has similar characteristics to deep water. The spectra are, however, directionally broader in finite depth conditions.

A $\cos^{2s}\theta/2$ function was found appropriate for the directional spread with the directional spreading factor (s) being dependent on f/f_p.

No dependence on either the inverse wave age (U_{10}/C_p) or the dimensionless depth parameter ($k_p\ d$) was established although a dependence on the dimensionless depth parameter is not ruled out. Nonlinear interactions may play an important role in determining the directional spreading.

It was observed that for $f > 2f_p$ the spreading becomes bi-modal. This feature cannot be fully explained, although it is very likely that nonlinear interactions control this process.

1. Introduction to the Lake George Shallow Water Experiment

1.1 Experimental Concept

This experiment was conceived, to obtain a better understanding of the growth of waves in finite water depths. Not only coastal engineering but other activities, such as shipping, coastal management and recreation along coasts, are dependent on accurate prediction of the wave climate in shallow waters. The majority of human activities that involve water take place in shallow water, yet very little is known about the growth of wind generated waves in this area.

There have been a number of deep water experiments (e.g. Hasselmann et al. 1973, Donelan et al. 1985, etc.), but there have been no comprehensive shallow water experiments. The shallow water experiments that have taken place (Bretschneider 1958, Bouws 1986) were single point measurements in lakes. With different water depths and wind speeds they were able to estimate dimensionless growth different to that of deep water. However, a shallow water experiment measuring simultaneously growth at several places had never been undertaken.

To obtain a better understanding of the growth of wind generated waves, measurements along an array of wave measuring stations would be ideal. This would enable the study of the differential growth between the stations. A large body of water with constant depth would be needed, preferably without any outside wave disturbances. The closest approximation to these requirements would, aside from a man-made construction, probably be a lake. Lake George (fig 1.2), near Canberra Australia (fig 1.1), was chosen for this experiment. This lake is approximately 24 kilometres long and 12 kilometres

wide, with nearly a constant depth of around 2 metres. The surrounding areas are relatively flat which ensured the undisturbed flow of the wind from land to water.

In addition to measuring the evolution of wave energy and peak frequency along the direction of the wind (called the fetch), the experiment also provided direct measurements of both the one-dimensional and directional spectra.

1.2 Lake George

Lake George (35.0 S 149.4 E) is located 40 km northwest of Canberra Australia (fig 1.2). Joseph Wild "discovered" the lake in 1820 (Woolley 1990). The native population, aborigines, had already called the lake "Wee-ree-waa." The English however, (re)named the lake after King George. This name is still used today. The elevation is 673 metres above sea level. On the western side of the lake there is a 50 metre high hill (fig 1.3) caused by a geological fault (Woolley 1990). This fault started in Palaeozoic times and until the post-Palaeozoic times there was still movement along the fault. Three small creeks on the eastern side and one on the southern side feed the lake from the catchment area. The water can only leave the lake by evaporation. The lake depth varies seasonally (fig 1.5) and as well yearly (fig 1.4). Variations in lake level and the absence of an obvious outlet are the subject of considerable public speculation. Stories range from underground caverns to holes connecting it to other lakes in Australia, New Zealand, and even China. Just the mentioning of the name Lake George to locals can spark spectacular stories about strange unexplained phenomena. However, the scientific world has been satisfied by the standard hydrological explanation given by Woolley (1990).

During the experiment the lake level ranged in depth from 1.7 metres to 2.2 metres at the measurement stations. However over the last 150 years the lake has dried out completely and has risen to more than 8 metres depth. There is evidence to indicate that

in Pleistocene times the lake was 35 metres deep. In these times the lake used to have a drainage river out to the Yass river at Geary's Gap on the western side of the lake (fig 1.6) (Woolley 1990). The fact that the lake is so shallow, and therefore has little heat "capacity," also causes the water temperature to fluctuate over short periods.

The lake bottom is very flat (fig 1.7) and muddy. The surrounding topography is free of large hills. The topography ensures an undisturbed flow of the wind. Although the lake is situated 100 km inland, it does have a sea breeze effect in summer. Throughout the summer around four o'clock in the afternoon, there was a distinct wind change. The wind increases in magnitude and comes from the East (fig 1.8). The lake has a clayish, thick mud bottom. Its waters are slightly brackish due to evaporation leaving minerals behind and the "sea breeze" bringing in salt from the ocean. Due to the shallow wave climate the mud is stirred and therefore the water is very turbid. This wave climate is very uncomfortable for small boats because of the short steep waves. This and the fact that the water temperatures can approach freezing in winter, have caused numerous fatal boating accidents. Even during the experiment two unfortunate fishermen drowned in Lake George. This was the reason warning signs (fig 1.9) were erected along the lake shores.

1.3 Thesis Outline

The purpose of this experiment was to measure wave growth in finite depth water. Therefore a large experiment was setup in Lake George, Australia. A total of eight wave measuring stations with specialised equipment, like anemometers and radio's, were placed along an array in the lake. Onshore, a receiver station was established with computer equipment for data acquisition. A detailed description of all the equipment is given in chapter 2.

The raw results that came back were processed and analysed. The methods and results of the processing and analyses are given in chapter 3. These wave results were in turn analysed for general trends. From this, new growth curves for wave height and peak frequency and limits in finite water were calculated in chapter 4. In chapter 5 the shape of the one-dimensional spectrum in finite depth water is discussed.

In addition to the one-dimensional wave gauges, a two-dimensional wave measuring gauge was placed in the lake to obtain information on the directional spread in finite depth water. The directional array is described in chapter 1 and the results are discussed in chapter 6.

Although all analysis chapters end with conclusions, chapter 7 is included to provide a summary of the findings of the full thesis.

2. Description of the Lake George Experiment

2.1 Introduction to the Experiment Description

This Chapter will give some insight into the experiment design, and the equipment which were used for the experiment. Further, it will explain details of the setting up of the equipment, together with the problems which were encountered. It must be stressed that setting up a field experiment in theory is often quite different from setting up the actual field experiment. This experiment had the good fortune to have the support of very capable staff. Still, many small problems occurred which no amount of planning could have foreseen. Therefore, an innovative and practical approach was required in much of the work. The ideal personnel would have the following attributes: Have two right hands, graduate electronics knowledge, practical soldering experience on small components, have a boat licence, diving licence & pilot licence, experience in diving with dry and wet suits, ability to predict weather on 1/2 hour and long term basis, don't get sea sick, knowledge of how to get a 4-wheel drive vehicle out of mud, how to change tyres, how to fix engines (both car and boat), full working knowledge of DOS and any programming language used, ability to walk tight rope, be an acrobat, very fit body to do heavy work, be very light to tighten screws/ guy wires on top/side of structures that have yet to be assembled, be able to work in cold rain, and blazing sun, etc... In short, the environment was such that successful completion of the research required a very high level of innovation.

There are many differences between field and laboratory experiments. Unlike a laboratory experiment, the field experiment usually can only determine the input parameters up to a certain extent. Things like bottom topography, wind (speed, direction and boundary layer adjustments), water levels (drying, flooding and seising) etc. can be

measured but not controlled. Therefore, in order to obtain data under all desired conditions, the field experiment needed to be of extended duration. Because of this long time span, all instruments need to operate more or less independently in an unattended mode and be able to withstand the elements for a long period of time. In contrast, a laboratory experiment, is in a controlled environment where both the input elements and the instruments are controlled while the experiment is running. The time span to obtain the required data is much shorter. Despite the apparent advantages of laboratory experiments many physical processes are such that field experiments are required. In the present application, it would be extremely difficult to develop an appropriate atmospheric boundary layer over a flume sufficiently wide to generate realistic directional seas. Even if this were possible, the influence of scale effects would still be of concern. The Lake George site represents a compromise between the completely "uncontrolled" ocean and the "fully" controlled laboratory.

In section 2.2 a description is given of the experimental site and the mode of access. Due to safety hazards on the lake, special safety precautions, which are described in section 2.3, were taken. The experimental instrumentation is discussed in section 2.4. Section 2.5 provides a detailed descriptions of the data and data processing. The last section 2.6 discusses details of the directional array instrumentation.

2.2 Experimental Site and Bathymetry

2.2.1 Lake George

The site chosen for the experiment was Lake George, which is just north of Canberra, Australia (fig 1.2). The lake is about 24 km long and 12 km wide. An existing survey of the lake was available from the Australian Bureau of Mineral Resources. However, since this was a very old survey, which proved to be inconsistent with sample measurements made during the preliminary investigations, a new survey was conducted to establish the bathymetry of the lake.

The initial plan was to use a depth sounder and a global positioning system (GPS), both coupled to a personal computer to make a survey of the bottom of the lake. Because most depth sounders have been made for depths greater than 2 metres, it was planned to convert a depth sounder to take shallow water measurements. The reason why most depth sounders will not measure depths below two metres is the following. When a sonic pulse is released from the sensor, reflections occur from material surrounding the transducer. To ensure that the real depth is measured and not a false reflection, a small time delay is build into the system. In a modified design the time delay would be reduced and the counter would be enhanced to run faster, thus giving a higher resolution and shallower depths. This depth sounder would then be coupled to a portable personal computer. To obtain an accurate position a portable Global Position System (GPS) was used (Trimble Inc.). The plan was to couple the GPS to the same personal computer and take simultaneous measurements from the depth sounder and the GPS while boating around the lake. However, the converted depth sounder proved unreliable. The problem was overcome by the use of a manually read "yard stick" together with the GPS to provide the position.

Survey data were only collected while there was a minimum reception of 4 satellites for the GPS. The method used to check the inaccuracies of the GPS (also know as the Selective Availability, where the signal is purposely made inaccurate (or offset) by the US Department of Defence) was to take periodic readings from the GPS at know points (towers, platform, boat launching ramp). In between these fixed points, depth readings were made by using a survey staff and noting the position given by the GPS. The inaccuracies of the GPS proved to be 30 metres or less. With a differential GPS it is possible to get much higher accuracy but that effort was not necessary for this survey.

The lake was crossed from side to side by boat and point measurements were made on the sides of the lake to establish the shore line. The path of the survey is shown in figure 2.1, in total 115 depths were taken. Determination of the position of the shoreline took considerable effort. The north west section of the lake (fig 2.2) is, because of its

very mild slope, very shallow for a long distance. Therefore, it was necessary to wade through the mud on foot for quite a distance. The question also arose: where does the lake end? In this area the shoreline was defined by the point where thick grassy vegetation started. This vegetation effectively stopped all wave action. The results are shown in fig 2.2.

2.2.2 Boats

The limited water depth precluded the use of large boats on the lake. Different types of boats were used during the experiment. The first boat, was an inflatable AVON with an inflatable keel instead of a wooden keel (fig 2.3). Although this assembled very easily, the keel was not particularly strong and therefore caused bending along the length of the boat. This resulted in cavitating of the outboard motor. To avoid the cavitation, boat speed needed to be reduced. As distances of tens of kilometres needed to be traversed in any day, a reduction in boat speed was unacceptable.

Because of a road accident with the AVON and its poor performance, another boat was purchased. This was a 4-metre aluminum fishing boat, called "tinny" (fig 2.4). This boat served its purposes well. It was capable of moving heavy equipment (with sharp edges) and tools across the lake. On flat water the boat reached speeds up to 65 km/h (checked with GPS receiver). In rough conditions, however, the boat's performance was less then ideal and considerable doubt was raised over its safety in such conditions.

The third boat used was a large assault craft provided by the Royal Australian Army. This craft was used to deploy the large structures such as the towers (fig 2.5) and the directional array. Because of its size and its questionable sea keeping abilities it was baptized "the Titanic." It was however a very useful craft capable of moving and deploying large structures and heavy equipment.

The fourth and last boat used, was a large inflatable boat provided by the Royal Australian Navy (RAN) (fig 2.6). This boat was used for the sole purpose of going to

the lake in extremely poor weather when the "tinny" would not only be uncomfortable but maybe even dangerous. This inflatable (with a wooden keel) was very stable in the small steep waves. The craft was capable of safe and efficient operation in wind speeds up to 15 m/s.

Throughout the experimental program, the various craft were powered by an EVINRUDE 30 HP outboard motor. This motor proved to be remarkably reliable.

2.3 Safety

Lake George is a dangerous lake due to several factors. First of all, it is very big. In the middle of the lake it is more than 6 kilometres to the nearest shore. Swimming to the nearest shore would take a considerable time. Even then, the bottom is very muddy. Walking the last bit to shore would tire a fit person. Secondly, due to the shallowness of the lake the temperature can drop quite quickly with a (cold) wind blowing. Thirdly, also due to the shallowness of the lake the waves were short and steep if the wind blowed. This made boating a very uncomfortable and very wet experience.

Due to the dangerous nature of Lake George, a series of safety measures were taken, to avoid accidents on the lake. There was a minimum "crew" of two people. Life jackets were worn whilst on the lake (also to protect against the spray and cold). Protective clothing against the cold and water was purchased. There was a spare tank of petrol in the boat. To communicate from all positions on the lake in case of an emergency, there was a mobile phone. People who went on the lake were made aware of the safety equipment and dangers of the lake. All these items contributed to the fact that the only accident which occurred during the experiment was sea sickness.

2.4 Instrumentation

2.4.1 Wave measuring gauges

The central requirement in the selection of instrumentation for the project was that it would be capable of operating unattended for long periods of time. In order to collect data under a wide range of conditions, the full experiment operated for approximately three years. With the limited resources available, frequent maintenance would not have been possible. The most important instruments utilised in the experiment were the wave gauges. The short fetch, shallow water and hence high frequency waves generated in Lake George, precluded the use of conventional field instruments such as Wave Rider Buoys. Resistance or capacitance wave staffs were also considered unsuitable due to the high level of maintenance required in keeping such instruments free of aquatic growth, the regular requirement for calibration and their limited robustness. The instrument finally chosen was the surface piercing transmission line gauge described by Zwarts (1974) (fig 2.7). These instruments had been previously utilised by Hardy and Young (1996) and found to be reliable and very robust.

Physical properties of the Zwarts poles

The Zwarts poles were constructed of two concentric aluminium tubes (fig 2.8). Holes in the outer tube allowed the water to flow freely into the gap between the tubes thus maintaining the same water elevation within the pole, as outside. The inner and outer tubes had outside diameters of 25 mm and 50 mm respectively with a gap between the tubes of 8 mm. To allow for possible fluctuations in the mean water level in the lake, the poles were constructed to a length of 4 metres. On top of the pole, a small watertight box with the essential electronics was placed.

Electrical properties of the Zwarts poles

The Zwarts poles act as the equivalent of a coaxial cable. The air water interface provides a discontinuity in the dielectric properties of the "cable" and causes a "reflection" of an electric wave. Zwarts (1974) showed that an electromagnetic standing wave can be established along the pole. The period of this wave is directly proportional to the length of the air gap between the head or top of the pole and the air-water interface (dielectric discontinuity). This identical principle is used by telecommunication companies to find the positions of breaks in underground coaxial cables. The electronics required to produce the standing wave is contained within a small water proof enclosure fixed to the top of the pole (fig 2.9 and fig 2.10). Although the period and hence the frequency of the electrical wave in the pole varied with the length of the air gap, its extremes were in the range from 6.4 MHz to 9.2 MHz (from a pole out of water to a completely submerged pole). Typically the frequency was around 8 MHz. This frequency was divided by 8192. The final output from the electronics was an analogue square wave. The period of this wave was proportional to the air gap. The square wave output from the Zwarts pole was connected to a counter circuit which contained two Programmable Array Logic (PAL) chips programmed to convert the frequency signal to a two byte number. The counter was triggered by a positive edge of the square wave. To avoid the output varying by one count in stable conditions, the counter sampled a total of 4 square wave forms. The period of the square wave was determined with a high speed counter with a frequency of 9.8304 MHz. The output from the counter circuit was a two-byte binary number representing the instantaneous water elevation at the Zwarts pole. For the experiment a sampling frequency of 8 Hz was found to be sufficient. The circuitry for both the Zwarts pole and the counter were produced by the Electronics Section of the Department of Civil Engineering, University College, University of New South Wales.

Static calibration of the Zwarts poles

Static calibrations of all Zwarts poles were performed prior to deployment. A significant advantage of the Zwarts pole over resistance or capacitance gauges is that the calibration is independent of the physical properties of the water. The salinity or conductivity of the water, for example, has no influence on the calibration of the instrument. The static calibration system consisted of a 4 metre length of PVC tubing, in which the Zwarts pole was placed. The tube was filled completely with water. The water was then lowered in steps whilst output from the Zwarts pole was logged. The level in the tube and therefore the submergence of the Zwarts pole was determined to an accuracy of ± 0.5 mm by the use of a simple manometer tube fixed to the outer wall of the PVC tube. The Zwarts pole was connected to a computer that read the counter signal. Both readings were stored in a file for further processing. This calibration was repeated at least once. The mean offset varies depending on the precise fixing position of the pole upon deployment. The slope of the curve can be approximated by a straight line whose slope found, by linear regression, is given by 1 count = 0.245 cm. The calibration curves for all 8 poles used in the North-South array were almost identical. Therefore, this calibration result was subsequently used in the analysis of data from all poles. The calibrations of all the poles were checked when taken in for inspection (and cleaning) every 3 to 6 months.

Dynamic calibration of the Zwarts poles

Since there was no information on the frequency response of our Zwarts poles, an investigation had to be conducted to ensure that the Zwarts poles' frequency response was sufficient for the frequencies of the waves that would be measured. The number and configuration of holes in the outer tube would largely determine the frequency response of the instrument. The holes in the outer tube of the Zwarts pole should not significantly impede the flow of water into and out of the annulus between the concentric tubes (fig 2.8). This would decrease the frequency response of the Zwarts poles. Naturally, there is a limit to the number of holes that can be placed in the tube as eventually the structural integrity of the pole will be degraded. To investigate the appropriate selection

of the porosity for the outer tube, a dynamic calibration of the pole was performed. The calibration system is shown in figure 2.11.

The Zwarts pole was placed vertically in a water storage tank (fig 2.12). A chain connected to the top of the pole passed over a toothed cog fixed to the roof of the laboratory. The other end of the chain was connected to an eccentric arm fixed to a variable speed electric motor (fig 2.13). By varying both the speed of the motor and the length of the arm, the pole could be oscillated vertically at a range of desired frequencies and amplitudes. A multiple turn variable resistor was fixed to the shaft of the toothed cog. A constant voltage was applied across the resistor and its output logged with a conventional analog to digital board in a PC (fig 2.14). The output from the Zwarts pole was sampled coincidently with that of the variable resistor. As the resistor measures the actual position of the pole relative to the stationary water surface, it provides a reference for the determination of the transfer function for the Zwarts pole.

A number of experiments were conducted for realistic wave amplitudes and frequencies (table 2.1). There was no measurable phase lag between the Zwarts pole and the resistor in any of the experiments. The amplitude transfer function for most frequencies and amplitudes is near to one. However, at 2 Hz the difference between the resistor and the Zwarts pole is about 15%.

Transfer Function of the Zwarts Pole									
		Amplitude in Metres							
		0.05	0.07	0.1	0.25	0.5	0.75	1	1.25	1.5
Frequency in Hz	2	0.84	0.86							
	1.33	0.96	0.96	0.96						
	1	0.99	0.99	1.00	0.98					
	0.5	1.00	0.99	1.01	1.00	1.00	0.98	0.95		
	0.33	1.00	0.98	1.00	1.00	1.00	0.98	0.99	1.00	0.99

Table 2.1 Transfer Function of the Zwarts Pole

Field comparison of the Zwarts poles

Although laboratory tests provided a well controlled dynamic calibration of the poles, there was some doubt as to whether the vertical oscillation of the pole in still water accurately simulated the passage of a spectrum of waves past the poles. To test this point an *in situ* field calibration was conducted. The Zwarts pole on the central platform was compared with three resistance wave gauges. The resistance wave gauges had a sampling frequency of 20 Hz and were statically calibrated before and after the experiment on site to ensure that the calibration had not changed over the "short" experiment time. Since the resistance gauges have a very high frequency response, comparison of the spectra would determine both the frequency response of the Zwarts poles and whether aliasing was significant at the 8 Hz sampling rate. Tests were conducted for a number of different wave heights and wind speeds. A total of 18 tests were conducted with wind speeds varying from 5 m/s to 14 m/s. The transfer function between the Zwarts pole spectra and the resistance gauge spectra were not only a function of the frequency but also differed with wave height. When non-dimensionalized in terms of the peak spectral frequency, f_p , the individual transfer functions collapsed onto a single relationship. The reasoning behind this is that the smaller waves (higher frequencies) are superimposed on the larger waves (lower

frequencies) and thus increase the slope of the wave front. The level of the water in the Zwarts pole has to rise faster for a wave with a steep slope. Therefore, the water has to enter the Zwarts pole faster if the waves are steeper. This again is limited by the hole size in the outer pole (fig 2.8). Since the laboratory tests were all done at single frequencies, this did not show up in the laboratory transfer function. Hence, the frequency response in the presence of a full spectrum of waves is poorer than in the monochromatic laboratory tests. A new transfer function, dependent on dimensionless frequency was developed as shown in fig 2.15 .The transfer function indicates that the instrument is incapable of resolving spectral components above $f/f_p = 5$. Hence, all analysed spectra were truncated at this point. The transfer function below $f/f_p < 1$ is very sensitive to noise due to the very low energy levels in this part of the spectrum. Therefore it was assumed that the transfer function is equal to one in this region. The smoothed transfer function shown by the dashed line in fig 2.15 was used to correct all recorded spectra.

Limitations of the Zwarts poles

Overall, the Zwarts pole system proved a remarkably reliable. A number of limitations of the system were, however, identified during the coarse of the experimental program. Firstly, the mean offset of the pole calibration was temperature sensitive and would vary with daily temperature fluctuations. Typical variations were of order 10 mm. Hence, the instruments are not ideal for the measurement of very low frequency oscillations such as tides, infra gravity waves or seiches. The first two of these long wave phenomena are of no interest in a lake. Seiching, however, could have some influence on the mean water level and will be addressed in a later section. Mean water levels could still be measured with reasonable accuracy by averaging measurements over a 2 or 3 day period. The second, and far more serious problem that was encountered with the Zwarts poles, was fouling of the poles with algae. This proved to be a persistent problem, particularly during summer when the water temperature in the lake typically rose to 25 deg C. The algae would "grow" across the holes in the poles and block the water from entering and exiting, thus degrading the frequency response, and finally rendering poles unusable.

The problem was overcome by periodic removal (generally at 3 month interval) and thorough cleaning of the poles. Cleaning the poles in situ proved to be an inefficient method.

2.4.2 The towers

To keep the wave staffs upright and to house the associated electronics, 7 towers were constructed. Besides being stable enough to resist rough weather, the towers had to be large and stable enough to enable work by maintenance crews. Needless to say, interference of the towers on the waves had to be minimal. Since these towers were 5 kilometres from shore, they had to be self contained. To provide for electrical power large solar panels were mounted on the towers.

Physical description of the towers

The towers were designed so as to provide minimum disturbance to the waves (fig 2.16). To allow for possible changes in mean water level, the towers were build to a height of 4.5 metre. The towers were free standing but additional stability was provided by four steel guy ropes fixed to the lake bed with anchors manually driven into the bed (fig 2.17). The Zwarts pole was connected to the tower (fig 2.18) by two U-bolt brackets, one near the bottom and one near the top of the tower.

Electrical equipment on the towers

From the Zwart pole an electrical wire ran to the counter card. This card together with the radio and the radio modem, which made up the data telemetry system, were housed in a watertight box on top of the tower (fig 2.19). Two 6 volt lead-acid batteries were located beside the watertight box on the tower covered to protect them from the elements. The batteries were connected in series to provide 12 volt power to the system. These batteries were charged with two solar cells. With no solar input, the batteries could power the system for approximately 6 days. Although battery failures did occur as the batteries aged, power failures were extremely rare. The solar panels (fig 2.20) were fixed with hinges on the top of the tower facing North. The angle of the solar panels

with the horizon could be adjusted so that the optimum angle to the sun could be obtained.

On one side of the tower a Yagi antenna was mounted to transmit the data. The antenna pointed across the water at the base station. This was the standard equipment on all towers.

The Bureau of Meteorology, Melbourne, Australia, provided a range of additional instrumentation. During the experiment, 10 metre high anemometer masts (VDO anemometers, model 402 715) were installed on four towers, to measure the wind speed and direction (fig 2.21). The data from the anemometers were recorded as 10 minute mean values using on-board data loggers. On two of those towers, water temperature at 3 different depths, the air temperature and air humidity was also measured and recorded on the data loggers. These additional meteorological instruments were not integrated into the telemetry system as they were added after the initial measurement program had commenced. As the quantity of data generated by these instruments was not large, the on-board data loggers proved an acceptable compromise. Data were down-loaded to a portable PC on regular maintenance visits. Although these additional instruments enhanced the experiments, they required a high degree of maintenance and failed on numerous occasions.

Deployment of the towers in the lake

The towers were fully constructed at the University College and transported to the lake shore by truck. On the shore the Zwarts poles were mounted. The bottom mounts of the Zwarts poles were between 1.5 and 2 metres below the water surface once the towers were standing in their upright position. The deployment of these towers was done from the "assault craft" borrowed from the Royal Australian Army (fig 2.22). This craft brought the towers to premarked spots (buoys) in the lake. The craft was then lined up facing North while two people would slide the tower off the front. When two of the tower feet hit the lake bed, the boat driver had to increase the engine power to move the boat slowly forward thus pushing the tower upward. With too much power, the boat

would overrun the towers pushing them over, and with too little power the tower would fall back into the lake. The deployment of the towers could only be achieved in very calm weather. Even in such conditions the process was often precarious. Once the tower was upright, a 40 kg pole was used to drive the anchors into the mud to which steel guy ropes were attached (fig 2.17). Needless to say, this was a very physically demanding job. Finally, the electronics, batteries and solar panels were placed on the upright towers.

2.4.3 Radio telemetry

To avoid numerous trips to the wave gauge towers to collect data, a telemetry system was setup to send the data to a base station (see section on base station) located on the shore. At the base station the data were stored for later collection.

As maintenance of the telemetry system in the field would be a difficult task, it was designed to be as simple as possible. Hence, microprocessor control was not attempted. Rather, the system had very little "intelligence". The communication was real time and "one-way." Any data lost in the transmission could not be recovered. Simple checks were implemented to determine if data were corrupted or lost during transmission.

The data path

The best way to describe the electronic/radio system is to follow the data path from the point the data have been measured to the point where they are safely stored. The Zwarts pole produces an analog square wave output (see section 2.4.1 on the Zwarts pole) which varied in frequency. This signal was passed via a cable with watertight connectors to a watertight box on the towers (see section on towers). These watertight boxes contained the "signal to count" converters, radio modems and the radios themselves. The counter converted the analog square wave to a digital count proportional to the period of the square wave. To keep the system as simple as possible, programmable array logic (PAL) chips were used to perform most tasks. The counter system described above, digitized the water surface elevation at a rate of 8 Hz. The output from the counter card consisted of a 2-byte string representing the water surface

elevation together with a further 2 byte sequence number used to identify lost or erroneous data. The data were in RS232 serial form which could be directly entered to a (portable) PC for testing and diagnosis. In the field operation, the data were transmitted via the radio telemetry system. This system consisted of a radio modem, a radio transmitter and an 8-element Yagi antenna. The radios operated continuously with the transmitters for each pole operating at differing carrier frequencies within the frequency band 850 MHz to 920 MHz. At the base station, on the shore of the Lake, a matched set of radio receivers were located (one for each transmitter/pole system). The system is shown schematically in figure 2.23. In order to reduce cost and power requirements, the system was strictly "one-way." As there was no "two-way" communication, there was no opportunity to re-transmit lost or corrupted data. The two-byte sequence number was later used in the processing to identify such occurrences. All poles were in line of sight of the base station with the maximum distance being approximately 20 km. With time the transmitter/receiver pairs would drift "off-frequency" and transmission errors would become a problem. On-site repairs were attempted, but eventually the radios had to be returned to the manufacture to be tuned. Generally, however, errors were rare. When they did occur, they were handled by the data processing software. From the radio receivers the signal went into the radio modems and into a multi-channel communication board attached to a Personal Computer (PC). This PC logged all the incoming data to disk and performed error checking on the incoming signals. The PC also contained software to check the functioning of the poles. Both programs could be started via a telephone modem from the university. This enabled continual checking for errors and the correct functioning of the system from the university.

A spatial array of Zwarts poles was established at the central platform to measure the directional properties of the waves (see section 2.6). In contrast to the other locations, the directional array had a "two way" radio link to the base station. The reason for this was that the directional array did not log data continuously due to the high volume of data. The "two way" link was used to transmit a signal to the array to switch on and commence logging data. A full description of this system appears in section 2.6.

2.4.4 Platform

At Station 6 in the centre of the lake a large platform was erected. The main purpose of the platform (fig 2.24) was to provide a work space for various experiments. It consisted of a wooden deck (4.5 x 4.5 metres) supported by steel poles at each corner. The deck was about 4 metres above the lake bed. The platform was assembled on the lake side floated out on drums and raised by lowering its legs onto the bottom and jacking the deck up, in the same manner as "jack-up" oil rigs. The platform was secured at the corners to the lake bed by guy wires attached to anchors. On the eastern side a ladder was constructed for access.

One of the major items on the platform was the Zwarts pole at the north west corner of the platform. This corner was selected for the Zwarts pole as the main wind direction was from the North to North West. The platform legs had little influence on the waves passing under the platform. At the north east corner a 10 metre high aluminium anemometer mast was erected. The mast supported an R.M.Young anemometer (model 05103). The mast was held steady by guy wires attached to the platform and anchors in the lake bed. The anemometer was connected to a data logger and the data logger to a one-way radio link to the base station. One second samples of the wind speed and direction were taken by the data logger. The telemetry system was the same as described in the section on telemetry (section 2.4.3). At a latter stage of the experiment several other instruments were also attached to the data logger. These consisted of a set of temperature probes to measure the temperature of the water at 0.5 m, 1 m and 1.5 m water depth, a hydrometer, an air temperature probe and a solar radiation meter (limited deployment). These data were averaged over a minute period by the data logger and transmitted by the telemetry system together with the wind data.

A light-weight aluminium structure was built on the platform to shelter equipment. This structure housed the computer (an AT Personal Computer) and the two-way radio link that controlled the directional array, located 15 metres north of the platform (see section 2.6 on the directional array). The computer was powered by an inverter, attached

to a bank of batteries, that could be switched on or off by radio signals (see section 2.6 on the directional array). Towards the end of the experiment the directional array, the anemometer mast and the aluminium structure were all extensively damaged during a particularly violent storm.

To power the equipment, solar cells facing the North were installed on the rail of the platform and on the roof of the aluminium structure. The energy from these solar cells was stored in batteries. The batteries were located on the platform deck under covers to protected them from the sun and rainwater.

A 4 metres long measurement bridge was also constructed on the western side of the platform, one end resting on a specially placed tower and the other end on the platform itself. The bridge enabled undisturbed wind flow measurements from the North or South to be made (fig 2.25). As part of a series of measurements not discussed in this report, a series of resistance wave gauges, a video camera, a hydrophone and a sonic anemometer were deployed from the bridge (fig 2.26).

2.4.5 The base station

A base station was established on the Western shore of the lake (fig 1.7). For security and logistic purposes this was located on a private farming property. A transportable construction building was used for the base station (fig 2.27). To ensure line-of-site for radio communication to the towers, the base station was located on slightly elevated ground. A 12 metre high mast was erected adjacent to the base station to support the receiver antennas for each of the telemetry systems (fig 2.28). Equipment within the base station consisted of a bank of radio modems and radio receiver pairs (one pair for each tower), together with a conventional Personal Computer (PC) for data acquisition. The radio receivers were powered with a regulated 12 volt power supply. A standard 240 volt power connection was made to the base station from the standard electricity grid. The output from each of the radio modems consisted of an RS232 data stream. As the PC had only two standard serial RS232 ports, a multiple "coms" port board was

added to the system. This provided eight additional RS232 ports, one for each of the wave measuring stations. The data stream for the anemometer and meteorological equipment at Station 6 (platform) were logged through one of the standard RS232 ports.

A telephone line was established to the base station and a telephone modem connected to the second of the RS232 ports. With the aid of the public domain computer package "PC-Elsewhere" (similar to PC-Anywhere) it was possible to monitor the operation and control the system remotely via this telephone connection from the University. This link, together with an electronic switch, was later used to control the directional array from the University. After establishing a link from the university modem to the base station modem, a special character could be send to the electronic switch. This then either established a link with the computer at the base station, or a link with the computer controlling the directional array at the platform.

2.5 Analysis of the Data

2.5.1 Data acquisition software

At the base station a Personal Computer (PC) logged all the data received from the radio modems and stored this to disk. The data were retrieved from the base station once a week. All the data collection and checking software were custom developed for this experiment.

Acquisition of all data at the base station was achieved with a Quick Basic program written specifically for the task. This software was far from trivial as it needed to run continuously and be sufficiently robust to handle possible radio communication errors and failures of the instruments. A flow chart showing the structure of the software appears in figure 2.29.

The software operated on a 30 minute duty cycle. Although the data stream from the various instruments was continuous, the software would collect data from all

instruments for a period of 30 minutes commencing at the start of an hour. At the completion of each 30 minute logging session, the data from each of the instruments was written to disk. The software then waited until the next hour to recommence logging. This apparently "wasted" time was often used to interrogate the base station computer via the telephone modem line from the university and check on instrument performance and data quality.

The normal cycle of the software was to commence by clearing the buffers of the RS232 ports. Then it would check whether the wave poles were working correctly. The way this was done is described below. Any pole not working correctly would be switched "off" (logically) by the software and not logged. The program then logged the data from the working Zwarts pole systems and the anemometer for 30 minutes.

The method used by the program to clear the buffers and log data was as follows. All the data in one RS232 port (from one Zwarts Pole) would be logged by the program until the buffer was empty. It would then switch to the next RS232 port and so on. During the switching the program also checked if the input from the Zwarts poles was still valid.
Each of the RS232 ports on the expansion card had an onboard buffer of 32 KBytes. Hence, there was capacity for the storage of incoming data. This buffer was insufficient, however, to store the full 30 minute data stream (approximately 57 KBytes). Therefore, clearing of the data buffers and storing of the data was required during the logging period. This procedure posed some problems as there was no simple method of determining how much data resided in the onboard data buffers. To retrieve too little data from the buffer would mean that the buffer would eventually overflow and data would be lost. To retrieve too much data would mean that the program would spend too much time at that Zwarts pole, with the possibility that one of the other buffers would overflow. This problem was overcome using a system of three possible timing checks during the data retrieval.

(1) 32 bytes (2 data bytes + 2 sequence counts * 8 Hz) of data should be entering the buffer each second. If there was no data in the buffer the expansion card would, upon transfer request, return a zero after a second. This would indicate that the buffer was empty and the program should go on and log the data of the next pole. This was also used as a check if a Zwart pole system had ceased to operate.

(2) With the data buffer flushed but new data entering the buffer, data could be extracted at the 32 Hz rate mentioned above.

(3) If the data buffer held stored data it could be retrieved at a rate of 1000 bytes per second. Data should, however, enter the buffer at only 32 bytes per second. Sometimes a Zwarts pole system would malfunction and send data at much higher rates than the 32 Hz. This could be checked by the time it would take to clear the buffer. This also, was used as a check if a Zwart pole system had ceased to operate correctly.

The anemometer and meteorological data from Station 6 were input to one of the standard RS232 ports. The data buffer of this port was sufficient to hold the full 30 minute logging period for this lower data rate. Hence, the data buffer for these data was only flushed at the conclusion of the logging period. Approximately 80 MByte of data were stored each week and this was downloaded to a portable PC on weekly visits to the base station (fig 2.30).

Additional software was written to check and display incoming data from the Zwarts poles in real time. These programs provided a real time graphical representation of the water surface elevation (waves) from a selected pole. Two versions of this software were developed: a crude ASCII based system for use over the telephone modem link and a graphics based version for use at the base station. These programs proved to be valuable diagnostic tools enabling the checking of both the wave height and the correct functioning of the Zwarts poles from the base station and more importantly from the university.

Due to the extremely long duration of the experiment, preliminary analysis of the recovered data was performed on a weekly basis. This analysis consisted of determining the significant wave height, H_s, and the frequency of the spectral peak, f_p, for each of the stations together with the wind speed and direction from Station 6. These results were stored in a data base for subsequent analysis. They were also summarised in weekly summary plots used to verify instrument performance. A typical example is shown in figure 2.31.

2.5.2 Processing of wind data

The raw data files from the meteorological package at Station 6 consisted of wind speed and direction sampled at a rate of 0.8 Hz. In addition, the raw data contained values representing the air temperature and humidity and water temperatures at three depths sampled at the lower rate of once per minute. In addition, occasional transmission errors due to the telemetry system either introduced spurious data or resulted in data gaps. The wind processing program, which was written in Quick Basic, removed data errors and corrected for missing data. From the resulting time series of wind speed and direction, 10 minute mean values of wind speed and direction were saved to a data base. The full time series were written to tape along with the unprocessed data.

2.5.3 Processing of wave data

Initially, the wave data were processed on a personal computer using a program written in Lahey Fortran. During the period of the experiment however, the analysis was ported to an IBM RS6000/530. All the analysis was repeated with new software. The programming language used on the IBM was Matlab.

As the wave data were to be subjected to spectral analysis, it was important that any possible gaps in the time series due to data transmission errors be accurately determined. Such gaps could be recognised since the sequence count information was available. The data were subdivided into contiguous blocks of 256 points. These blocks

were subjected to standard spectral analysis. The spectra from each block were ensemble averaged to yield the final smoothed spectral estimate (Bendat and Piersol, 1971). The number of available blocks depended on the number of transmission errors in the record, but 57 was a typical number. Thus, the spectra typically had 112 degrees of freedom with a spectral resolution of 0.031 Hz. The Nyquest frequency is half the sampling interval and therefore equal to 4 Hz. Transmission errors occasionally also introduced spurious data into the data blocks. Any data which deviated from the mean by more than 4 σ, where σ was the standard deviation of the block, were flagged as erroneous and eliminated. The erroneous values were replaced by values obtained from linearly interpolating between their neighbours. Obviously, an excessive number of such errors could bias the resulting spectral estimate. A number of numerical tests were conducted to assess this effect. It was concluded that even with as many as 30 erroneous values in a block, little bias was introduced. Hence, blocks containing more than 30 errors were not included in the ensemble average. As the telemetry system was very reliable, exclusion of data blocks for this reason was very rare.

The main parameters estimated from the spectra were the significant wave height (H_s) and the peak frequency (f_p). The significant wave height H_s or more precisely H_{m0}, (see section on the definition of H_s ,section 3.5) was determined from the integral of the spectrum and the frequency of the spectral peak using the weighted mean technique of Young (1995).

$$f_p = \frac{\int f\,[F(f)]^5\,df}{\int [F(f)]^5\,df} \qquad \textbf{(2.1)}$$

where f_p is the frequency of the spectral peak and $F(f)$ the spectrum at frequency f. These values were stored in a database together with their 95% confidence limits (Young 1995). The spectral estimates together with the raw water surface elevation time series were written to 8 mm streaming tape.

The mean daily water level was determined at each station using a zero phased 5th order Butterworth smoothing technique. Because of the influence the temperature had on the calibration offset, it was not possible to distinguish seiching from temperature variations. Although the seiching effects were very small (maximum that was calculated was 10 cm and visual observations were even smaller) and were ignored in the analysis, they do introduce a possible error in the estimates of mean water level. This effect has been considered in the error analysis (section 4.4.3).

2.6 The Directional Array

In addition to the measurement of the evolution of the significant wave height, peak frequency and one-dimensional spectrum, the experimental design also required measurements of finite depth directional spreading. Such measurements were made with a spatial array located adjacent to the platform at Station 6.

Young (1994) has investigated measurement methods for directional spectra. The use of a directional buoy was not possible due to the shallow water and relatively high frequency waves in the lake. The measurement system was required to operate remotely and for long periods of time. Therefore Zwarts poles (see section 2.4.1) were used as elements in a directional array. The directional resolving power of such multi-element arrays increases with the inclusion of additional measurement elements (Isobe *et al.* 1984, Young 1994). Following Young (1994) a series of Monte Carlo simulations were performed to determine the optimum number and placement of the elements in the array (and thus the shape of the array). Two general approaches were considered in the array design. One was to construct an array to provided higher directional resolution from one particular direction. The other was to design an array with equal resolving power for all directions. A symmetric design with equal resolving power in all directions was finally adopted. The array consisted of 7 elements arranged in the form of a "Mercedes" star (fig 2.32).

The Zwarts poles which comprised the array were housed within a frame consisting of a top and a bottom holder separated by three thin vertical rods. These rods were sufficiently thin to avoid any disturbance of the waves before they reached the directional array. They were designed to simply separate the top and bottom holders and thus provided little structural rigidity. When the 7 aluminium Zwarts poles were installed however, the full array could support the weight of one person. The top and bottom holders had radial sliders with U-bolt clamps to hold the Zwarts poles. These sliders could be relocated at different radial positions along the holder to adjust the position of the Zwarts poles in the array. This feature allowed for field adjustments to the array geometry although such adjustments were not actually required. To provide the array with additional cross bracing, very thin wires were strung to the opposite corners (fig 2.33). Furthermore, for stability and, to make sure the array did not blow over, three anchors were driven into the lake bed and attached with guy wires to the top holder.

The Zwarts pole array was located 15 metres north of the main platform at Station 6. On the platform there was a garden shed with a personal computer (AT). Data from the array were logged by a personal computer (AT), housed within the aluminium structure on the platform. A program was written in Turbo Pascal to log the 7 poles at a rate of 8 Hz. All the data were kept in memory until the logging session of half an hour was complete. This was necessary because the writing of the data to the hard disk caused delays in the sampling. All the poles in the array were attached to the PC via waterproof cables. These cables ran from the PC, via one of the legs of the platform into the water and across the bottom of the lake to the array. The cables were securely attached to the legs of the platform to avoid damage to the cables. On the lake bed, the cables were held in place using weights.

The computer on the platform was powered by an inverter connected to 12 volt storage batteries (or two 6 volts in series). These batteries were recharged by the solar cells which were placed on the platform. To conserve energy, the computer could be

switched on via the telemetry link to the base station from the university in Canberra. To make sure that the computer switched off after logging the array in the event of losing the radio link, a timer was installed that switched the computer off after 45 minutes. This system made it possible to log the directional array remotely. This was necessary for two reasons. Firstly, the measurements could be taken at any time of the day, without organizing a team to go out to the platform. Secondly, measurements could be taken in rough weather. Sometimes it was not safe to go to the platform by boat because of bad weather or the onset of night. Logging the array remotely avoided these problems. The data were down loaded onto a portable computer when the hard disk of the computer on the platform was nearly full. This required a trip to the lake and platform.

The logging sessions were 30 minutes. Once initiated, the logging worked automatically. The data logged from the 7 poles at 8 Hz, was kept in memory due to the slowness of the disk writing interfering with the logging. After the logging period, all the data were retrieved from memory and written to disk. These data were retrieved at regular intervals (before the harddisk was filled). The amount of data collected per session was approximately 600 KByte.

The first deployment of the array was disastrous. The initial design of the array did not include the vertical rods or the cross bracing and relied completely on the Zwarts poles themselves for structural rigidity. The army assault craft (see section 2.2.2) was used to launch the array. Just after launching and before the ground anchors could be attached to the array, it collapsed sidewards as a parallelogram. The U-bolts which connected the Zwarts poles to the top and bottom holders could not resist the moment applied by out-of-balance forces on the structure. The collapsed array was recovered, re-designed and later successfully deployed.

The second problem which was encountered with the array, was with the watertight heads on top of the Zwarts poles which contained all the electronics. These were a

different design to those used on the Zwarts poles deployed at the towers. Although the heads were watertight, they were not airtight. During the day warm air with a high moisture content entered the head. During the evening the water in the air condensated within the watertight head. The continual buildup of moisture eventually destroyed the electronics requiring a re-design of the head assembly.

The last problem encountered with the array was the algae growth on the poles. This required complete dismantling of the array. Because the Zwarts poles were part of the structural strength of the array, they had to be replaced by similar poles. Three aluminum poles with the same diameter were used to replace the Zwarts poles while the Zwarts poles were cleaned. The dismantling of the Zwarts poles was done by one person on top and one diver on the bottom to undo the U-bolts. The cleaning of the Zwarts poles was done using a high pressure water jet. After the cleaning, the poles were returned, remounted (fig 2.34), and the three temporary supports removed.

Although the directional array was deployed later in the experiment, it functioned for more than one and a half years. At the end of this period unfortunately some of the guy wires of the array were corroded and in a severe storm, the array collapsed.

3. Results from Lake George

3.1 Introduction to the Results of the Measurements

The previous chapter provided a description of the instrumentation used to measure both wind and wave data. This chapter provides an overview of the data measured during the extended measurement program. The overview includes the wave and wind data collected at the individual stations, together with the directional data from the array at Station 6.

The chapter also includes two short notes on the definitions of wave height and wind speed to be used in later analysis.

3.2 Results of the Wave Measurements

Although wave measurements were conducted on Lake George over a 3 year period, the period from 6 March 1992 until 7 October 1993 has been used for the data analysis. In this period there were 67,225 usable wave records each with a duration of half an hour collected. The samples in these records were taken at a frequency of 8 Hz. For the spectral analyses the samples were split into 256 point data blocks. In total there were 3,675,819 blocks analysed. Table 3.1 shows the quantity of usable data obtained from each station during the analysis period.

Station Number	1	2	3	4	5	6	7	8
Records	8731	8171	8642	8594	8880	6918	8618	8671
number of 256 sample blocks	468,291	449,134	481,803	477,453	490,114	385,673	469,895	453,456

Table 3.1 Stations with the number of records and 256 sample blocks

Because of the quantity of wave data, an automatic analysis and quality control program was written. This program applied the following checks:

- Gaps in the sequence count, indicating missing data were noted. For small gaps (less than 30 data points) the data were interpolated. Whilst for larger gaps, the data block was discarded.
- The total number of gaps and their total length in the record were noted. If the total number of missing data points in a record exceeded 30, the block was also disregarded.
- Possible data spikes were flagged. If individual readings exceeded 4 times the standard deviation of that block, they were considered a spike, and treated in the same manner as data gaps.

This data quality control process, together with occasional instrument failures (especially Station 6), accounts for the varying number of records and blocks reported in table 3.1.

From the preliminary analyses the following quantities were derived and recorded. A brief explanation of the recorded variables is given.

1	Date	This is a normal date including the hour in the following format YYMMDDHH.
2	Station number	There were 8 stations in the lake. The most northern one being Station 1 and the southern wave measuring station being Station 8. The platform was Station 6.
3	H_s	The H_s is calculated from the variance of the spectrum.
4	Lower 95% H_s	The lower 95% confidence limit is calculated from the number of degrees of freedom of the spectrum (Young 1995).
5	Upper 95% H_s	The upper 95% confidence limit is calculated from the number of degrees of freedom of the spectrum (Young 1995).
6	f_p	The peak frequency is calculated with the weighted method described by Young (1995).
7	Number of blocks	The wave record was split up into blocks of 256 samples for the analysis. The number of these sample blocks was recorded as a quality indicator.
8	U_{10} Wind Speed	This was a mean of the wind speed measured at 10 metres height at Station 6 during the recording period.
9	θ_{10} Wind Direction	This was a mean of the wind direction measured at 10 metres height at Station 6 during the recording period (not a vector mean).
10	σu_{10}	The standard deviation calculated from the wind speed records measured at 10 metres height.
11	$\sigma \theta_{10}$	The standard deviation calculated from the wind direction records measured at 10 metres height.
12	Number of wind points	Number of points used to determine the wind speed (U_{10}) and direction (θ).
13	Water depth at Station 5	Water depth at Station 5 in metres (ie. lake average). Due to the position of Station 5 in the middle of the lake, it was used as the average water depth that could be used for all the stations.
14	Actual water depth	Actual water depth at the station (field 2) in metres.

Table 3.2 Variables calculated for all the wind and wave records.

For the wind that came from North or South (± 20°) direction the following extra quantities were calculated.

15	Actual fetch	Distance (m) from the north or south shore.
16	Fetch using JONSWAP	The fetch at the most upwind station is calculated from the measured energy at this station and the JONSWAP (energy-fetch) relationship. The fetch at the other locations is determined as an offset from the most upwind station.
17	Fetch using JONSWAP with NaN	Same as above but the fetch at the most upward station is flagged as Not a Number (NaN)
18	Number of the stations	Number of the stations along the fetch (1 is first station along fetch)

Table 3.3 Extra items which were calculated for North and South winds

The wind was not measured at every station. There are however different methods for estimating the wind speed for each station. Therefore, the wind was calculated with these different methods and stored for easy accessibility and comparison.

19	U_{10} Taylor	Using the boundary layer theory of Taylor and Lee (1984) a value of U_{10} at each station was calculated from the measured wind at Station 6. See section 3.6.
20	Averaged U_{10} Taylor	Using the boundary layer theory of Taylor (1984) (see section 3.6) a value of U_{10} at each station was calculated for the measured wind at Station 6. This was then averaged along the downwind path of the fetch. Note this doesn't give the same answer as the measured wind (field 8).
21	Averaged U_{10} Taylor $\cos(\theta)$	Using the boundary layer averaged wind speed (field 20) and the wind direction (field 9) the effective wind speed was calculated. See section 3.6.
22	U Wu	The wind speed according to Wu (1980). See section 3.6.
23	U HEXOS	The wind speed according to HEXOS (1992). See section 3.6.
24	U [$\lambda/2$]	The wind speed U [$\lambda/2$] is the wind speed half a wave length above water surface at the station. The wind speed is calculated by using a logarithmic wind profile and the measured wind at 10 metres.
25	Averaged U [$\lambda/2$]	The values in field 24 averaged along the fetch.
26	Average downwind path depth	This depth is averaged along the downwind path. This means that the average depth was calculated over the distance which the wind had travelled. Note that this means that the averaged downwind path depth differs for every station. Also, note that this is a different depth to field 13.

Table 3.4 Extra wind speed calculations which were included for North and South winds

To give an indication of the data which was returned, histograms of two parameters have been prepared. The significant wave height (H_s) of the data from all eight stations is shown in figures 3.1 and 3.3. One interesting feature of the graphs in figure 3.3 is that the measuring stations in the middle of the lake have higher waves on average than the measuring stations at the ends. This occurs since a large proportion of the data are for easterly and westerly winds. For these cases, both stations 1 and 8 have short fetches.

The histograms of frequency (fig 3.2 and 3.4) do not exhibit any obvious position dependent trend.

Cases for which the wind direction was closely aligned ($\pm 20^\circ$) with the north-south instrument array provided the opportunity to investigate fetch limited growth at multiple stations. Hence, such cases were extracted from the full data set. This sub-set was entitled the "North-South" data set. To ensure well defined conditions, only data which corresponded to steady-state cases were retrained. Only cases for which the wind speed varied by less than 10%, not only during the 30 minute measurement period but for one hour previously were retained. Also cases where the wind speed was less than 4 m/s were discarded.

North-South data distribution histograms have also been prepared (fig 3.5 to 3.8). In figure 3.7 again the measuring stations close to the shore on average have smaller significant wave heights than the ones in the middle of the lake. In figure 3.8 there can now be seen a difference in the peak frequency for the different measuring stations. In the middle of the lake the measuring stations have a lower peak frequency than for the stations at the ends of the lake. The North-South data contains a wide range of fetches. This increased dynamic range more clearly shows the variation in peak frequency with fetch.

A more detailed frequency distribution of the full data set is given in figure 3.9. In this figure there is a clear low frequency spike. These data were checked manually and in all cases the wind speed was very low and both the wave height and frequency were not consistent with the other measuring stations. Subsequently such records were deleted for the North-South analysis. Some of the North-South cases exhibited rather unusual behaviour at long fetch. As expected, the significant wave height generally increased with increasing fetch. In some cases, however, the significant wave height began to decrease again at long fetch. The reasons for this behaviour are yet to be explained. Possible causes are: Changes in water depth, changing aerodynamic roughness of the

water surface and the influence of the lake sides. For the present analysis, such cases were excluded.

3.3 Results of the Wind Measurements

In total, five anemometers were mounted on the stations. However four anemometers (the VDO type 402 715) failed on numerous occasions. These anemometers were mounted on Stations 2, 4, 7 and 8. On Station 6 (the platform) the R.M. Young anemometer was used as wind reference during the experiment. In figure 3.10, the times that the anemometers were operational is shown. Times when all five anemometers were working are limited. To investigate boundary layer development along the lake only cases where the wind speed was greater than 4 m/s were considered (see section 3.6). As can be seen in figure 3.11 the window for that opportunity is even smaller. As the record at station 6 was most complete, this station was used for the bulk of the analysis to be described in subsequent sections.

As with the wave data, the wind data were analysed after transfer to the university. The data logger at station 6 recorded a sample every 1.25 seconds and averaged these samples every minute. These data were then sent to shore and stored on the base station computer. At the university, both the wind speed and wind direction were averaged over a 10 minute period. This would result in three average wind speeds and wind directions during a 30 minute logging period.
Both the vector mean and the arithmetic mean were calculated. The two averages, as shown in table 3.5, did not differ significantly.

Mean difference between arithmetic and vector average of the wind speed & direction				
	Difference in wind speed (m/s)		Difference in direction (degrees)	
	Difference in mean	Difference in sdev	Difference in mean	Difference in sdev
All winds	0.09	0.51	2.46	13.84
Wind > 3 m/s	0.07	0.39	0.45	3.96

Table 3.5 Differences between the "vector mean" and the "arithmetic mean" wind speed and direction. The reason that the directional difference is larger for wind speeds less than 3 m/s is that during periods of very low winds the slightest gust could turn the anemometer around, which gives a larger difference in the two values.

Distribution histograms for wind speed and direction are shown in figures 3.12 to 3.17. In figure 3.12 the wind speed histogram for all data is shown. There are numerous events with moderate to strong winds. The corresponding wind direction histogram is shown in figure 3.13 and a joint scatter plot of the wind speed and direction in figure 3.14. The experiment was designed for North-South winds. As shown by these plots, such events were not particularly common. Hence, the extended data gathering period was required to acquire sufficient suitable data.

The most common wind direction is west (fig 3.13). The wind direction histogram indicates that an east-west array geometry would have represented a more effective experimental design. Although North-South events are relatively rare, the longer fetch in this direction was seen as a significant parameter in the experimental design, thus justifying the array alignment.

As noted earlier, strict quality controls were imposed for the North-South data set. These criteria ensured that the data were collected in truly fetch limited conditions and with homogeneous wind fields. These strict criteria, together with the fact that

North-South wind events were not common, reduced the data set significantly. However, as the measurement period lasted for a long period, the resulting data set consisted of approximately 1000 observations. The distribution in terms of wind speed and direction for this data set are shown in figures 3.15 and 3.16 respectively. As shown in figure 3.16 southerly winds are more common than northerly events. A scattergram showing wind speed and direction appears in figure 3.17.

3.4 Results of the Directional Spectra Measurements

There was one directional array with 7 elements placed at Station 6. This directional array was operated from the university through a series of (radio) modems. With this connection, the controlling computer could be switched on. Unless the computer had received a command to be switched off earlier, it would remain on for a period of 45 minutes and then would switch off. This ensured that if the data link was lost, the remainder of the session would be logged, without excessive drain on battery power. Because the array could be monitored and controlled from the university via telemetry and modem links, it could be switched on when the wind was of suitable strength and direction. Of coarse there was no way of knowing if the wind would remain steady in both direction and magnitude when starting the logging session. The array functioned for more than one and a half years.

The water depth during this period was between 1.8 and 2.4 metres. The wind speed, which was monitored by the anemometer at Station 6, ranged between 3 and 15 m/s. In this period 156 directional spectra were recorded. Many of the directional spectra were recorded under slantly fetch conditions. This resulted in directionally skewed spectra with significant differences in the directions of the wind and waves. Such cases were excluded by considering only easterly and westerly cases where the wind direction was $\pm 10^\circ$ from the shore normal. This resulted in 58 records. There were no suitable North-South events recorded by the directional array.

These 58 records ranged from very young seas ($U_{10}/C_p = 4$) to fully developed seas ($U_{10}/C_p = 1$). The ratio U_{10}/C_p is often referred to as the inverse wave age in which U_{10} is the wind speed measured at 10 metres height above the surface and C_p is the phase speed of the peak frequency,

$$C_p = \frac{L_p}{T_p} \tag{3.1}$$

where L_p is the peak wave length and T_p the peak period of the wave. Although the majority of the cases were around $U_{10}/C_p = 2.3$ (see fig 3.18) the data set covers a broad range of wave-ages. This range is comparable to the deepwater data set of Donelan et al. (1985), and significantly broader than the well know data set of Mitsuyasu *et al.* (1975) and Hasselmann *et al.* (1980)

Figure 3.19 shows the non-dimensional parameter $k_p d$ which is often used to indicate whether the record is taken in shallow water ($k_p d < 0.25$), deep water ($k_p d > \pi$) or transitional water ($0.25 < k_p d < \pi$). Here k_p is the wave number of the spectral peak and d the water depth. As shown in figure 3.19 the majority of the data are between $1 < k_p d < 2$. Hence, the data set is entirely in transitional water depth where significant bottom effects could be expected.

3.5 A Note on H_{mo} Versus $H_{1/3}$

Before describing wave development in detail, a comment on the definition of significant wave height (H_s) is warranted. The significant wave height (H_s) is often defined as $H_s \equiv H_{1/3}$, with $H_{1/3}$ being the average of the highest 1/3 of the waves (computed from zero crossing analysis). Alternatively it is defined as $H_s \equiv H_{mo}$ (computed from the area of the energy density spectrum). There seems to be no consensus on the matter. As long as H_s is well defined by the author(s) there can be no confusion. Here $H_s \equiv H_{mo}$ is used. There is a difference between $H_{1/3}$ and H_{mo}. Thompson

and Vincent (1985), conducted experiments in the CERC wave tank with a 1:30 slope. They found differences up to 40% between $H_{1/3}$ and H_{mo}. Hardy (1993), working in very shallow water (0.5 to 2.5 metres water depth) on the edge of a reef, found differences ranging from 0 to 15%. Forristall (1978) conducted an analysis of 116 hours of hurricane spectra and concluded that the $H_{1/3}$ is 0.942 times H_{mo} . A comparison was conducted for the Lake George data set. Because the raw wave records were available, a true $H_{1/3}$ could be calculated together with the H_{mo}. For all the data H_{mo} is less than 1.5 % higher than $H_{1/3}$ (fig 3.20). A linear regression to the data of figure 3.20 yields $H_{1/3} = 0.9864\ H_{mo}$ .When limited to the North-South data, $H_{1/3}$ is lower than H_{mo} by about 4-6 % (fig 3.21). Because of the longer fetch, these waves are relatively larger than waves from other directions. This possibly accounts for the larger difference.

3.6 Wind Speeds

There has been significant debate about which wind speed to use in converting the wave height, wave frequency, fetch length and water depth to dimensionless parameters. The most widely used wind speeds are the value at 10 metres above the "average" surface and the friction velocity, defined as

$$U_* = \left(\frac{\tau}{\rho}\right)^{\frac{1}{2}} \qquad \textbf{(3.2)}$$

where τ is the wind stress and ρ the density of air.

Of the two, the most frequently used is the wind speed at 10 metres above the surface level (U_{10}) although this can sometimes be difficult to measure. For instance, most ships at sea measure the wind speeds at 19.4 metres above the sea surface. If the wind speed is measured at a level other than 10 metres above the surface, it can be converted to U_{10} using the logarithmic form of the boundary layer profile

$$U_z = \frac{U_*}{\kappa} \ln\left(\frac{z}{z_o}\right) \tag{3.3}$$

in which z is the elevation at which U_z is measured, κ is the von Karman's constant ($\kappa = 0.4$), z_o is the roughness length of the surface and U_* is the friction velocity.

Wu (1980) proposed a relationship between U_*, U_{10} and the drag coefficient C_{10}.

$$\begin{aligned} U_* &= (C_{10})^{1/2}\, U_{10} \\ C_{10} &= (0.8 + 0.065\, U_{10}) \times 10^{-3} \end{aligned} \tag{3.4}$$

The HEXOS results (Smith *et al.* 1992) showed that the roughness length is a function of the wave age (C_p/U_*)

$$z_0 = 0.48 \frac{U_*^3}{g C_p} \tag{3.5}$$

This together with equation 3.3 yields

$$U_z = \frac{U_*}{\kappa} \ln\left(\frac{z\, g\, C_p}{0.48\, U_*^3}\right) \tag{3.6}$$

which can be solved iteratively. A good starting point is using Wu's U_* as a first guess. Another major problem is knowing the exact speed along the fetch. This is a serious problem when there is a change of roughness length of the surface (e.g. from land to water). Taylor and Lee (1984) provide some guidelines. The basic principle is that the boundary layer adjusts itself after a certain length. The flow will have an internal boundary layer with a depth of δ_i. Outside this internal boundary layer the wind velocity is the same as equation 3.3. The internal boundary layer grows according to the relationship

$$\delta_i = 0.75\, z_0 \left(\frac{x}{z_0} \right)^{0.8} \tag{3.7}$$

where x is the distance along the fetch and z_0 is the roughness length at x. Inside the boundary layer ($z \leq \delta_i$) the wind speed at elevation z is

$$U_z = \frac{\ln\left(\frac{z}{z_0}\right) \ln\left(\frac{\delta_i}{z_{0u}}\right)}{\ln\left(\frac{\delta_i}{z_0}\right) \ln\left(\frac{z}{z_{0u}}\right)} U_{0u} \tag{3.8}$$

with z_{0u} being the roughness length of the upwind boundary, U_{0u} the upwind wind velocity and U_z the wind speed at elevation z.

The wind is usually only measured at a point or a few points along the fetch. As indicated in equations 3.7 & 3.8, the wind speed varies after a change of roughness length. Since the wave growth is dependent on the wind speed, it is wise to calculate an average wind speed for the fetch. One could also argue that even a mean of the wind speed along the fetch is not good enough and a more sophisticated calculation should be made.

As explained in the chapter on wind speed measurements, there were five stations where the wind was measured. Unfortunately due to technical failures, there was only a small period when all 5 stations were working (fig 3.10 and fig 3.11). Therefore it was decided to use the wind measuring Station 6 (on the platform) as the wind speed indicator for the calculations, since this record was most extensive. The equations given by Taylor and Lee 1984 (equations 3.7 and 3.8) were calibrated and verified in the small period that all the stations were working.
Based on these relationships and the measurements at station 6, wind speeds at the other stations along the fetch were calculated.

3.7 Dimensionless Parameters

One of the basic assumptions of wind-wave research is that wind generated waves are "self similar". When expressed in non-dimensional form gravity waves of different magnitude will behave in a similar fashion. Much of the data analysis in the subsequent chapters will present data in terms of non-dimensional variables. The common variables to be introduced are defined in table 3.6.

Name	Dimensionless Quantity
Dimensionless Wave Height	$\Lambda = \frac{g H_s}{U^2}$
Dimensionless Frequency	$\nu = \frac{f_p U}{g}$
Dimensionless Fetch	$\chi = \frac{g F}{U^2}$
Dimensionless Energy	$\varepsilon = \frac{g^2 E}{U^4}$
Dimensionless Depth	$\delta = \frac{g d}{U^2}$

Table 3.6 Dimensionless form of several quantities. g = 9.81 m/s^2, U is the wind speed (either U_{10}, U_*, $U_{1/\lambda}$, or any other U) , H_s is the significant wave height (either $H_{1/3}$ or H_{mo}), f_p is the peak frequency, F is the fetch, E is the energy of the waves, and d the depth of the water.

4. Growth Curves for Shallow Water

4.1 Introduction to the Depth and Fetch-limited Growth of Waves in Finite Depth Water

One of the major objectives of the Lake George experiment was to determine growth curves for fetch limited waves in finite depth water. As described in the previous chapters, wave and wind measuring stations were placed along the longest axis of the lake to measure the wave and wind characteristics. As this took place over long periods of time, there is a significant amount of data including some extreme events.

This chapter mainly deals with determination of growth curves for depth-limited and fetch-limited finite depth water waves. First, an overview of existing knowledge and observations for wave growth is given. Thereafter the section splits into two parts:

- First the maximum wave height in finite depth water is discussed. In this section the data selection at Lake George is discussed. Then the derived depth-limited asymptote will be given. Finally a comparison is provided between the Lake George data and data from other experiments.
- In the second part of this chapter, the fetch-limited growth of the waves in finite depth water will be discussed. Again firstly the data selection is presented. Thereafter, proposed growth curves are presented. A thorough error analysis is included at the end of this section.

4.2 Wave Growth

4.2.1 The Physics of Wind Wave Evolution

Even in deep water, a comprehensive understanding of the physical mechanisms responsible for the wind wave evolution is not available. A reasonable description can however be formed in terms of the action-balance or radiative transfer equation (Hasselmann *et al.* 1973).

For constant depth, fetch limited conditions this becomes

$$C_g \cos\theta \frac{\delta E}{\delta F} = S \qquad \textbf{(4.1)}$$

where C_g is the group velocity, θ the wind direction, E the directional (two-dimensional) wave spectrum, F the fetch and S a source/sink term representing all processes which add, subtract or transfer energy to/within the spectrum.

Two first order, S is often represented as the summation of a series of separate processes

$$S = S_{in} + S_{nl} + S_{ds} + S_{bf} \qquad \textbf{(4.2)}$$

where

S_{in} = atmospheric input from the wind

S_{nl} = nonlinear interactions within the spectrum

S_{ds} = dissipation due to white-capping

S_{bf} = dissipation at the bottom (bottom friction, percolation etc.)

The present experiments are not aimed directly at determination of S but at defining the left hand side of equation 4.2. That is, the experiment is aimed at the determination of

$$E = E(f, \theta, F) \qquad \textbf{(4.3)}$$

4.2.2 Previous observations of wave growth in finite depth water

Thijsse (1949) performed the first study of finite depth wave evolution. In his article he refers to the diagram made by Sverdrup and Munk (1946) for deep water. Thijsse (1949) argues that as the waves grow, bottom friction increases in finite depth waters and at a certain stage the energy of the wind input and the energy lost due to bottom friction are counterbalanced. The waves will be in a state of equilibrium. Thijsse (1949) based these assumption not on theory but on the results of observations which the Hydraulic Laboratory at Delft (now called Delft Hydraulics) had at its disposal. These observations included both field and laboratory data.

The first major field experiment to investigate the growth of waves in finite depth water was conducted by CERC (the U.S. Army Corps of Engineers 1955 and Bretschneider 1958) in Lake Okeechobee (Florida, USA). This experiment consisted of only one measurement station and was aimed at establishing the maximum wave height in shallow water rather than investigating the growth of waves along the fetch. Bretschneider (1958) used the data from Lake Okeechobee to develop depth-limits to growth. He used the wind speed at 10 metres as the scaling wind speed for the growth curves, yielding

$$\varepsilon = 1.4 \times 10^{-3} \delta^{1.5} \qquad \textbf{(4.4)}$$

$$\nu = 0.16 \ \delta^{-0.375} \qquad \textbf{(4.5)}$$

Where ε is the dimensionless energy, ν the dimensionless frequency and δ the dimensionless depth. (see table 3.6 for the definition of the dimensionless quantities)

As an upper limit the integrated spectrum of Pierson Moskowitz (1964) was used, where the dimensionless wave energy is equal to

$$\varepsilon = 3.54 \times 10^{-3} \qquad \textbf{(4.6)}$$

Ijima and Tang (1966) used the above equations in a computer model as they were of the opinion that "numerical analysis will be more expedient than graphical operations". Their model incorporated both deep and shallow water equations to hindcast wave conditions. They developed a set of growth curves for both ε and ν.

Vincent (1985) used a full spectral approach. He states in his paper that the characteristics of wind seas propagating into shallow water appear to be fundamentally different from monochromatic waves. He used the shape of the spectrum to determine the total energy (E) of the waves. Vincent (1985) used Phillips' (1958) spectrum modified by Kitaigordskii *et al.* (1975) for his analytical solution

$$E_m(f,d) = E_m(f) \cdot \Phi(2\pi f,d) = \alpha g^2 f^{-5} (2\pi)^{-4} \cdot \Phi(2\pi f,d) \qquad \textbf{(4.7)}$$

in which $E_m(f)$ is the deep water Phillips' spectral form. Kitaigordskii *et al.*(1975) suggest that α is 0.0081. Adopting linear wave theory $\Phi(2\pi f,d)$ can be given as

$$\Phi(2\pi f,d) = \left[R(\omega_d) \right]^2 \cdot \left\{ 1 + \frac{2\omega_d^2 \; R(\omega_d)}{\sinh\left[2\omega_d^2 \; R(\omega_d) \right]} \right\}^{-1} \qquad \textbf{(4.8)}$$

where

$$\omega_d = 2\pi f \left(\frac{d}{g} \right)^{\frac{1}{2}} \qquad \textbf{(4.9)}$$

and

$$R(\omega_d) \tanh\left[\omega_d^2 \; R(\omega_d) \right] = 1 \qquad \textbf{(4.10)}$$

Another solution for $\Phi(2\pi f,d)$ in a simplified form has been proposed by Thompson and Vincent (1983)

$$\begin{aligned} &for\ \omega_d \le 1 \qquad \Phi(2\pi f,d) = \frac{1}{2}\omega_d^2 \\ &for\ \omega_d > 1 \qquad \Phi(2\pi f,d) = 1 + \frac{1}{2}(2 - \omega_d)^2 \end{aligned} \tag{4.11}$$

Vincent (1985) used this to integrate the spectrum from high frequencies to a low frequency cutoff (f_c).

$$E = \int_{f_c}^{\infty} \alpha g^2 f^{-5} (2\pi)^{-4}.\ \Phi(2\pi f,d)\ df \tag{4.12}$$

Vincent and Hughes (1985) used the TMA spectrum described by Bouws *et al.* (1985) for further analyses. The TMA spectrum is similar to the JONSWAP (Hasselmann *et al.* 1973) spectrum but with the inclusion of the Kitaigordskii *et al.*(1975) modifications.

$$F(f) = \alpha g^2 f^{-5} (2\pi)^{-4}\ e^{\frac{-5}{4}\left(\frac{f}{f_p}\right)^{-4}}\ \gamma^{\exp\left[\frac{(f_p - f)^2}{2\sigma^2 f_p^2}\right]}\ \Phi(2\pi f,d) \tag{4.13}$$

Bouws *et al.* (1985) fitted the TMA spectrum to a large number of spectra and found a relation for α and γ. With $\sigma = 0.07$ for $f \le f_p$ and $\sigma = 0.09$ for $f > f_p$.

$$\left.\begin{aligned} \alpha &= 0.0078\ \kappa^{0.49} \\ \gamma &= 2.47\ \kappa^{0.39} \end{aligned}\right\} \qquad \kappa = \frac{U_{10}^2\ k_p}{g} \tag{4.14}$$

where k_p is the peak wave number and U_{10} the wind speed at 10 metres above the sea surface. As the wave frequency is decreased in finite depth water, a point is eventually reached where the waves become non-dispersive. Waves with a frequency lower than this frequency will propagate at the same group velocity $C_g = \sqrt{(gd)}$. Vincent and Hughes (1985) proposed that the shallow water limit to wave growth should be determined approximately by the frequency where the shallow water dispersion relationship holds. To account for the continual shift of energy by nonlinear processes, a

slightly lower value was adopted for f_p as shown

$$2\pi f_p \left(\frac{d}{g}\right)^{\frac{1}{2}} = 0.9 \qquad \textbf{(4.15)}$$

Bouws (1986) conducted a single point wave measurement in Lake Marken (The Netherlands). This type of experiment has the disadvantage that the fetch only differs when the wind blows from a different direction. Although the fetch may differ in length so do many other factors which could influence the growth of the waves. Another disadvantage is that although the dimensionless fetch (χ) differs with wind speed so does the dimensionless depth (δ) (see table 3.6). Hence, only a relatively narrow range of the non-dimensional variables will be explored by such an experiment. Bouws (1986) used the friction velocity of the wind (U_*) as the scaling wind speed, claiming it reduced the scatter in the data. He claims that he found a close agreement with the Bretschneider (1958) growth curves in the Shore Protection Manual CERC (1977).

In the revised Shore Protection Manual CERC (1984) the results of the JONSWAP (Hasselmann *et al.* 1973) experiment were taken into account.

$$\varepsilon = 1.6 \times 10^{-2}\, \chi \qquad \textbf{(4.16)}$$

This ensured that the deep water results from the Shore Protection Manual CERC (1984) (see equation 4.17) were consistent with the deep water results from JONSWAP (Hasselmann *et al.* 1973).

$$E(f) = \alpha g^2 (2\pi)^{-4} f^{-5} e^{\frac{-5}{4}\left(\frac{f}{f_p}\right)^{-4}} \gamma^{\exp\left[\frac{(f_p - f)^2}{2\sigma^2 f_p^2}\right]} \qquad \textbf{(4.17)}$$

The dimensionless energy (ε) becomes

$$\varepsilon = 5\times10^{-3}\left[\tanh\left(0.53\ \delta^{3/4}\right)\tanh\left(\frac{5.65\times10^{-3}\ \chi^{1/2}}{\tanh\left(0.53\ \delta^{3/4}\right)}\right)\right]^2 \qquad \textbf{(4.18)}$$

It should be noted that this relationship is constrained to agree with the asymptotes of equations (4.4) and (4.6) for large χ and JONSWAP(1973) for small χ (equation 4.16). The transition between these limits is defined by the "tanh" function. No experimental data were available to confirm the validity of this transitional curve.

These are the most widely used fetch limited wave prediction equations. There is no clear evidence in the literature as to which is the preferable parameter for the wind. Battjes *et al.* (1987) and Kahma and Calkoen (1992) have attempted to explain the discrepancies, but at this point it remains debatable as to which wind speed should be used.

4.2.3 Previous observations for the maximum wave height in finite depth water

A number of methods have been proposed for the prediction of the maximum wave height in shallow water. Some methods use a monochromatic approach, others have a simple depth limitation, while again others present spectral solutions. Most methods can be reduced to a simple depth limitation. The formulations for maximum wave height given here are limited to flat bottoms. For sloping and rapidly changing bottom topography other processes play important roles and should not be neglected.

A simple solution method using monochromatic waves was proposed by Miche (1944)

$$H_{\max} = 0.14\ L\ \tanh\ \frac{2\pi d}{L} \qquad \textbf{(4.19)}$$

in which H_{max} is the maximum wave height, L the wave length and d the water depth. For shallow water this becomes $H_{max} = 0.88\ d$. The solitary wave theory gives a breaking limit of $H_{max} = 0.78\ d$ in shallow water. Nelson (1994), who based his conclusions on an extensive data set, claims that the maximum wave height in very flat regions is only $H_{max} = 0.55\ d$.

Another method of calculating the wave height in shallow water is to take each

component of the spectrum and model it as a monochromatic wave (Wang and Yang, 1977).

Vincent (1985) used the shape of the spectrum to determine the total energy (E) of the waves. From this he finds the wave height

$$H_{mo} = 4\sqrt{E} \tag{4.20}$$

Hence, using Vincent (1985) equation 4.12 and 4.8, H_{mo} can be determined as

$$H_{mo} = \frac{1}{\pi}(\alpha g d)^{1/2} f_c^{-1} \tag{4.21}$$

Thus, the relation between the wave height and the water depth is $H_{mo} \propto d^{0.5}$. As the low frequency face of the wind wave spectrum is typically very steep, the cutoff frequency (f_c) is assumed to be only slightly less than the peak frequency (f_p) (ie. $f_c = 0.9 f_p$).

Adopting equations 4.14, 4.15 and 4.21 and expressing this in dimensionless wave height (Λ) yields

$$\Lambda = \frac{g H_{mo}}{U_{10}^2} = 0.210 \left(\frac{g d}{U_{10}^2} \right)^{\frac{3}{4}} \tag{4.22}$$

Based on observations in Lake Okeechobee, Bretschneider (1958) found, the not dissimilar limit

$$\Lambda = 0.238 \tanh \left[0.53 \left(\frac{g d}{U^2} \right)^{\frac{3}{4}} \right] \tag{4.23}$$

Note, although not stated in the original paper it is assumed that $U = U_{10}$ in the above

equation. At large values of d, equation 4.23 approaches a maximum value of $\Lambda = 0.238$. Integrating the Pierson Moskowitz (1964) spectrum yields a limit of $\Lambda = 0.2433$, in good agreement with Bretschneider (1958). Equations 4.22 and 4.23 for Λ both indicate $H_{mo} \propto d^{0.75}$.

The data from Lake Okeechobee presented in Vincent (1985) and Vincent and Hughes (1985) are presented in a similar graph to figure 4.1. It can be noted that there is no clear proof for the upper limit of Λ in these data. Both lines with the exponents 0.5 and 0.75 seem to fit the data reasonably well. However neither of the two lies on "top" of the data, therefore indicating a clear upper limit for Λ.

As stated, in the revised Shore Protection Manual CERC (1984) the results of the JONSWAP (Hasselmann *et al.* 1973) experiment were taken into account. For the dimensionless significant wave height (Λ) and dimensionless peak frequency (ν) this resulted in the following relationships,

$$\Lambda = 0.238 \tanh\left(0.53\ \delta^{3/4}\right) \tanh\left(\frac{5.65\times10^{-3}\ \chi^{1/2}}{\tanh\left(0.53\ \delta^{3/4}\right)}\right) \qquad \textbf{(4.24)}$$

$$\nu = 0.133 \left[\tanh\left(0.833\ \delta^{3/8}\right) \tanh\left(\frac{3.79\times10^{-2}\ \chi^{1/3}}{\tanh\left(0.833\ \delta^{3/8}\right)}\right)\right]^{-1} \qquad \textbf{(4.25)}$$

Note that (4.24)is equivalent to (4.18), although expressed in terms of Λ rather than ε.

4.3 Depth-Limited Wave Growth

4.3.1 Data selection for depth-limited growth

In the following analysis all the data collected from March 1992 to October 1993 are used. These data consist of winds blowing from all directions. Despite the quality

control methods described previously, occasionally erroneous data still entered the database. These isolated occurrences were removed from the extensive database by application of the simple empirical limit

$$H_s < 0.2 + 0.033\ U_{10} \qquad \textbf{(4.26)}$$

where H_s has the units of (m) and U_{10} units of (m/s). Equation 4.26 enabled the removal of clear data errors whilst leaving plausible data unaffected. In addition, only wind speeds greater than 3 m/s were automatically retained. For wind speeds less than 3 m/s, the wind was often quite variable in both speed and direction. Therefore, considerable caution needs to be exercised in the use of these low wind speed data. Such data were examined manually before inclusion in the database. For all wind speeds lower than 3 m/s, both the wind speed and direction for the interval from eight hours before the time under consideration to four hours after were inspected. From these periods steady state wind records were manually selected. There were 18,791 cases of wind speeds smaller than 3 m/s examined. The final data set consisted of 48,339 points with wind speeds greater than 3 m/s and only 58 points with wind speeds between 0 and 3 m/s (see fig 4.2).

4.3.2 Depth-limited growth for the Lake George data

Figure 4.2 shows a plot of the non-dimensional wave height (Λ) against non-dimensional water depth (δ). The wind speed (U_{10}), measured at Station 6, and the water depth (d), measured at Station 5, were used to make the variables non-dimensional.

The data comes from a wide range of non-dimensional fetches and hence there is large scatter. There does however, seem to be a clear upper limit to the growth (depth limited state). Because of the automatic data selection that excludes wind speeds less than 3 m/s there are almost no data with dimensionless depth (δ) greater than 2. For winds with speeds smaller than 3 m/s, a period of eight hours before and four hours after, were examined. Only if the wind was constant (both in speed and direction) over that period

of time were the records used in the analyses. These data are also shown in figure 4.2 An edge enhancement technique was used to accurately define the depth limit to growth shown in figure 4.27 and a least squares power law fitted. This yielded the result

$$\Lambda = 0.13\ \delta^{0.65} \qquad \textbf{(4.27)}$$

Equation 4.27 defines an upper limit to growth where the waves are completely defined by δ. This result can also be expressed in terms of non-dimensional energy (ε) (fig 4.3).

$$\varepsilon = 1.06 \times 10^{-3}\ \delta^{1.3} \qquad \textbf{(4.28)}$$

Fig 4.4 shows the non-dimensional peak frequency, ν as a function of δ. Again, a clear limit to growth exists, which can be approximated by the relationship

$$\nu = 0.20\ \delta^{-0.375} \qquad \textbf{(4.29)}$$

Examination of the data at large values of δ, indicates that an upper limit to the value of the non-dimensional wave height also exits.

4.3.3 Comparison between lake data and previous proposals

The present data set spans a considerably wider range of δ than the limited previous observational data. It is however, interesting to compare these results with previous proposals. The Vincent and Hughes theoretical (1985) result (equation 4.22) lies above all the present data (fig 4.2) and nearly above all the Lake Okeechobee data. Bretschneider's (1985) empirical result (equation 4.23) is a better fit than the Vincent and Hughes (1985) result, to both the Lake Okeechobee data and to the Lake George data. However, at the lower dimensionless depth (δ) it seems to have a lower dimensionless wave height (Λ), and at the higher dimensionless depths (δ) it has a higher dimensionless wave height (Λ) than the present data. Bretschneider's (1985) empirical result doesn't fit the Lake Okeechobee data at the lower dimensionless wave height (Λ). It therefore seems that the slope of the Bretschneider solution is too steep.

Data at large values of δ are shown in figure 4.5 . Like Bretschneider's (1958) curve, the

data asymptotes close to the Pierson Moskowitz limit (dimensionless wave height (Λ) = 0.238), although slightly higher. Because of the limited number of data points in this area, it is hard to make an accurate judgement of the precise value of the asymptote, but there is a clear indication of an upper limit consistent with the Pierson-Moskowitz value.

4.3.4 Error analysis of the depth-limited growth curves

4.3.4.1 Spurious correlations for the fetch-limited growth

As the wind speed, U_{10} appears in all the non-dimensional quantities, care must be exercised to ensure that apparent correlations between quantities are not the result of fluctuations in U_{10} (Kahma and Calkoen 1972).

Spurious relations which might result from this source are given in table 4.1. The two spurious relationships that have to be investigated here are the relationships between the dimensionless depth (δ) versus dimensionless energy (ε), and versus dimensionless frequency (ν).

Spurious Relationships for the Growth curves		
	Dimensionless Energy versus Dimensionless Depth	Dimensionless Frequency versus Dimensionless Depth
Spurious relationship	$\varepsilon \equiv \frac{E}{d^2}\,\delta^2$	$\nu \equiv f_p \left(\frac{d}{g}\right)^{1/2} \delta^{-1/2}$
Derived relationship	$\varepsilon \propto \delta^{1.3}$	$\nu \propto \delta^{-0.375}$
Exponents ratio	1.5	1.3
Multiplier range	$10^{-4} \rightarrow 10^{-2}$	$10^{-1} \rightarrow 1$

Table 4.1 Spurious relationships between the dimensionless depth (δ) and both the dimensionless energy (ε) and the dimensionless frequency (ν).

The exponent of δ in equation 4.28 for the growth of ε is 1.3 both in deep water and in shallow water. The exponent of the spurious relationship is 2. Therefore the exponential ratio between the derived equation and the spurious relationship differs by a factor of 1.5. This is a good indication that the derived equation is genuine and not a spurious relationship. The multiplier range of the relationship also spans two orders of magnitude. Therefore it can be concluded that the relationship in equation 4.28 for the growth of ε is genuine and not one caused by a spurious relationship.

For ν a similar reasoning can be followed. The exponents of the spurious relationship and equation 4.29 are not greatly dis-similar with a ratio of 1.3. This relationship is not necessarily spurious, however the ratio of the exponents is close to 1 and therefore caution must be exercised. The multiplier range does, however, vary by an order of magnitude. This means that the influence of spurious correlations will be relatively small.

4.3.5 Conclusions of depth-limited growth in finite depth water

The data from Lake George indicates an upper limit to the dimensionless wave height (Λ) as a function of dimensionless depth (δ). There are little data to determine with great accuracy the upper limit of the dimensionless wave height (Λ) for large dimensionless depth (δ), but the available data tend to indicate a limit slightly greater than the Pierson-Moskowitz value.

The relationship between dimensionless wave height (Λ) and dimensionless depth (δ) yields a result only slightly different to previous experiments. The best fit for the Lake George data was,

$$\Lambda = 0.13\ \delta^{0.65} \tag{4.30}$$

or expressed in dimensionless energy (ε).

$$\varepsilon = 1.06 \times 10^{-3}\ \delta^{1.3} \tag{4.31}$$

For dimensionless frequency (ν) the data yields,

$$\nu = 0.20\ \delta^{-0.375} \tag{4.32}$$

The Lake Okeechobee data generally agrees with the Lake George data, although it has more outliers. In summary, the Lake George data are consistent with the limited existing data but more clearly define the depth limitations to growth.

4.4 Fetch Limited Wave Growth in Finite Water Depth

4.4.1 Data selection for fetch-limited growth

A description of the data selection process has already been given in some detail in section 3. Only the North-South data were selected for the fetch-limited analysis with very stringent data control. The wind had to be constant not only in speed and direction during the measurement period but also in the periods before and after the measurement.

This ensured that no data were included that did not correspond to constant wind, fetch-limited conditions. In all, nearly 1000 spectra have been analysed for the North-South winds. No wind speed less than 4 m/s was considered, as at very low wind speeds the winds tended to vary significantly in direction.

The wind speeds ranged from 4 to 15.2 m/s, the dimensionless depth (δ) ranged from 0.08 to 1.2, the dimensionless fetch (χ) from 40 to 10,000 and the depth parameter ($k_p d$) from 1.6 to over 6. The last parameter is a good indication of whether the waves are in shallow water, transitional depth or deep water. The present data set is mainly from transitional to deep water.

For verification of the analysis the East-West data (perpendicular to the array) will also be used. Only data from Station 6 were used for this purpose. The data were further restricted to cases where the wind speed was constant in magnitude and direction, above 4 m/s and within 10° of perpendicular to the shore line. For the North-South data, the wind speed averaged over the down wind fetch, and measured at a height of 10 metres was used as the scaling wind speed. The wind speed variation along the fetch was determined from the recommendations of Taylor and Lee (1984) (see section 3.6). As there was no "along fetch" information, no similar correction was made to the east-west data. On the western side of the lake there was a small hill that would have had some influenced on the wind for the east-west cases. Another deficiency of these data is that it is for a single point measurement with a fixed fetch of 5 kilometres. Therefore as the data is not completely reliable and spans a limited range of χ and δ, it is only used to verify the higher quality North-South data.

4.4.2 Growth parameter fitting for fetch-limited growth in finite depth water

The data which were used are shown in figures 4.6 and 4.7. For the analysis the non-dimensional energy (ε) is used instead of the non-dimensional significant wave height (Λ). In figures 4.6 and 4.7 the data are split up into 4 dimensional depth (δ) sections for clarity.

A generalised form of the Bretscheinder (1958) relationship was used to model the data. As can been seen from figures 4.6 and 4.7 the deep water limit proposed by Hasselmann *et al.* (1973) for the energy (equation 4.33) and the deep water limit proposed by Kahma and Calkoen (1992) for the peak frequency (equation 4.34) are consistent with the data.

$$\varepsilon = 1.6\times10^{-7}\chi \tag{4.33}$$

$$\nu = 2.18\,\chi^{-0.27} \tag{4.34}$$

These relationships provide a short fetch/large water depth asymptote. For the upper limit (when χ is very large) there is a maximum to which the waves can grow. This is given in section 4.3.2. Equation 4.28 and 4.29 give both the maximum dimensionless energy and the minimum dimensionless peak frequency. Both are repeated here for the readers convenience.

$$\varepsilon = 1.06\times10^{-3}\,\delta^{1.3} \tag{4.35}$$

$$\nu = 0.20\,\delta^{-0.375} \tag{4.36}$$

With these four limits, a generalised form of Bretscheinder's (1958) result can be written as:

$$\varepsilon = 3.64\times10^{-3}\left(\tanh A_1 \tanh\left(\frac{B_1}{\tanh A_1}\right)\right)^n \tag{4.37}$$

$$A_1 = 0.292^{1/n}\,\delta^{1.3/n}$$

$$B_1 = (4.396\times10^{-5})^{1/n}\,\chi^{1/n}$$

for the dimensionless energy and

$$\nu = 0.133 \left(\tanh A_2 \tanh \left(\frac{B_2}{\tanh A_2} \right) \right)^m \tag{4.38}$$

$$A_2 = 1.505^{1/m} \delta^{-0.375/m}$$

$$B_2 = 16.391^{1/m} \chi^{-0.27/m}$$

for the dimensionless peak frequency.

A least squares method was used to determine "*m*" and "*n*." This resulted in n = 1.74 and m = -0.37. With these values, equations 4.37 and 4.38 become

$$\varepsilon = 3.64\times10^{-3} \left[\tanh\left(0.493\ \delta^{3/4}\right) \tanh \left(\frac{3.13\times10^{-3}\ \chi^{0.57}}{\tanh\left(0.493\ \delta^{3/4}\right)} \right) \right]^{1.74} \tag{4.39}$$

$$\nu = 0.133 \left[\tanh\left(0.331\ \delta^{1.01}\right) \tanh \left(\frac{5.215\times10^{-4}\ \chi^{0.73}}{\tanh\left(0.331\ \delta^{1.01}\right)} \right) \right]^{-0.37} \tag{4.40}$$

These curves are displayed in figures 4.6 and 4.7. Note there is still some scatter in the data. The above data were from a situation where the lake was long and narrow. To ensure that the data were not influenced greatly by the shape of the lake, the East-West data were examined. The selection and shortcomings of these data have been explained in section 4.4.1 . The results shown in figure 4.6 and 4.7 and indicate that the lake geometry had no measurable influence on the results.

Growth relationships for ε and ν as a function of χ and δ are shown in figures 4.8 and 4.9

4.4.3 Error analysis of the fetch-limited growth curves

4.4.3.1 Monte Carlo simulations

The results in figures 4.6 and 4.7 do show some scatter in the data. The question arises as to whether the scatter is the result of measuring errors, analysis methods, inadequate theory (more or even different variables involved such as air-water temperature, stability of the atmosphere etc.) or the influence of spurious correlations or instrument errors.

To investigate the magnitude of the observed scatter, a Monte Carlo analysis was undertaken to determine the confidence limits for the collected data. Each measured quantity was considered as a stochastic variable with a known probability distribution. The four variables that were investigated are wind speed, fetch length, energy of the waves and peak frequency.

The wind speed was measured at a sampling interval of 1.25 seconds, therefore each 30 minute value is the average of many readings (over 1000 samples per sampling session). Both the mean (U_{10}) and the standard deviation (σ_u) can be determined from the recorded data. Following Walpole and Myers (1972) or van Soest (1983), the probability distribution of the mean will follow a normal distribution with a standard deviation (σ_{u10}).

$$\sigma_{u_{10}} = \sqrt{\frac{\sigma_u^2}{N}} \tag{4.41}$$

where N is the number of samples used to form the mean (N large).

Determining the fetch length between the wave measurement stations involved little error. However, determining the fetch length from shore to the first station involved potential error. The northern and southern shorelines were fringed with grass which complicated the determination of the exact location of the boundary. In addition, wind setup during strong winds and seasonal fluctuations in the mean lake level could result

in considerable movement of the effective shoreline. Hence, a precise determination of the position of the shoreline was not possible. An estimate of the error was made on site. It was assumed that the error was normally distributed with a standard deviation (σ_f) of 300 metres.

The total energy (E) of the waves was calculated from the raw wave samples by integrating the variance spectrum $F(f)$, where f is the frequency. Note, often the variance spectrum $F(f)$ is also called the energy spectrum. The significant wave height (H_s) was calculated from the total energy of the spectrum

$$H_s = 4 \left[\int F(f)\, df \right]^{\frac{1}{2}} \tag{4.42}$$

Due to sampling variability, the significant wave height (H_s) follows a chi-squared distribution (χ_α) with α_f degrees of freedom (Young 1986), where α_f is defined as

$$\alpha_f = \frac{n\left(\int F(f)\, df \right)^2}{\int \left(F(f) \right)^2 df} \tag{4.43}$$

and n is the number of degrees of freedom in the spectral estimate, which in this case was 112.

The last variable is the peak frequency (f_p). Like the significant wave height (H_s) it was determined from the variance spectrum $F(f)$ using Young's (1995) (see section 2.5.3 equation 2.1) weighted method. The probability function for f_p as defined by Young (1995) depends on the spectral shape $F(f)$, the discrete frequency interval (Δf) used in the spectrum, and the number of degrees of freedom in the spectral estimate (n)

A large number of simulated measurements (10,000 each) were computed for each individual measured variable described above. Each variable following its respective

probability distribution around the mean. These values were then randomly multiplied to obtain the non-dimensional quantities. The output is an unknown distribution due to the nonlinear products. The values were then sorted in magnitude and the 2.5 and 97.5 percentile value selected to define the 95% confidence limits. The results can be seen in figures 4.10 and 4.11 The length of the "crosses" represent the confidence limits. The results show that the uncertainty in the variables can account for most of the scatter. Note that the dimensionless depth (δ) has not been included in this Monte Carlo simulation. The dimensionless depth (δ) in itself is also a statistical parameter which has not been taken into account. The statistical variability cannot, however, account for the fact that the measured values of non-dimensional wave height appear anomalously low at short fetch compared to previous deep water measurements. This result may be due to an incorrect specification of the wind velocity at the first station. As there was no anemometer at this site, the wind speed could not verified. Other factors such as the shore conditions or dimensionless depth (δ) could also play a more important role than assumed.

4.4.3.2 Spurious correlations for the fetch-limited growth

To ensure that the relationships that have been determined are not due to errors in the data, spurious relations must also be investigated. The two spurious relationships that have to be investigated here are the relationship between the dimensionless fetch (χ) versus dimensionless energy (ε), and the dimensionless fetch (χ) versus dimensionless frequency (ν).

Spurious Relationships for the Growth curves		
	Dimensionless Energy versus Dimensionless Fetch	Dimensionless Frequency versus Dimensionless Fetch
Spurious relationship	$\varepsilon \equiv \frac{E}{x^2}\chi^2$	$\nu \equiv f_p \left(\frac{x}{g}\right)^{1/2} \chi^{-1/2}$
Derived relationship	$\varepsilon \propto \chi^1 \rightarrow \varepsilon \propto \chi^0$	$\nu \propto \chi^{-0.27} \rightarrow \nu \propto \chi^0$
Exponents ratio	$2 \rightarrow \infty$	$1.9 \rightarrow \infty$
Multiplier range	$10^{-9} \rightarrow 10^{-11}$	$8 \rightarrow 20$

Table 4.2 Spurious relationships between the dimensionless fetch (χ) and both the dimensionless energy (ε) and the dimensionless frequency (ν) in relation to the growth curves analysis.

The exponent of χ in equation 4.39 for the growth of ε varies from 1 in deep water to 0 in shallow water. The exponent of the spurious relationship is 2. Therefore the ratio of exponents between the derived equation and the spurious relationship ranges from 2 to ∞. This alone is a good indication that the derived equation is genuine and not a spurious relationship. However, the multiplier range of the spurious relationship also spans two orders of magnitude. This indicates that the relationship represented by equation 4.39 for the growth of ε under fetch-limited conditions is not influenced by spurious correlations.

For the non-dimensional frequency ν a similar reasoning can be adopted. The derived equation 4.40 has nearly the same exponential ratio relationship as above, namely from 1.9 in deep water to ∞ in shallow water. Therefore again, with reasonable confidence, one can assume that the derived relationship is real and not obtained as the result of

spurious correlations.

4.4.4 Conclusions for fetch-limited growth in finite depth water

The measured growth rates of waves under fetch limited conditions are smaller than in deep water. Rather than there being a single relationship between ε and χ or ν and χ, a family of curves exists in each case. The family of curves occurs since the non-dimensional depth, δ represents an additional variable.

The Lake George data have accurately defined these growth relationships, which are consistent with the limited previous finite depth studies and with deep water observations. These results have been represented in terms of the relationships given by equations 4.39 and 4.40

5. One Dimensional Spectra

5.1 Introduction to One-Dimensional Spectra

The evolution of deep water one-dimensional spectra has been studied extensively (e.g. Hasselmann et al.1973). In contrast, few studies of spectra in finite depth situations exist (e.g. TMA, Bouws et al. 1985).

As a part of the Lake George Experiment, the evolution of the one-dimensional spectrum was measured as a function of fetch.

This chapter firstly provides an introduction to previous work and theories that have been developed. Some parts of the discussion will refer back to the chapter on "Growth Curves for Shallow Water" as some parts of the theory have been discussed there. Data selection and preparation are then discussed. Results of the fitting of the parameters for the one-dimensional spectra are also discussed, together with an error analysis.

5.1.1 Frequency spectra

The first detailed studies of the shape of the spectrum were conducted by Phillips (1958). Based on dimensional arguments, he proposed a form for the high frequency portion of the spectrum

$$F_p(f) = \alpha g^2 (2\pi)^{-4} f^{-5} \qquad \textbf{(5.1)}$$

where $F_p(f)$ is the energy at frequency (f) and α is a constant ($\alpha = 8 \times 10^{-3}$). Based on the theory of Phillips (1958) and Kitaigorodskii (1961), Pierson and Moskowitz (1964) proposed a form for the fully developed spectrum. Kitaigorodskii (1961) argued in his paper that the wave spectrum could be expressed in terms of four variables, namely the frequency of the wave (f), the friction velocity (U_*), the fetch (F), and the gravitational

acceleration (g). Pierson and Moskowitz (1964) assumed that the properties deduced from the friction velocity (U_*) would hold for the wind velocity (U) measured at a fixed reference height. They introduced the following spectrum for fully developed conditions.

$$F_{pm}(f) = \alpha g^2 (2\pi)^{-4} e^{\frac{-5}{4}\left(\frac{f}{f_p}\right)} f^{-5} \quad \textbf{(5.2)}$$

with $F_{pm}(f)$ being the Pierson Moskowitz spectrum, and f_p being the frequency of the spectral peak. Kitaigorodskii (1961) argued if $U_2 > U_1$ then for all frequencies the following must hold.

$$F(f, g, U_2) \geq F(f, g, U_1) \quad \textbf{(5.3)}$$

Although this holds true for the Pierson Moskowitz spectrum, due to the exponential factor, this is not strictly true for the JONSWAP spectrum with the added peak enhancement factor.

The Joint North Sea Wave Project (JONSWAP, Hasselmann *et al.* 1973) was a major experiment aimed at investigating the growth of waves in deep water. This experiment showed that wave-wave interactions play an important role in forming and stabilising the shape of the spectrum. Based on these measurements, Hasselmann *et al.* (1973) developed the so-called, JONSWAP spectral form

$$F(f) = \alpha g^2 (2\pi)^{-4} f^{-5} e^{\frac{-5}{4}\left(\frac{f}{f_p}\right)^{-4}} \gamma^{\exp\left[\frac{-(f-f_p)^2}{2\sigma^2 f_p^2}\right]} \quad \textbf{(5.4)}$$

where $\sigma = 0.07$ for $f \leq f_p$ and $\sigma = 0.09$ for $f > f_p$. Here α is a variable, unlike the Pierson Moskowitz (1958) spectrum. In the JONSWAP publication a best fit result for α and γ (the peak enhancement factor) was derived from the data,

$$\alpha = 0.0076\ \chi^{-0.22}$$
$$\gamma = 3.3 \qquad \textbf{(5.5)}$$

where χ is the dimensionless fetch. The peak frequency of the spectrum is calculated as

$$f_p = 3.5 \left(\frac{g}{U_{10}} \right) \chi^{-0.33} \qquad \textbf{(5.6)}$$

The JONSWAP form is well know and widely used. However, alternative relationships have been proposed for the parameters of both equations 5.2 and 5.4. For example, Mitsuyasu (1981) proposed the following relationship for the peak enhancement

$$\gamma = 7.0\ \chi^{-0.143} \qquad \textbf{(5.7)}$$

One of the things all the above spectral forms have in common is the decrease in energy at high frequencies proportional to f^{-5}. However, there are numerous authors who have proposed alternative forms (Toba 1973, Kitaigorodskii *et al.* 1975, Mitsuyasu *et al.* 1975, Forristall 1981, Kahma 1981, Donelan *et al.* 1985, Battjes *et al.* 1987 and Resio 1987). These authors suggested different exponential constants for the high frequency part of the spectrum. Their constants for the exponential decrease in the high frequency part range from -3.5 to -5. Donelan *et al.* (1985) proposed the following spectrum based on field data;

$$F(f) = \alpha g^2 (2\pi)^{-4} f^{-4} f_p^{-1} \exp\left[-\left(\frac{f}{f_p} \right)^{-4} \right] \gamma^{\exp\left[\frac{(f_p - f)^2}{2\sigma^2 f_p^2} \right]} \qquad \textbf{(5.8)}$$

This suggests a high frequency slope of f^{-4}. Donelan *et al.* (1985) and Donelan *et al.* (1992) avoided working with the fetch, which was difficult to determine for their data, by using the inverse wave age,

$$inverse\ wave\ age = \frac{U_{10}}{C_p} \tag{5.9}$$

where U_{10} is the wind speed measured at 10 metres above the water surface and C_p is the phase speed of the spectral peak. They claim that the use of the inverse wave age avoids inaccuracies introduced due to inhomogeneous winds over long fetches and changing winds due to the abrupt roughness change from land to water. They found that the inverse wave age scaled well against dimensionless energy

$$\varepsilon = 0.00274 \left(\frac{U_{10} \cos\theta}{c_p} \right) \tag{5.10}$$

where θ is the angle between the direction of the waves and the direction of the wind. Young and van Vledder (1993) suggest that non-linear interactions play an important role in stabilizing the high frequency part of the spectrum as Hasselmann *et al.* (1973) had speculated. Banner and Young (1994) confirm this, but also state that other processes such as atmospheric input and white-capping play a role in shaping the high frequency part of the spectrum.

5.1.2 Wave number spectra

As indicated above, there are few data sets for shallow water spectra. Kitaigorodskii (1962) and Kitaigorodskii *et al.* (1975) tried to derive a form for the spectrum for both deep and finite water depths. For this they used a wave number spectrum

$$F(k) = \frac{\alpha}{2} k^{-3} \Psi(k, f_p, d) \tag{5.11}$$

where $F(k)$ is the wave number spectrum, α is a depth independent constant, k is the wave number and $\Psi(k, f_p, d)$ is a non-dimensional shape function. $\Psi(k, f_p, d)$ approaches 1 for $k \gg k_p$. Using linear wave theory, equation 5.11 can be transformed to a

frequency spectrum with a variable high frequency exponent. Using JONSWAP (equation 4.17) this yields

$$F(f) = \alpha g^2 f^{-5} f_p^{-1} (2\pi)^{-4} e^{\left[\frac{-5}{4}\left(\frac{f}{f_p}\right)^{-4}\right]} \gamma^{\exp\left[\frac{-(f-f_p)^2}{2\sigma^2 f_p^2}\right]} \Phi \qquad \textbf{(5.12)}$$

where Φ is an extra shape function which is equal to

$$\Phi = \left\{ \frac{[k(f,d)]^{-3} \frac{\partial k(f,d)}{\partial f}}{[k(f,\infty)]^{-3} \frac{\partial k(f,\infty)}{\partial f}} \right\} \qquad \textbf{(5.13)}$$

The term Φ has been specified in detail in the chapter on Growth Curves for Shallow Water (section 4.2.2 equation 4.8). The result of transforming equation 5.11 into a frequency spectrum is that the exponent for the high frequency part of the spectrum varies from -3 in shallow water to -5 in deep water.

Bouws *et al.* (1985) suggested a new form which was based on data from three different experimental sites, Texel (Dutch North Sea), Marsen (German Bight) and Arsloe (east coast of the United States of America). They suggest that, although they mainly work in frequency space, a more appropriate form of the spectrum will be in wave number space which will hold for both deep water and shallow water. They use Kitaigorodskii *et al.* (1975) equation 5.11 as their base. They obtain an estimate of the energy by neglecting the shape factor (Φ) and integrating the spectrum,

$$E = \frac{\alpha}{2} \int_{k_p}^{\infty} k^{-3} \, dk \tag{5.14}$$

Which yields in non-dimensional form

$$\varepsilon = \frac{\alpha}{4} \kappa^{-2} \tag{5.15}$$

where ε is the dimensionless energy and κ is the non-dimensional wave number

$$\kappa = \frac{U_{10}^2 \, k_p}{g} \tag{5.16}$$

and k_p is the wave number corresponding to the peak frequency.

Bouws *et al.* (1987) concluded that the use of a frequency spectrum in finite depth water is not appropriate and suggest use of the wave number spectrum, which is applicable in both deep and shallow water. Despite adoption of the wave number form, Bouws *et al.* (1987) still had considerable scatter in their data for α, γ and σ.

Miller and Vincent (1990) expanded Kitaigorodskii's (1975) theory by using the general theory but changing the coefficients. They fitted data from the Corps of Engineers Field Research Facility to the model and concluded that an f^{-4} power law in deep water would be consistent with the observations. Rather than using k^{-3}, a $k^{-2.5}$ form of the wave number spectrum was used. Miller and Vincent (1990) transformed this into a frequency space (FRF) spectrum which they then used to determine the coefficients. They also found that by using a mean value for the coefficients α (=0.0029), and σ ($\sigma_a = 0.115$ and $\sigma_b = 0.114$) a direct relationship was found between the peak enhancement factor γ and the wave steepness ε_f .

$$\gamma = 3500\,\varepsilon_f^{1.39} \tag{5.17}$$

The wave steepness is given by

$$\varepsilon_f = \frac{H_{mo}}{4\,L_p} \tag{5.18}$$

where L_p is the wave length at the peak frequency.

5.2 Data Selection and Preparation for the One-Dimensional Spectra

In order to investigate the fetch limited development, the high quality North-South data set was used.

Although the wave measuring gauges were tested in the lab and gave a good frequency response (fig 5.1), *in situ* testing against resistance wave gauges showed poorer frequency response (see section 2.4.1). This was due to the fact that the high frequency waves were superimposed on lower frequency waves, thus increasing the slope of the high frequency components. This was not taken into account during the dynamic frequency response testing in the laboratory. To overcome the decrease in response with frequency, a transfer function was calculated. The transfer function was dependent on the peak frequency (f_p) and therefore expressed in terms of f/f_p (fig 5.2). The high frequency limit of the transfer function was taken at $5\,f_p$. A more detailed section on the transfer function is given in the description of the Lake George Experiment (section 2.4.1).

Figures 5.3 and 5.4 show typical examples of recorded spectra. The case shown is for a wind speed of U_{10} = 10.8 m/s (measured at Station 6). As mentioned earlier, the wind

speed increases along the fetch due to the development of the internal boundary layer. The increase in total spectral energy and the migration of the peak to lower frequencies with fetch are clear in these figures. The relatively fetch insensitive high frequency face of the approximate form f^{-n} is also clear.

For the analysis approximately 1000 spectra were selected that met the stringent selection criteria.

5.3 Analysis and Results of the One-Dimensional Spectra

5.3.1 High frequency tail of the spectrum

For this section of the analysis, only the high frequency part of the spectrum was taken into account ($f > 2f_p$). As stated in the previous paragraphs, there are three main thoughts on the slope of the high frequency part. All theories indicated the high frequency part of the spectrum should be of the form

$$F(f) \propto f^n \tag{5.19}$$

where n differs in the theories. In JONSWAP n is equal to -5, whereas Donelan has n equal to -4. Both theories have a constant n. The TMA spectral form (section 4.2.2, equation 4.13) has a variable n, which is dependent on water depth, d.

In order to assess the most appropriate value of n, a relationship of the form

$$F(f) = \beta f^n \tag{5.20}$$

was independently fitted (least squares) to each of the recorded spectra. There was no one value for n which would fit all spectra. In figure 5.5 the values of n are grouped by non-dimensional depth (δ). Only two ranges have been shown here for clarity. The ranges shown are $\delta = 0.1$ to 0.2 and $\delta = 0.5$ to 0.6 . At short non-dimensional fetches (χ) or high non-dimensional depths (δ), thus deep water, the coefficient n is approximately

equal to -5. However, as the non-dimensional fetch (χ) increases the magnitude of n decreases. As the fetch increases, the effects of the bottom are increasingly felt by the waves. The decrease in non-dimensional depth (δ) also decreases n. Again, the bottom effects seem to play a significant role, the deeper the water, the higher the coefficient n. This seems to indicate that n is not a constant, but a function of the water depth.

5.3.2 Spectral form

The above results suggest the spectral form is dependent on the water depth. In deep water (high non-dimensional depths, δ) the coefficient n seems to be equal to -5, which is consistent with the JONSWAP spectrum (section 5.1.1 equation 5.4). In very shallow water (low non-dimensional depths, δ) the coefficient n seems to approach -3. This result is not consistent with the deep water Donelan *et al.* (1985) form where n = -4. There is, however, considerable scatter within all data sets.

A generalized form of the wind-wave spectrum can be proposed as:

$$F(f) = \alpha g^2 (2\pi)^{-4} f_p^{-(5+n)} f^n \exp\left[\frac{n}{4}\left(\frac{f}{f_p}\right)^{-4}\right] \gamma^{\exp\left[\frac{-(f-f_p)^2}{2\sigma^2 f_p^2}\right]} \qquad \textbf{(5.21)}$$

Using n = -4 or -5 will give the Donelan or JONSWAP spectrum, respectively. For this investigation, equation 5.21 and the TMA spectrum (section 4.2.2 equation 4.13) were investigated.

5.3.3 Analysing the spectral parameters

There are several techniques which can be used to determine the parameters of the above spectral forms. A straight forward technique is to use a multi-parameter, non-linear least squares curve fitting technique (Press *et al.* 1986). This method determines all the parameters simultaneously. Other authors (Günther 1981, Battjes *et al.* 1987, Donelan *et al.* 1985.) have used methods in which the spectral parameters were fitted individually. In theory, both methods should yield the same results. In practice, both

noise and sampling variability are present, and the data are defined on a rather coarse spectral grid. To determine which method could most robustly produce the parameters, a Monte-Carlo simulation was applied. A TMA spectrum (section 4.2.2 equation 4.13) which was typical for the Lake George situation was specified. Each of the spectral bins, defining the spectrum, was allowed to vary around its mean while following a Chi-squared probability distribution with 112 degrees of freedom (section 2.5.3). In addition to this, the discrete frequency grid was allowed to vary Δf assuming a uniform distribution (Young 1995). A total of 10,000 simulations were computed.

The results of these Monte-Carlo simulations are shown in figures 5.6 and 5.7. The individually fitted parameters show some bias from the mean. The spectral parameter α is 3% too small, the spectral parameter γ is 12% too high, and the peak frequency is 3% too high. The results of the multi-parameter fitting however are not biased, and symmetrically distributed around the mean values. Therefore, the multi-parameter fitting technique was adopted for the analyses.

To determine how well each spectral form (equation 5.21 and 4.13) fitted the North-South data set, the following RMS error statistics were defined.

$$Er_1 = \left[\frac{1}{N} \sum_{i=1}^{N} \varepsilon_i^2 \right]^{1/2} \qquad \textbf{(5.22)}$$

$$Er_2 = \left[\frac{1}{(N - P + 1)} \sum_{1=p}^{N} \varepsilon_i^2 \right]^{1/2} \qquad \textbf{(5.23)}$$

where N is the number of spectral bands analysed and P the spectral band which contains the peak frequency (f_p). ε_i is defined as:

$$\varepsilon_i = \frac{F_i(fit) - F_i(data)}{F_i(data)} \qquad \textbf{(5.24)}$$

where F_i *(fit)* is the *i*'th spectral band of the fitted spectrum, and F_i *(data)* is the *i*'th spectral band of the measured spectrum. Er_1 gives an indication of how well the fitted spectrum corresponds to the original measured spectrum. The indication of how well the form of the tail of the spectrum agrees between the fitted spectrum and the original measured spectrum is given by Er_2. The results are given in the next paragraph.

5.3.4 The spectral parameters

The results of the 1000 spectra were averaged and the values for of Er_1 and Er_2 are shown in the table 5.1.

Errors in the fit between the measured spectra and fitted spectra		
	Er_1	Er_2
General form of JONSWAP	0.37	0.36
TMA	0.24	0.19

Table 5.1 Errors in the fit between the measured spectra and fitted spectra

Although the general form of the JONSWAP spectrum (equation 5.21) has one more free parameter *(n)* to fit, the error statistic (Er_1) indicates that the TMA spectrum (equation 4.13) is a better fit. Also the high frequency part of the spectrum is, according to the error statistic (Er_2), described better by the TMA spectrum (equation 4.13). This seems to indicate that a constant *n* in the description of the high frequency part of the spectrum is not appropriate. A variable *n*, such as in the TMA spectral form (equation 4.13), that is frequency dependent is more suitable. Therefore the TMA spectral form (equation 4.13) is a better approximation than the generalized form of the JONSWAP spectrum (equation 5.21).

Further support for using the TMA spectral form (equation 4.13) is given in figure 5.8 where the non-dimensional energy (ε) is given as a function of $\alpha\kappa^{-2}$. The quantities of α and κ are determined from the multi-parameter fit. A least squares fit to the data in figure 5.8 yields the result

$$\varepsilon = 0.14 \left(\alpha \kappa^{-2}\right)^{0.91} \quad \textbf{(5.25)}$$

which is quite close to equation 5.15 . Equation 5.15 is obtained by the integration of equation (5.14), the wave number spectrum proposed by Kitaigorodskii (1962) (in section 5.1.2). The above results tend to support the conclusion that the wave number spectrum is of the form

$$F(k) \propto k^{-3} \quad \textbf{(5.26)}$$

The transformation of equation 5.26 to a finite depth frequency spectrum is given by the TMA form (equation 4.13).

The dependence of the spectral parameters α , γ and σ on κ needs to be determined. These parameters have been plotted in figures 5.9, 5.10 and 5.11. As with previous deep water experiments, there is considerable scatter. Of the three parameters, the dependence on κ is clearest for α. The result of a least squares fit is:

$$\alpha = 0.0091 \, \kappa^{0.24} \quad \textbf{(5.27)}$$

Results for α from other studies, such as TMA (equation 4.13) and JONSWAP (equation 5.4), assuming the linear dispersion relationship is applicable, are respectively;

$$\begin{aligned} \alpha_{TMA} &= 0.0078 \, \kappa^{0.49} \\ \alpha_{JONSWAP} &= 0.01 \, \kappa^{0.33} \end{aligned} \quad \textbf{(5.28)}$$

These results are also shown in figure 5.9. Although there are differences, these relations all indicate that there is a trend toward decreasing values of α with increasing

maturity of the waves. This result has previously been observed in deep water situations, the present data set confirms the same trend in finite depth water.

The relations for γ and σ with κ are not as clear. Previous studies, such as TMA (equation 4.13) and JONSWAP (equation 4.17) yielded similar results. The mean values for the present data set are

$$\begin{aligned} \gamma_{mean} &= 2.70 \\ \sigma_{mean} &= 0.12 \end{aligned} \qquad \textbf{(5.29)}$$

5.3.5 The spectral peak enhancement factor

Integration of the TMA spectrum (equation 4.13) with the above mentioned parameters yields the total energy (E). The same results should be obtained by calculating E with the results of growth curves in chapter 4. In the mean, these two approaches are consistent. However, in some regions of the parameter space, discrepancies in the values of E exist. These discrepancies can be as high as 30%. The reason for these discrepancies can be explained in terms of the dependence of γ on κ. Adoption of a constant mean value for γ is insufficient to yield a self-consistent set of relationships. The variable κ may be dependent on other factors. The same applies for σ. The total E, however, does not differ significantly with changes in σ. Therefore, the 30% difference in E cannot be attributed to an incorrectly specified dependence of σ on κ.

To investigate the dependence of γ on other factors, the following technique was applied. For given values of non-dimensional fetch (χ) and non-dimensional depth (δ), the non-dimensional energy (ε) and non-dimensional peak frequency (ν) can be calculated via the growth curves presented in chapter 4. From these, via the linear dispersion relationship, the non-dimensional peak wave number (κ) can be calculated. The parameter α can be derived from equation 5.27 and for σ the mean value from equation 5.29 can be used. Then an iterative approach is used to determine the correct

value for γ so that ε agrees with the growth curves in section 4 . These results are shown in figure 5.12.

One of the things that is quite apparent in figure 5.12 is that with decreasing non-dimensional depth (δ) the peak-enhancement factor (γ) increases. The peak-enhancement factor (γ) also increases with an increase of the non-dimensional fetch (χ). Therefore the peak-enhancement factor (γ) is dependent on both the non-dimensional depth (δ) and the non-dimensional fetch (χ).

In deep-water the peak-enhancement factor (γ) is nearly equal to one. It then increases along the fetch until the waves become fully depth-limited. Once the waves reach the depth limited state, the peak-enhancement factor (γ) stays constant.

There were numerous occasions during the extended Lake George experiment when boating operations were required during very strong winds. On these occasions, it was clear that the waves were well "organised" with a clear dominant period. In addition, the waves were very steep. These observations are consistent with large values of γ under these strongly depth limited conditions. Indeed, these conditions made operation of small boats extremely uncomfortable and even sometimes dangerous (see section 2.2.1 on boating).

These results are apparently inconsistent with results from previous deep water studies. Hasselmann *et al.* (1973), using the JONSWAP data set, found a mean value of 3.3 for the peak-enhancement factor (γ). They used an average because they could find no consistent trend in their data set. Donelan *et al.* (1985) using equation 5.8 found that the peak-enhancement factor (γ) decreased along the fetch. In contrast, the present finite depth results indicate that (γ) increases with fetch.

The probable cause for this is the following. In the chapter 4 on growth curves, the non-dimensional energy (ε) relationship asymptotes to JONSWAP for deep water.

However the non-dimensional frequency (ν) asymptotes to the form proposed by Kahma and Calkoen (1992). If one lets the non-dimensional frequency (ν) asymptote to the JONSWAP limit the result for γ would be as shown in figure 5.13.

Here the deep-water limit decreases along the fetch as predicted by Donelan. However the results of Kahma and Calkoen (1992) fitted the present data set better than the JONSWAP limit. Even with the large data set available in this study, an authoritative statement on the behaviour of γ with χ cannot be made.

Figure 5.14 shows the peak-enhancement factor (γ) as a function of the non-dimensional depth (δ) when the waves are fully developed. This result is independent of the chosen deep water asymptotic form for ν, as a function of χ . There is a distinct decrease in the peak-enhancement factor (γ) with increasing non-dimensional depth (δ). A least squares fit gives the following depth limited result

$$\gamma_\delta = 1.1 - 5.8 \log_{10} \delta \qquad for \ 0.05 < \delta < 1 \tag{5.30}$$

Note, this is for fully depth limited cases only.

5.4 Error Analysis of the Results of the One-Dimensional Spectra

To determine if the scatter in the Lake George one-dimensional spectral data set is a result of the natural measurement variability or the result of unsuitable forms for the fitted spectral form, an investigation was setup to determine the natural scatter that could occur in the data set. This was done using a Monte-Carlo simulation similar to the one used to determine the most appropriate form of the spectrum. The TMA spectral form was adopted with the following parameters

$\alpha = 0.01$	$\sigma = 0.1$	$\gamma = 2.5$
$d = 1.8$ m	$f_p = 0.4$ Hz	$\Delta f = 0.031$ Hz

The resulting spectrum is considered as a statistical variable with each of the spectral ordinates following a Chi-squared probability distribution. To simulate the position relative to the spectral peak, the discrete frequency grid was allowed to vary by Δf following a uniform distribution. For each realization of the spectrum, a multi-parameter least squares fit (like the one in section 5.3.3) was used to determine the spectral parameters. A total of 10,000 spectra were produced and fitted.

The results indicated (section 5.3.3), that all parameters approximately followed a normal distribution, with the mean values close to those of the initial spectral shape. This shows that the fitting technique is not biased.

The 2.5 and 97.5 percentile values were determined and the resulting 95% confidence limits are shown in table 5.2

95% confidence limit of the Monte-Carlo simulation	
Parameter	Span of 95% Confidence Limit
α	± 13 %
f_p	± 2.5 %
γ	± 28 %
σ	± 44 %

Table 5.2 Confidence limits for the fitted spectral form obtained from the Monte-Carlo simulation.

As can be seen from table 5.2, determining the exact value of γ and σ is very difficult with significant spread about the mean values. Hence, the large scatter apparent for these parameters in the Lake George data set can be attributed to the difficulty of obtaining these parameters from discretely sampled data. Other processes, such as, variable wind speed and direction, uneven bottom, different depths, irregularities in the upwind shoreline, temperature difference and other atmospheric instabilities, may however, also contribute to the observed scatter.

5.5 Conclusions of the One-Dimensional Spectral Analysis

In this chapter, the shape of the spectrum has been investigated. The wave number spectral form of TMA (section 4.2.2, equation 4.13) provides a better approximation to the data than other forms investigated.

For the shape of the high frequency part of the spectrum the following main conclusions can be drawn. The exponent of the high frequency part of the spectrum is not a constant. The coefficient seems to vary between -3 in shallow water to -5 in deep water. Furthermore, the slope of the high frequency part of the spectrum steepens as a function of the frequency. This is explained since the higher frequencies are in "deep" water and the lower frequencies are in "shallower" water (in terms of kd).

For the TMA spectrum (section 4.2.2, equation 4.13) the spectral parameters α, γ and σ were investigated. It was found that α is a function of non-dimensional wave number (κ) (equation 5.27). For the peak enhancement factor (γ) no dependence on non-dimensional wave number (κ) was found. However there seems to be an indication that the peak enhancement factor (γ) could be dependent on other factors such as the non-dimensional fetch (χ) and/or the non-dimensional depth (δ). The data indicate that the peak enhancement factor (γ) increases with a decrease in non-dimensional depth (δ). This has been visually confirmed in Lake George. For the last factor, σ, no clear relationship was found with any other parameters. However, since changes in the value of σ make very little difference to the total energy of the spectrum, an average value of 0.12 can be used. Certainly for engineering purposes this is more than sufficient.

It is interesting to note that the Lake George data set has been measured in a lake with a cohesive mud bottom. Despite this, the results are similar to the TMA (Bouws *et al.* 1985) mobile bed results. This seems to indicate that bed friction might not play a significant role in finite depth fetch-limited growth. This is consistent with the results obtained in the chapter on growth curves (chapter 4).

6. Directional Wave Spectra

6.1 Introduction to the Two-Dimensional Spectra

Although many engineering problems are still solved with only significant wave height (H_s) and peak frequency (f_p), for more complex problems the complete spectrum is required. Although the one-dimensional spectrum often provides sufficient information, two-dimensional wave spectra are important for the calculation of transformation processes such as diffraction, refraction and reflection. Holthuijsen *et al.*(1992) and Verhagen *et al.*(1992) showed that knowledge of the directional spreading is very significant in engineering design. They modelled short and long crested waves entering a harbour/river entrance. The difference in the results between the short and long crested waves penetrating the harbour was profound. Other fields where directional spreading is important for engineering purposes are sediment transport, shore protection, and satellite surveillance. A good knowledge of the directional spreading is needed to calculate the nonlinear energy terms accurately (Dungey & Hui, 1979). Field measurements of two-dimensional spectra are more difficult (and more expensive) to make than measurements of one-dimensional spectra. For deep water there are a number of types of directional buoys that can be used. However, for finite depth water there are no readily available products or methods. This is in a way ironic since the greatest use of two-dimensional spectra is in finite depth waters. To date, no comprehensive data sets of fetch-limited, finite depth directional spectra have been published.

The following section reviews previous descriptions and theories on two-dimensional spectra. This is followed by a short section on data selection. Proposed models will then be fitted to the Lake George data set. Finally there will be a brief note on bimodal spreading of the directional spectrum.

The description of the array and the equipment used is given in chapter 2 (the directional array is described in section 2.6).

6.2 Representation of the Two-Dimensional Spectrum

Longuet-Higgins *et al.* (1963) introduced a directional spreading function

$$E(\omega,\theta) = E(\omega)\, D(\omega,\theta) \tag{6.1}$$

where $D(\omega,\theta)$ is the directional spreading function, $E(\omega,\theta)$ the directional spectrum, $E(\omega)$ the one-dimensional spectrum, ω the radian frequency and θ the wave direction. By definition

$$\int_{-\pi}^{\pi} D(\omega,\theta)\, d\theta = 1 \tag{6.2}$$

They suggested that the spreading function should be proportional to

$$\cos^{2s}\left(\frac{1}{2}\theta\right) \tag{6.3}$$

with s varying from 4 at low frequencies to 1 at higher frequencies. For completeness the translation from ω to f is as follows;

$$\omega = 2\pi f \quad and \quad \omega_p = 2\pi f_p \tag{6.4}$$

where f is the frequency in Hz, and ω_p and f_p the peak frequencies.
Mitsuyasu *et al.* (1975) used a cloverleaf buoy in which they could measure the vertical acceleration (η_{tt}), the slope in two directions (η_x, η_y), and the curvature in three directions ($\eta_{xx}, \eta_{yy}, \eta_{xy}$) of the water surface ($\eta(t,x,y)$). However, only the first three of these quantities were used in their analysis. The form of the spreading function they found was similar to Longuet-Higgins *et al.* (1963).

$$D(\omega,\theta) = Q(s)\, \cos^{2s}\left(\frac{\theta - \theta_m(\omega)}{2}\right) \tag{6.5}$$

where $Q(s)$ is a normalizing function to satisfy equation 6.2 . The parameter s was fitted by Mitsuyasu *et al.* (1975) to their data.

$$s = \begin{cases} s_p \left(\dfrac{\omega}{\omega_p} \right)^5 & for\ \omega < \omega_p \\ s_p \left(\dfrac{\omega}{\omega_p} \right)^{-2.5} & for\ \omega \geq \omega_p \end{cases} \tag{6.6}$$

and s_p is the value of s at the peak frequency (ω_p)

$$s_p = 11.5 \left(\frac{U_{10}}{C_p} \right)^{-2.5} \tag{6.7}$$

where C_p is the phase speed of the spectral peak

$$C_p = \frac{g}{\omega_p} \tag{6.8}$$

and g is the gravitational constant.

In this representation, the directional spreading is dependent on the inverse wave age in addition to ω/ω_p. Hasselmann *et al.*(1980) used the 1973 JONSWAP data. They argue that the directional spreading parameter s is more dependent on f/f_p than the inverse wave age (U_{10}/C_p). Young (1994), showed that for the data region covered by the data of Mitsuyasu *et al.* (1975), the spreading function is not very different from that of Hasselmann *et al.* (1980). Outside this region, however, the differences are quite significant. Hasselmann *et al.* (1980) developed the following representation

$$s = \begin{cases} 6.97 \left(\dfrac{\omega}{\omega_p} \right)^{4.06} & for\ \omega < 1.05\ \omega_p \\ 9.77 \left(\dfrac{\omega}{\omega_p} \right)^{\mu} & for\ \omega \geq 1.05\ \omega_p \end{cases} \tag{6.9}$$

where μ is

$$\mu = -\left\{ 2.33 + 1.45 \left(\frac{U_{10}}{C_p} - 1.17 \right) \right\} \qquad \textbf{(6.10)}$$

The dependence on the inverse wave age is considerably reduced compared to Mitsuyasu *et al.* (1975) .

The data measured and analysed by Donelan *et al.* (1985) did not seem to fit the cosine distribution well. Donelan *et al.* (1985) proposed a sech^2 distribution.

$$D(\omega,\theta) = 0.5\beta \; sech^2 \beta\left(\theta - \bar{\theta}(\omega)\right) \qquad \textbf{(6.11)}$$

with β

$$\begin{aligned} \beta &= 2.61\,(\omega/\omega_p)^{+1.3} && for \quad 0.56 < \omega/\omega_p < 0.95 \\ \beta &= 2.28\,(\omega/\omega_p)^{-1.3} && for \quad 0.95 < \omega/\omega_p < 1.6 \\ \beta &= 1.24 && for \quad \omega/\omega_p > 1.6 \end{aligned} \qquad \textbf{(6.12)}$$

Note that in equation 6.12 there is no dependence on the inverse wave age. Donelan *et al.* (1985) could find no evidence of any relationship between the inverse wave age and the directional spreading, although they had a larger data set than both Mitsuyasu *et al.* (1975) and Hasselmann *et al.* (1980). The Donelan *et al.* (1985) spectra are narrowest at frequencies slightly less than the peak. Both above and below his point the spectra broaden. Donelan *et al.* (1985) only analysed their data up to 1.6 times the peak frequency. Beyond this point, Donelan *et al.* (1985) assumed that the spreading stays constant. However, Banner (1990) argues that this is incorrect. After examining high frequency stereo photography data and re-examining the data collected by Donelan *et al.* (1985), he proposed,

$$\beta = 10^{-0.4 + 0.8393 \exp\left[-0.567 \ln(\omega/\omega_p)^2\right]} \qquad for \quad \omega/\omega_p > 1.6 \qquad \textbf{(6.13)}$$

The directional spreading predicted by the above relationships varies significantly, especially near the spectral peak. As stated, Donelan *et al.* (1985) spreading is narrower than Mitsuyasu *et al.* (1975) and Hasselmann *et al.* (1980).
Young (1994) made an extensive study of the different analysis techniques, measuring methods, and the three proposed spectral forms. One of his main conclusions was that the spreading given by pitch-roll buoys is broader than that of multi-gauge arrays (where multi > 3). The number of elements in the array together with the placing of the elements will determine the performance of such a measuring device. Donelan *et al.* (1985) also concluded that pitch and roll buoys give poor directional resolving power.

6.3 Analysis Methods

There are several methods for measuring 2-dimensional spectra. They can be divided into remote sensing measurements and *in situ* measurements. The first attempts to measure 2-dimensional spectra were made by Cote *et al* (1960) using aerial photogrammetry. Holthuijsen (1981 & 1983) also used stereophotography to look at directional spectra in the North Sea. However, the most common method employed is *in situ* measurements. The most widely used technique at present uses the pitch and roll buoy. This buoy measures the vertical acceleration and the pitch and roll angles. Variations have been made to this kind of buoy such as the cloverleaf buoy described by Mitsuyasu *et al.* (1975). Another method is a spatial array of wave gauges. These gauges can be resistance gauges, current metres, pressure gauges, or other types. The gauges don't have to be of one type but can be mixed. These wave gauges can be positioned in various configurations (Young 1994), the most common of which is in some form of a symmetrical star pattern. If however one wants to measure directional spectra from one specific direction an asymmetrical pattern can also be used. The purpose of the pattern is to obtain as many different spatial lags between the wave gauges as possible. The spacing of the wave gauges is critical to avoid spatial aliasing.

The analysis of the data is not a straight forward task. The most commonly used analysis methods are the Direct Fourier Transform Method, the Maximum Entropy Method (MEM) and the Maximum Likelihood Method (MLM). There are several variations of these methods. The first method was proposed by Barber (1963). He developed a method in which the directional spectrum is estimated from the cross-spectra between the measurement elements. Longuet-Higgins *et al.* (1963) expanded this method for data with pitch-roll buoys. The Direct Fourier Transform Method relies on the assumption that the directional spreading is of the general form $\cos^{2s}\theta/2$. In contrast, the MEM and MLM make no apriori assumptions about the spreading. The MEM tends to produce excessively peaked directional spectra, and sometimes overestimates the peak energy (Tsanis and Brisette, 1992a). The MLM tends to have a too broad spread of the energy. Although the MLM makes the directional spread too wide, it was chosen as the preferred analyses method since the MEM sometimes produces peaks in the spectra that do not exist. A complete comparison has been conducted by Young (1994).

The general extended form of the MLM (Isobe *et al.* 1984) is

$$F(\omega,\theta) = \frac{s(\omega)}{\sum_m \sum_n C^{-1}_{mn}(\omega)\, H^*_m(\omega,\theta)\, H_m(\omega,\theta)\, e^{i\underline{k}\cdot(\underline{x}_n - \underline{x}_m)}} \qquad \textbf{(6.14)}$$

This form has the advantage that it can be used with different kinds of instruments in the array by appropriate specification of the transfer function H. The detailed form of the transfer function H can be found in Isobe (1984) and in Young (1994). In table 6.15 some of the transfer function forms of H are given. The term C^{-1}_{mn} is the inverse cross-spectrum matrix between the measured quantities. $s(\omega)$ is a scaling factor so that the total energy of the directional spectrum and the one-dimensional spectrum are equal. The wave number is represented by $\underline{k}$ and $\underline{x}$ is the spatial coordinate vector.

Transfer Table for Function H		
Measured Quantity	Symbol	Transfer Function $H(\underline{k},\omega)$
Water surface elevation	η	1
Water pressure	P	$\rho g \frac{\cosh(kz)}{\cosh(kd)}$
Vertical velocity of water	η_t	$-i\omega$
Vertical acceleration of the water	η_{tt}	ω^2
Surface slope of the wave (x direction)	η_x	$ik\cos(\theta)$
Surface slope of the wave (y direction)	η_y	$ik\sin(\theta)$
Surface curvature of the wave (x direction)	η_{xx}	$-k^2\cos^2(\theta)$
Surface curvature of the wave (y direction)	η_{yy}	$-k^2\sin^2(\theta)$
Surface curvature of the wave (xy direction)	η_{xy}	$-k^2\cos(\theta)\sin(\theta)$
Water particle velocity (x direction)	u	$\omega\cos(\theta)\frac{\cosh(kz)}{\sinh(kd)}$
Water particle velocity (y direction)	v	$\omega\sin(\theta)\frac{\cosh(kz)}{\sinh(kd)}$
Water particle velocity (z direction)	w	$-i\omega\frac{\sinh(kz)}{\sinh(kd)}$
Water particle acceleration (x direction)	u_t	$-i\omega^2\cos(\theta)\frac{\cosh(kz)}{\sinh(kd)}$
Water particle acceleration (y direction)	v_t	$-i\omega^2\sin(\theta)\frac{\cosh(kz)}{\sinh(kd)}$
Water particle acceleration (z direction)	w_t	$-\omega^2\frac{\sinh(kz)}{\sinh(kd)}$

Table 6.1 Transfer Table for Function H

The transfer function H for instruments that measure the surface elevation is simply unity (i.e. $H = 1$). Therefore equation 6.14 reduces to

$$F(\omega,\theta) = \frac{s(\omega)}{\sum_m \sum_n C^{-1}_{mn}(\omega)\, e^{i\underline{k}\cdot(\underline{x}_n - \underline{x}_m)}} \qquad (6.15)$$

and

$$\begin{aligned} x_n &= R_n \cos\theta_n \\ x_m &= R_m \cos\theta_m \end{aligned} \qquad (6.16)$$

where R_n is the radius of element n and θ_n is the angle between the wave propagation direction and the line between the array origin and element n. As the cross-spectral matrix can be calculated from the measured time series and the positions of the elements in the array are known, the equation can be solved. Some practical problems must however be overcome. Since there are always small calibration errors in each individual measuring device, it is wise to normalize the spectra of all the measuring devices. Another practical problem is that C^{-1}_{mn} can become singular. Capon (1969) therefore, suggested multiplying the off-diagonal elements by a small quantity to overcome this problem.

6.4 The Selection of the Two-Dimensional data

The selection of the directional data is described in section 3.4 . In total, 156 spectral measurements were taken by the array. The wind speeds were between 3 m/s and 15 m/s, the mean water depth was between 1.8 m and 2.4 m during this part of the experimental period (18 months).

Because of the shape of the lake which was orientated north/south, data were only considered from steady wind periods where the wind was ±10° from the normal to the eastern and western shore lines. This left 58 spectra for the analysis.

In figures 3.18 and 3.19 there is some basic information on the spectra. In figure 3.18 the inverse wave ages of the spectra are shown. The majority of the data are near $U_{10} / C_p = 2.3$. However the range of data is quite extensive, from $U_{10} / C_p = 4$ (highly forced seas) to $U_{10} / C_p = 1$ (fully developed seas). In the next figure 3.19 the spread of the non-dimensional relative depth parameter ($k_p d$) is shown. As can be seen in figure 3.19 the directional data set is completely in transitional water depth.

6.5 Results of the Two-Dimensional Analyses

6.5.1 Fitting existing two-dimensional directional spreading models

As described in the earlier sections, there are a number of models that are commonly used to describe the directional spreading. The two most common ones are

$$\cos^{2s}\left(\frac{1}{2}\theta\right) \tag{6.17}$$

and

$$sech^{2}(\beta\theta) \tag{6.18}$$

There are also a number of techniques to analyse the data. Mitsuyasu *et al.* (1975) and Hasselmann *et al.* (1980) used the Fourier Expansion Method described by Longuet-Higgins (1963) and Young (1994). The first 2 components of the Fourier expansion were used to determine the value of s. Donelan *et al.* (1985) used a completely different technique. They matched the directional form to the half power points of the measured spreading function, since interest is concentrated on the energetic region of the directional distribution. Another method that could be used is the nonlinear least squares method described by Press *et al.* (1986). This method was also used in the

one-dimensional spectral analyse in chapter 5. This method fits the analytical form to the full directional distribution obtained by the MLM.

For this analysis, the least squares method was used as it gave the least scatter in the data. The MLM spectra were normalized by

$$\hat{D}(f,\theta) = \frac{\hat{E}(f,\theta)}{\hat{E}_{max}(f,\theta_{max})} \qquad \textbf{(6.19)}$$

where $\hat{E}(f,\theta)$ is the directional spectrum derived from the MLM, and $\hat{E}_{max}(f,\theta_{max})$ is the maximum ordinate of the directional spectrum in direction θ_{max}.

As discussed, the two most common directional spreading functions (equation 6.17 and 6.18) were fitted to the data. To determine the better fit an error analysis was conducted where

$$\Delta(f,\theta_i) = \hat{D}(f,\theta_i) - A(f,\theta_i) \qquad \textbf{(6.20)}$$

was calculated. The function $A(f,\theta_i)$ was either of the two directional spreading functions (equation 6.17 or 6.18). An error function $\varepsilon(f)$ was calculated through,

$$\varepsilon(f) = \frac{1}{N}\sqrt{\sum_{i=1}^{N}\Delta^2(f,\theta_i)} \qquad \textbf{(6.21)}$$

where N was the number of directional bands in the discrete spectral representation. Due to noise in the high frequencies, cases that had $\varepsilon > 0.01$ were disregarded. The results are shown in figures 6.1 and 6.2. The figures are qualitatively similar, with broad spreading away from the peak frequency and narrow spreading around the peak frequency. Values of the parameter s range over a factor of 10, whereas β_s has a small dynamic range, a factor of only 2. This means that the relative data scatter is greater in the $sech^2$ (equation 6.18) form than in the cos^{2s} (equation 6.17) form. The correlation coefficient for the two forms are

Correlation Coefficients		
	$f < f_p$	$f > f_p$
$cos^{2s}\theta/2$	0.89	-0.67
$sech^2 \beta_s \theta$	0.78	-0.62

Table 6 Correlation Coefficients

One of the reasons why the $sech^2$ form might not perform as well is because it contains a discontinuity where the wave direction is broader than π. In this data set the cos^{2s} form performed better than the $sech^2$ form. Therefore the cos^{2s} form is used for the remainder of the analysis.

6.5.2 Wave age dependence of the directional spreading

As stated, some authors (Mitsuyasu *et al.*, 1975 and Hasselmann *et al.*, 1980) claim a dependence on the inverse wave age for the directional spreading function. Other authors, including Donelan (1985) argue the opposite. To see if evidence could be found for either case, the data were split up into inverse wave age groups where the inverse wave age was taken as

$$inverse\ wave\ age = \frac{U_{10}}{C_p} \qquad \textbf{(6.22)}$$

The data were split into three groups,

group 1 $1 < \text{inverse wave age} \leq 2$

group 2 $2 < \text{inverse wave age} \leq 3$

group 3 $3 < \text{inverse wave age} \leq 4$

As can been seen in figure 6.3 there is no clear dependency on the inverse wave age in the data. The data of the three groups are completely mixed. Hasselmann *et al.* (1980) indicate this is caused by the fact that the nonlinear source term dominates over both the input and dissipation. Donelan *et al* (1985) also suggests this, although they caution that

there might be other reasons. Banner and Young (1994) in their calculations with an unconstrained model clearly show that the nonlinear source terms play an active role in the directional spread. No conclusion can be drawn from the measurements taken in Lake George as to whether the nonlinear terms play such an important role. However, together with the calculations made by Banner and Young (1994) it does seem to support the dominant role of the nonlinear source term.

6.5.3 Depth dependence of the directional spreading

In order to investigate the dependence of the directional spreading on the dimensionless water depth parameter ($k_p\ d$), the data were partitioned into three groups based on the relative depth.

group 1 $1 < k_p d \leq 1.5$

group 2 $1.5 < k_p d \leq 2$

group 3 $2 < k_p d \leq 2.5$

The results are shown in figure 6.4 Again there is no distinct pattern to show a clear dependence on the relative depth. However, it must be noted that most of the spectra were taken in transitional water depth and hence there is a relatively narrow range of values of $k_p d$.

6.5.4 Directional spreading parameter (s)

Another aspect which must be considered is the artificial broadening of the directional spreading factor (s) caused by the measurement array and the analysis method. To check to what extend the artificial broadening played a part in the results, a sensitivity test was performed. Artificial spectra with directional spreading factors (s_{in}) between 1 and 10 were generated. These spectra were subjected to the MLM analysis, resulting in the output directional spreading factor (s_{out}). As can be seen in figure 6.5 and 6.6 the analysis broadens the directional spreading significantly for the narrowest directional

spectra. To adjust for this, the directional data were corrected using the results in figure 6.6.

Although the narrowest point is hard to establish, the fit to the data was applied constraining the data to be the narrowest at $f/f_p = 1$. The fit resulted in the following form

$$s = \begin{cases} 11\left(\frac{f}{f_p}\right)^{2.7} & f < f_p \\ 11\left(\frac{f}{f_p}\right)^{-2.4} & f \geq f_p \end{cases} \quad \textbf{(6.23)}$$

The results of several deep water studies (Mitsuyasu *et al.*, 1975, Hasselmann *et al.*, 1980, Donelan *et al.*, 1985) and this study have been compared in figure 6.7. The mean values of the wave age dependent data from Mitsuyasu *et al.* (1975) and from Hasselmann *et al.* (1980) are used. Their data are broader than the data from this experiment. This could indicate that their instrumentation and/or analysis technique introduced artificial broadening (Young 1994). The Donelan *et al.* (1985) data were digitized from their figure 30 as they do not supply an equation in terms of the directional spreading factor (s). The Lake George data set is broader. The data set has been corrected for the artificial broadening due to the analysis. Therefore, the broadening could be due to the shallow water effects. However there is too little data (very small range of $k_p d$) to substantiate this claim.

6.5.5 Physical processes controlling the directional spreading

One of the physical possesses that could explain the growth of the directional spreading could be the non-linear interactions. In addition to transferring energy in frequency space, nonlinear transfer can also move energy from the mean direction to larger angles. This may influence the final directional spreading.

A numerical investigation of this form, is, however, beyond the scope of this study.

6.6 Bimodal Spreading of the Directional Spectra

During the analysis, a phenomenon that could not be simply explained was discovered. As discussed in the previous sections, the analysis of the directional data was done by the Maximum Likelihood Method (MLM). The directional spreading function $D(\omega,\theta)$ can also be normalized in the following fashion

$$D(\omega,\theta) = N(\omega)\ G(\omega,\theta) \qquad \textbf{(6.24)}$$

where $N(\omega)$ is the normalizing factor and $G(\omega,\theta)$ the directional spreading function with a maximum of unity (1). For completeness equation 6.1 (section 6.2) is rewritten in the above form

$$F(\omega,\theta) = F(\omega)\ N(\omega)\ G(\omega,\theta) \qquad \textbf{(6.25)}$$

where $F(\omega,\theta)$ is the directional spectrum and $F(\omega)$ the one-dimensional spectrum. The results from the analysis are spectra like the ones shown in figure 6.8 At the peak frequency, the spectra are single peaked. However at higher frequencies, starting from twice the peak frequency, a bimodal form becomes apparent.

The MLM analysis technique was checked with artificially generated data. The technique showed no sign of generating bimodal distributions if these did not occur in the input spectra. Hence, it is concluded that the bimodal spreading shown in figure 6.8 is not an artifact of the analysis methods.

The question arises, why haven't these bimodal spectra been noted before in other studies. Mitsuyasu *et al.* (1975) and Hasselmann *et al.* (1980) used an analysis technique that assumes a uni-modal form. This excludes any form of bimodal structure because of the analyses. Donelan *et al.* (1985) used a high resolution directional analysis technique but stopped their analysis at 1.6 times the peak frequency (f_p). The bimodal structure in the Lake George data does not become apparent until $2f_p$. Therefore Donelan *et al.* (1985) might not have noticed it in their analysis. Holthuijsen (1983),

who made stereophotographs over the North Sea, has a slight bimodal spreading in his results. Brissette and Wu (1992) did find bimodal spreading in their data from lake St. Clair, but were unable to explain it. They assumed that it was caused by currents. K.C. Ewans (personal communication) (Shell International Exploration and Production) analysed a recent deep water data set from New Zealand finding bimodal spreading in his data.

Assuming the analyses of the bimodal seas are true, then a cause for this effect must be sought. One source could be the directional spreading of the wind. There are not enough detailed wind data from Lake George to test this theory. Another more likely source is nonlinear interactions. Young and van Vledder (1993) and Banner and Young (1994) have investigated the growth with a numerical model which has no assumption about the high frequency part of the tail and has a full solution to the nonlinear source terms. The results can be seen in figure 6.9. Although there are some differences with the measured data, the trend toward bimodal directional spreading at higher frequencies is clear. Banner and Young (1994) claim that the magnitude of the bimodal peaks at higher frequency varies with the atmospheric input and dissipation terms of the model. The cause of the directional spreading is however the nonlinear interactions. They claim that nonlinear terms transport energy from the wind direction to "off-wind" angles.

No further attempt has been made to explain the bimodal form of the directional spreading in this thesis.

6.7 Conclusions for the Two-Dimensional Spectra

The directional array yielded 58 directional spectra from young to fully-grown seas. After processing these data a high resolution directional set was available for analysis.

The form of the spreading is best represented by

$$\cos^{2s}\left(\frac{1}{2}\theta\right) \tag{6.26}$$

and where s is a function of f/f_p .

There was no clear dependency on the inverse wave age nor on the non-dimensional depth parameter ($k_p\, d$).

Although the directional spreading was, in general, broader than in deep water experiments, the general trend in finite depth water is the same as in deep water; broad spreading at the higher frequencies and a narrow spreading near the peak frequency. This seems to indicate that nonlinear interactions play an important role. This however was not substantiated in this thesis.

Bimodal spreading was noted for frequencies above $2f_p$. This has also been observed in deep water data obtained with different analysis methods. Modelling shows that nonlinear interactions play an important role in forming the directional spreading.

7. Conclusions

7.1 General Conclusions of the Lake George Experiment

The main reason for conducting this experiment was to determine the characteristics of fetch limited wind-wave growth in finite depth water. It is believed these goals have been successfully achieved. The data set collected is extensive and will certainly be utilized for other scientific purposes.

7.2 Conclusions for the Growth Curves for Finite Depth Water

The Lake George data set has enabled the development of a family of growth curves for non-dimensional energy and non-dimensional peak frequency as a function of non-dimensional fetch. In contrast to deep water, the water depth introduces an additional variable. At short fetch, where bottom influences are small, the data are consistent with the well know deep water data sets. As the effects of the bottom increase, the growth rate is retarded compared to deep water. Finally, at long fetch or small non-dimensional depth, an asymptotic state is reached in which the waves become depth limited and hence independent of the fetch.

7.3 Conclusions for the One-Dimensional Spectra

The data clearly shows that the TMA spectral form is a good representation of the finite depth spectra.

A clear relationship exists between α and the non-dimensional wave number (κ). However, there was no relationship found between the peak enhancement factor (γ) and the non-dimensional wave number (κ). The data suggest a dependence of the peak

enhancement factor (γ) on the non-dimensional fetch (χ) and/or the non-dimensional depth (δ). There is clear evidence that γ increases with decreasing water depth.

7.4 Conclusions for the Two-Dimensional Spectra

Although the results of the two-dimensional spectral measurements taken by the directional array in Lake George are broader than in deep water they are consistent with deep water, trends. Broad directional spreading exists at high frequencies, with the spectrum being narrowest at the spectral peak.

The general form using $\cos^{2s} \theta/2$ is appropriate for the directional spreading, with the directional spreading factor (s) being dependent on f/f_p.

No dependence on either the inverse wave age (U_{10}/C_p) or the dimensionless depth parameter ($k_p\, d$) was established, although a dependence on the dimensionless depth parameter is not ruled out.

At frequencies greater than $2f_p$ the spectra exhibited bimodal spreading. It is very likely that nonlinear interactions play some part in this. However, it was outside the scope of this study to investigate this any further.

It is clear that more research will have to done into the role of the nonlinear interactions.

7.5 Final Conclusions for the Lake George Experiment

The data set described in this thesis is, by far, the most comprehensive collected under fetch limited finite depth conditions. Despite the extent of the data set a number of important questions remain unresolved. In particular, the detailed role played by finite water depth in influencing the directional spreading is yet to be resolved.

The experimental design was not such that it could define the physical processes responsible for finite depth wind wave evolution. It has, however, provided a valuable data set and a parametric description of this evolution. This description will prove valuable for both engineering design and model testing.

8. References

Banner M.L., Melville W.K., 1976. On the Separation of Air Flow over Water Waves, Journal of Fluid Mechanics, Vol. 77, part 4, pp. 825-842

Banner M.L. 1990. Equilibrium Spectra of Wind Waves, Journal of Physical Oceanography, Vol. 20, pp. 966-984

Banner M.L. and Young I.R. 1994. Modelling Spectral Dissipation in the Evolution of Wind Waves. Part I: Assessment of Existing Model Performance, Journal of Physical Oceanography, Vol 24, No. 7, pp. 1550-1571

Barber N.F. 1963. The Directional Resolving Power of an Array of Wave Detectors, Ocean Wave Spectra, Prentice-Hall Inc., New Yersey, pp. 137-150

Barnett T.P. 1968. On the Generation, Dissipation, and Prediction of Ocean Wind Waves, Journal of Geophysical Research, Vol. 73, No. 2, pp. 513-528

Barnett T.P., Wilkerson J.C. 1967. On the generation of Ocean Wind Waves as Inferred from Airborne Radar Measurements of Fetch-Limited Spectra, Journal of Marine Research, Vol. 25, No. 3, pp. 292-328

Battjes J.S., Zitman T.J. and Holthuijsen L.H. 1987. A Reanalysis of the Spectra Observed in JONSWAP, Journal of Physical Oceanography, Vol. 17, pp. 1288-1295

Bendat J.S. and Piersol A.G. 1971. Random Data: Analysis and Measurement Procedures, Wiley-Interscience, John Wiley & Sons Inc. , New York

Booij N., Holthuijsen L.H., de Lange P.H.M. 1992. Penetration of Short-Crested waves through a Gap, Proceedings of the 23rd Conference on Coastal Engineers ASCE, pp. 1044-1052

Bouws E. 1986 Provisional Results of a Wind Wave Experiment in a Shallow Lake (Lake Marken, The Netherlands), KNMI Afdeling Oceanografisch Onderzoek, OO-86-21, de Bilt, pp. 1-15

Bouws E., Günther H., Rosenthal W. and Vincent C.L. 1985. Similarity of the Wind Wave Spectrum in Finite Depth Water, Part 1. Spectral Form, Journal of Geophysical Research, Vol. 90, No. C1, pp. 975-986

Bouws E., Günther H., Rosenthal W. And Vincent C.L. 1987. Similarity of the Wind Wave Spectrum in Finite Depth Water, Part 2 Statistical Relations between

Shape and Growth Stage Parameters, Deutsche Hydrographische Zeitschrift, Vol 40, pp. 1-24

Bretschneider C.L. 1958. Revisions in Wave Forecasting: Deep and Shallow Water, Proceedings of the 6th Conference on Coastal Engineers ASCE, pp. 30-67

Brissette F.P. and Wu J. 1992. Wave Directional Spectra and Current Interaction in Lake St. Clair, Third International Workshop on Wind Hindcasting and Forecasting, Environment Canada, Montreal, Canada

Capon J. 1969. High-resolution Frequency-Wavenumber Spectra Analysis, Proceedings IEEE, 57, pp. 1408-1418

Cote L.J., Davis J.O., Marks W., McGough R.J., Mehr E., Pierson W.J. Jr, Ropek J.F., Stephenson G. and Vetter R.C. 1960. The Directional Spectrum of Wind-Generated Sea as Determined from Data Obtained by the Stereo Wave Observation Project. Meteor. Pap., New York University, College of Engineering, Vol. 2, No. 6, 88 pages

Dobson F., Perrie W. and Toulany B. 1989. On the Deep-Water Laws for Wind_Generated Surface Gravity Waves, Atmosphere-Ocean, No. 27, pp. 210-236

Donelan M.A., Hamilton J. and Hui W.H. 1985. Directional Spectra of Wind-Generated Waves. Phi. Trans. R. Soc. Lond. A 315, pp. 509-563

Dungey J.C., Hui W.H. 1979. Nonlinear Energy Transfer in a Narrow Gravity-Wave Spectrum, Proc. R. Soc. Lond. A 368, pp. 239-265

Forristall G.Z. 1978. On the Statistical Distribution of Wave Heights in a Storm, Journal of Geophysical Research, Vol 83, No C5, pp. 2353-2358

Forristall G.Z. 1981. Measurements of a Saturation Range in Ocean Wave Spectra. Journal of Geophysical Research, Vol 86, No C9, pp. 8075-8084

Günther H. 1981. A Parametric Surface Wave Model and the Statistics for the Prediction Parameters, Hamburger Geophysikalishe Einzelschriften, 90 pages

Ijima T. and Tang F.L.W. 1966. Numerical Calculations of Wind Waves in Shallow Water, Proceedings of 10th Conference on Coastal Engineering, Tokyo, Japan, Chap. 4, pp. 38-45

Isobe M., Kondo K., Horikawa 1984. Extension of MLM for Estimating Directional Wave Spectrum, Copenhagen Symposium on description and Modelling of Directional Seas, DHI & MMI, paper A-6, pp 1-15

Janssen P.A.E.M. 1991. Quasi-Linear Theory of Wind-Wave Generation Applied to Wave Forecasting, Journal of Physical Oceanography, Vol. 21, pp. 1631-1642

Jeffery's H. 1925. On the Formation of Water Waves by Wind, Proc. Royal. Soc., series A, Vol. 107, pp. 189-206

Hasselmann D.E., Dunckel M., and Ewing J.A. 1980. Directional Wave Spectra Observed during the JONSWAP 1973, Journal of Physical Oceanography, Vol. 10, pp. 1264-1280

Hasselmann K. 1962. On the Nonlinear Energy Transfer in a Gravity Wave Spectrum, Part 1 General Theory, Journal of Fluid Mechanics, Vol. 12, pp. 481-500

Hasselmann K., Barnett T.P., Bouws E., Carlson H., Cartwright D.E., Enke K., Ewing J.A., Gienapp H., Hasselmann D.E., Kruseman P., Meerburg A., Müller P., Olbers D.J., Richter K., Sell W., Walden H. 1973. Measurements of Wind-Wave Growth and Swell Decay during the Joint North Sea Wave Project (JONSWAP), Deutsches Hydrographisches Institut, Hamburg

Hardy T.A. 1993. The Attenuation and Spectral Transformation of Wind Waves on a Coral Reef, Ph.D Thesis, James Cook University of North Queensland, Townsville, Australia

Hardy T.A. and Young I.R. 1996. Field Study of Wave Attenuation on an Offshore Coral Reef, Journal of Geophysical Research, Vol 101, No C6, pp. 14311-14326

Holthuijsen L.H. 1981. The Directional Energy Distribution of Wind Generated Waves as Inferred from Stereophotographic Obervations of the Sea Surface, Ph.D. Thesis, Technical University Delft, Delft, Netherlands

Holthuijsen L.H. 1983. Observations of the Directional Distribution of Ocean-Wave Energy in Fetch-Limited Conditions, Journal of Physical Oceanography, Vol. 13 pp. 191-207

Kahma K.K. 1981.A Study on the Growth of the Wave Spectrum with Fetch, Journal of Physical Oceanography, Vol. 11 pp. 1503-1515

Kahma K.K., Calkoen C.J. 1992. Reconciling Discrepancies in the Observed Growth of Wind-Generated waves, Journal of Physical Oceanography, Vol 22, pp 1389-1405

Kitaigorodskii S.A. 1961. Applications of the Theory of Similarity to the Analysis of Wind-Generated Wave Motions as a Stochastic Process, Izv. Akad. Nauk. USSR, Ser. Geofiz, Vol. 1, pp. 105-117 (Rusian), English translation : Bull. Acad. Sci. USSR. Geoph. Ser. No. 1, 1962 *

Kitaigorodskii S.A., Krasitskii V.L., and Zaslavskii M.M. 1975. On Phillips' Theory of Equilibrium Range in the Spectra of Wind-Generated Gravity Waves, Journal of Physical Oceanography, Vol. 5, pp. 410-420

Longuet-Higgins M.S. 1952, On the Statistical Distribution of Heights of Sea Waves, Journal of Marine Research, Vol. 11, No. 3, pp. 245-266

Longuet-Higgins M.S., Cartwright D.E. and Smith N.D. 1963. Observations of the Directional Spectrum of Sea Waves using the Motions of a Floating Buoy. Prentice-Hall Inc., New Yersey, pp. 137-150

Miche R. 1944. Mouvement Ondulatoirs des Mers en Profonduer Constante ou Décroissante, Annales des Ponts et Chaussées, pp. 25-78, 131-164, 270-292, 369-406

Miles J.W. 1957. On the Generation of Surface Waves by Shear Flows, Journal of Fluid Mechanics, Vol.3, pp. 185-204

Miles J.W. 1960. On the Generation of Surface Waves by Turbulent Shear Flows, Journal of Fluid Mechanics, Vol. 7, pp. 469-478

Miller H.C., Vincent C.L. 1990. FRF Spectrum: TMA with Kitaigorodskii's f^{-4} Scaling, Journal of Waterway, Port Coastal, and Ocean Engineering, Vol. 116, No. 1, January, pp. 57-77

Mitsuyasu H., Tasai F., Suhara T., Mizuno S., Ohkusu M., Honda T., Rikiishi K. 1975. Obervations of the Directional Spectrum of Ocean Waves using a Cloverleaf Buoy, Journal of Physical Oceanography, Vol. 5, pp. 750-760

Motzfeld H. 1937. Die Turbulente Strömung an Welligen Wänden, Zeitschrift fur Angewandte Mathematiek und Physik, Vol. 17, pp. 193

Nelson R.C. 1994. Depth Limited Design Wave Heights in Very Flat Regions, Coastal Engineering, Vol. 23, pp. 43-59

*Note: This paper could not be obtained, but it would be unfair to the author not to cite the intellectual source.

Phillips O.M. 1957. On the Generation of Waves by Turbulent Wind, Journal of Fluid Mechanics, Vol. 2, pp. 417-445

Phillips O.M. 1958. The Equilibrium Range in the Spectrum of Wind-Generated Ocean Waves, Journal of Fluid Mechanics, Vol. 4, pp. 426-434

Phillips O.M. 1966. The Dynamics of the Upper Ocean, Cambridge University Press, first edition.

Pierson W.J. and Moskowitz L. 1964. A Proposed Spectral Form for Fully Developed Windseas Based on Similarity Theory of S.A. Kitaigorodskii, Journal of Geophysical Research, Vol. 69, pp. 5181-5190

Press W.H., Flannery B.P., Teukolsky S.A. and Vetterling W.T. 1986. Numerical Recipes, Levenberg-Marquardt Method, Cambridge University Press, chap. 14.4 pp. 523-528

Read W.W. 1986. Time Series Analysis of Wave Records and the Search for Wave Groups, Ph.D Thesis, James Cook University of North Queensland, Townsville, Australia

Resio D.T. 1987. Shallow Water Waves I: Theory. ASCE Journal, Waterway, Port, Coastal Engineering, Vol. 113, pp. 264-281

Shore Protection Manual 1984. US Army Engineer Waterway Experiment Station, Coastal Engineering Research Center (CERC), US Government Printing Office, Washington, D.C., 4th edition, 2 Volumes

Soest van J. 1983, Elementaire Statistiek, Vereniging voor Studie en Studentenbelangen te Delft (VSSD), Delftse Uitgevers Maatschappij (DUM), pp. 1-175

Smith D.S., Anderson J.R., Oost W.A., Kraan C., Maat N., DeCosmo J., Katsaros K.B., Davidson K.L., Bumke K., Hasse L., Chadwick H.M. 1992. Sea Surface Wind Stress and Drag Coefficients, The HEXOS Results, Boundary-Layer Meteorology, Vol. 60, pp. 109-142

Smith P.C., and MacPherson J.I. 1987. Cross-Shore Variations of Near-Surface Wind Velocity and Atmospheric Turbulence at the Land-Sea Boundary During CASP, Atmosphere-Ocean, Vol. 25, No. 3, pp. 279-303

Stanton T.E., Marshall, D. and Houghton, R. 1932. Proc. Roy. Soc., serie A, Vol. 137, pp. 282

Synder R.L., Cox C.S. 1966. A Field Study of the Wind Generation of Ocean Waves, Journal of Marine Research, Vol. 24, No. 2, pp. 141-178

Synder R.L., Dobson F.W., Elliott J.A., and Long R.B. 1981, Array Measurements of Atmospheric Pressure Fluctuations above Surface Gravity Waves, Journal of Fluid Mechanics, Vol. 102, pp. 1-59

Sverdrup H.U. and Munk W.H. 1946. Empirical and Theoretical Relations between Wind, Sea and Swell, Trans. Amer. Geophys. Union, Vol 27, pp. 823-827

Taylor P.A. and Lee R.J. 1984. Simple Guidelines for Estimating Wind Speed Variations due to Small Scale Topographic Features, Climatological Bulletin, Vol. 18, No. 2, pp. 3-32

Thijsse J.Th. 1949. Dimensions of Wind-Generated Waves. General Assembly of Association d'Océanographie Physique, Oslo. Procés-Verbaux No. 4, pp. 80-81

Thompson E.F. and Vincent C.L. 1985. Significant Wave Height for Shallow Water Design, Journal of Waterway, Port, Coastal and Ocean Engineering, Vol. 111, No. 5, pp. 828-842

Toba Y. 1973. Local Balance in the Air-Sea Boundary Processes, Part III: On the spectrum of wind waves, Journal of Oceanographic Society Japan, 29, pp. 209-220

Tsanis I.K. and Brissette F.P. 1992. Methods for Directional Spectra Measurements by Small Arrays, 3rd International Workshop on Wave Hindcasting and Forecasting, Montreal, May 19-22, pp. 12-23

Ursell F. 1956. Surveys in Mechanics, editor Batchelor G.K., Cambridge University Press, Wave Generation by Wind, pp. 216-249

U.S. Army Corps of Engineers 1955. Waves and Wind Tides in Shallow Lakes and Reservoirs. Summary Report, Project CW-167, Jacksonville District, Fla

Verhagen L.A., Holthuijsen L.H., Won Y.S. 1992. Modelling Ocean Waves in the Colombia River Entrance, Proceedings of the 23rd Conference on Coastal Engineers ASCE, pp. 2893-2901

Vincent C.L. 1985. Depth-Controlled Wave Height, Journal of Waterway, Port, Coastal and Ocean Engineering, Vol. 111, No. 3, pp. 459-475

Vincent C.L., Hughes S.T. 1985. Wind Wave Growth in Shallow Water, Journal of Waterway, Port, Coastal and Ocean Engineering, Vol. 111, No. 4, pp. 765-770

Walpole R.E. and Myers R.H. 1972 Probability and Statistics for Engineers and Scientists, Macmillan, New York, pp. 1-506

Wamdi Group 1988. The WAM Model- A Third Generation Ocean Wave Prediction Model, Journal of Physical Oceanography, Vol. 18, pp. 1775-1810

Woolley J. 1990. Lake George with Historical Notes on Bungendore and Collector, Goulburn & District Historical Society

Wu J. 1980. Wind-Stress Coefficients over Sea Surface near Neatral Conditions-a Revisit, Journal of Physical Oceanography, Vol. 10, Part 1, pp 727-740

Young I.R. 1986 Probability Distributions of Spectral Integals, ASCE J. Waterway, Port, Coastal and Ocean Engineering, No. 112, pp. 338-341

Young I.R., van Vledder G. Ph. 1993. A Review of the Central Role of Nonlinear Interactions in Wind-Wave evolution. Phil. Trans. Royal Society London, Vol A, No. 342, pp. 505-524

Young I.R. 1994. On the Measurements of Directional Wave Spectra, Journal of Applied Ocean Research, Vol. 16, pp. 283-294

Young I.R. 1995. The Determination of Confidence Limits Associated with Estimates of the Spectral Peak Frequency, Ocean Engineering, Vol. 22, No. 7, pp. 669-686

Zwarts C.M.G. 1974. Transmission Line Wave Height Transducer, Proceedings International Symposium on Ocean Wave Measurement and Analysis, New Orleans, ASCE, Vol. 1, pp. 605-620

9. Symbols

Symbol	Description
α	depth independent constant or variable, depending on the definition of the spectrum
α_f	f degrees of freedom
β	empirical growth parameter
β^*	Miles growth parameter
β_s	directional spreading parameter
γ	peak enhancement factor
δ	dimensionless water depth
δ_i	internal boundary layer of the wind
ε_f	wave steepness
ε	dimensionless energy
$\varepsilon(f)$	error function
η	the water surface
η_{tt}	vertical acceleration of the water surface
$\eta_x\eta_y$	the slope of the water surface
$\eta_{XX},\eta_{YY},\eta_{XY}$	the curvature of the water surface in three directions
θ	wave direction
θ_{10}	wind direction at 10 metres heigth
θ_n	angle between the wave propagation and the line between the fixed points and element n in the directional array
κ	von Karman constant
κ	dimensionless wave number
Λ	dimensionless wave height
μ	dimensionless Miles growth parameter

Symbol	Description
ν	dimensionless frequency
ξ	dimensionless height parameter
π	PI $\pi = 3.142$
ρ_a	density of air
ρ_w	density of water
σ	standard deviation
Φ	shape function
Φ_c	dimensionless parameter at critical height *c*
χ	dimensionless fetch, dimensionless distance along the fetch
$\Psi(k,f_p,d)$	non dimensional shape function
ω	radian wave frequency
ω_p	frequency of the spectral peak, peak period, in radian
$A(f_i,\theta_j)$	two directional spreading functions
c	critical height
Cp/U	wave age
Cp	phase speed of the spectral peak
C_g	group velocity
d	water depth
$D(\omega\theta)$	directional spread function
E	total energy of the spectrum
$E_i(data)$	i^{th} spectral band of the measured energy spectrum
E_m	maximum energy
F	fetch
$F(\omega)$	one dimensional spectrum
$F(\omega,\theta)$	directional wave spectrum
F(f)	variance spectrum at frequency f

Symbol	Description
$F(f,\theta)$	directional spectrum derived from the MCM
$F(k)$	wave number spectrum
f_c	cut off frequency
$F_{ma}(f)$	maximum energy at frequency f
f_p	frequency of the spectral peak, peak period
$F_{pm}(f)$	Pierson Moskowitz spectrum
g	gravitational force
$H_{1/3}$	average of the highest 1/3 of the waves
H_{max}	maximum wave height
H_{mo}	wave height derived from energy spectrum
H_s	significant wave height
k	wave number
k_p	wave number of the spectral peak
L	wave length
L_p	wave length of the peak frequency
n	number of spectral bands analysed, number of directional bands
P	spectral band which contains the peak frequency
$Q(s)$	normalizing function
R_n	distance from element n to a fixed point in directional array
s	directional spread factor
S	source/sink term
S_{in}	energy going into the waves, artificial widening of the directional spread factor
S_{nl}	nonlinear source term
S_{ds}	white-capping source term
S_{bf}	dissipation at bottom source term

Symbol	Description
U	measured wind velocity/wind speed
U_{10}	wind speed 10 metres above surface level
U_{ou}	upwind wind velocity
U_z	wind speed at elevation z above the surface
U_*	friction velocity or shear stress wind speed at Z_0 above mean "ground" level
x	distance along the fetch.
z	elevation (at which Uz is measured) above the surface
Z	elevation of the windspeed
Z_o	roughness length scale of the wind
Z_{ou}	roughness length of the upwind boundary

10. Acknowledgments

The person to thank the most would be Prof. Ian Young. The project was setup by him (together with Prof. Mike Banner) both in concept and financially. This made it possible for me to go to Australia. Once there, Ian has supported me in numerous ways. Ian's guidance throughout the complex project was an essential part of finishing. His painstaking review of this work (written by a non-native English speaker) has been a necessary and welcome addition. He has the great ability to inspire people and can explain the most complex things in simple manners. He still inspires me half way across the world. It has been a great pleasure working for Ian and I hope I to get this privilege again in the future.

I would like to thank Peter McMahon and Mary Dalton for their first rate work. Without them this project simply would not have worked. Their enthusiasm and determination got all problems solved. Mary spent many hours on the lake repairing/fixing/installing equipment sometimes under the most appalling conditions. Peter helped me with numerous electronics and computer problems (mainly at the university because Peter has some kind of water fear). With both I have spent many, very enjoyable hours in their office. Both have put a lot of extra effort into this project.

The project was funded by the Australian Research Council without who's funding it would not have been possible.

I would also like to express my thanks to:

Prof. Mike Banner for giving input and starting the project together with Prof. Ian Young.

John MacLeod, Doug Collier and Bernie Miller have delivered the finest craftsmanship one could wish for. The constructions they bolted/welded together were of quality that one could expect in the space industry.

Graham Johnston, Terry Lutze, David Sharp, Jim Baxter and Carl Shaw, all were the necessary muscle for the project. Without them things would not have moved.

CDR. Jon Delaney of the Royal Australian Navy, for arranging many boats (from large to small) and equipment. He is a keen diver with whom I have spend many hours underwater. I recommend his barbeque and his enjoyable company.

Tony Webb with whom I have spent many enjoyable hours and who has helped inspire me in finishing his thesis. I would also like to thank Tony for taking the time and effort reading the thesis and helping correct the English.

Both the Royal Australian Navy and Royal Australian Army for lending us boats and equipment

The "old fellas" John Sneddon, Bruce Golley, Ray Nelson and John Baird for having the most inspiring and, unlike the quality of the food, certainly very enjoyable lunches with me at the officers mess of the Australian Defence Force Academy.

Leo Holthuijsen for getting me started with waves and inspiring me to go to Australia. Leo even now regularly enquires about my general state (and the thesis).

Roeland Ris with whom I have spend many hours and conferences (and before/during/after-dinner drinks).

My new boss Toine van Riel of Fugro-Inpark B.V. for giving me days off to finish the last parts of the thesis.

Last but also not least, I would thank Mirjam de Vast (now Verhagen) for waiting so patiently all those years in the Netherlands for me to hurry up and return.

For those of you who also helped me but whom I have forgotten to mention due to my bad memory, please come by for a beer and accept my apologies.

The End

The University of New South Wales

The Growth of Wind Waves in Finite Water Depth

The figures for the Thesis submitted in candidature for
Doctor of Philosophy

by **Louis Verhagen**

Department of Civil Engineering
University College
University of New South Wales
Australian Defence Force Academy
1999

Picture, Graphs, and Maps

This part contains all the pictures, graphs and maps of the thesis for easy reading. The chapters are divided as in the thesis itself. Although the description in caption should provide enough information please refer to the main text for thorough explanations.

Chapter

page

1. Introduction to the Lake George Shallow Water Experiment

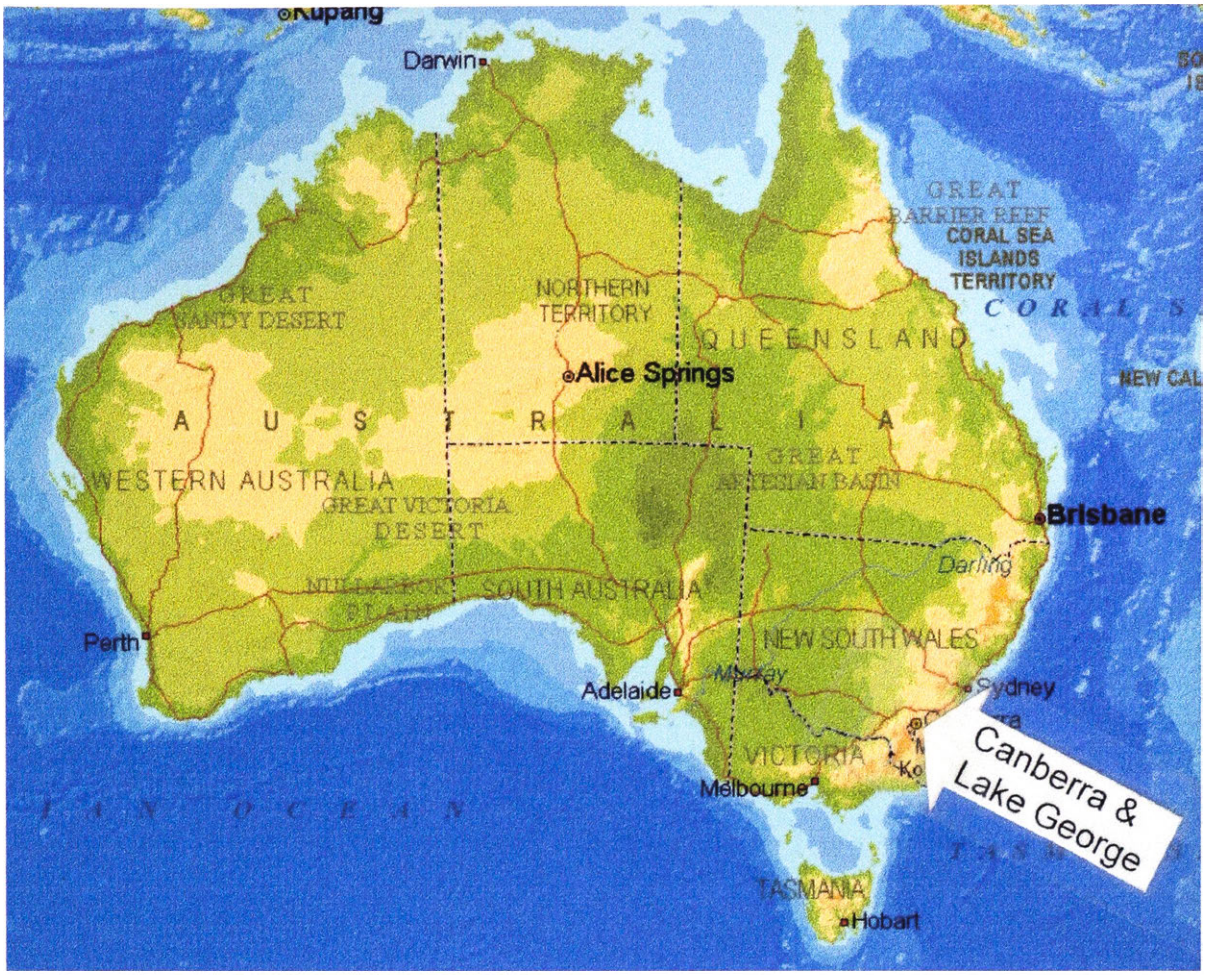

Figure 1.1 The site for the experiments is Lake George in the south east of the state of New South Wales and near to the capital, Canberra (in the Australian Capital Territory). Sydney is about 250 kilometres north of Lake George.

Figure 1.2 New South Wales from Canberra (south west of map) to Sydney (north east of map). The experimental location at Lake George is shown.

Figure 1.3 Photo of the "hill" caused by a geological fault. This hill runs from north to south along the western side of Lake George.

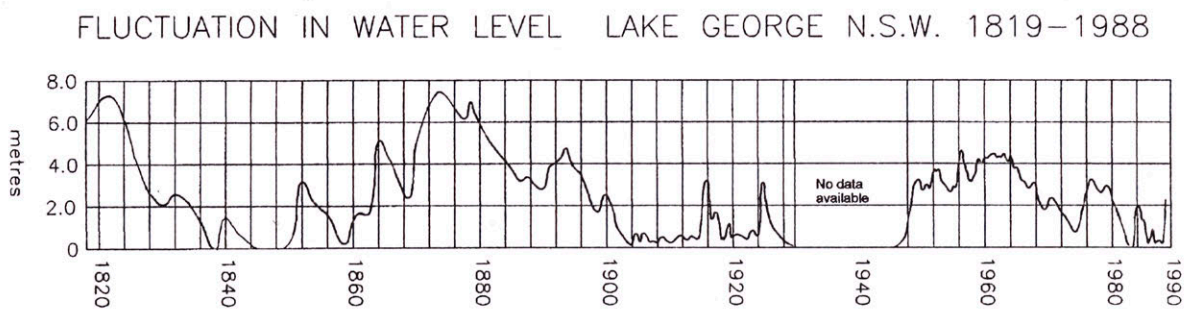

Figure 1.4 Fluctuation of the water level in Lake George from 1819 – 1988. Source of this information is the Bureau of Mineral Resources Canberra. Note, the datum of the water level is measured at the deepest spot in the lake.

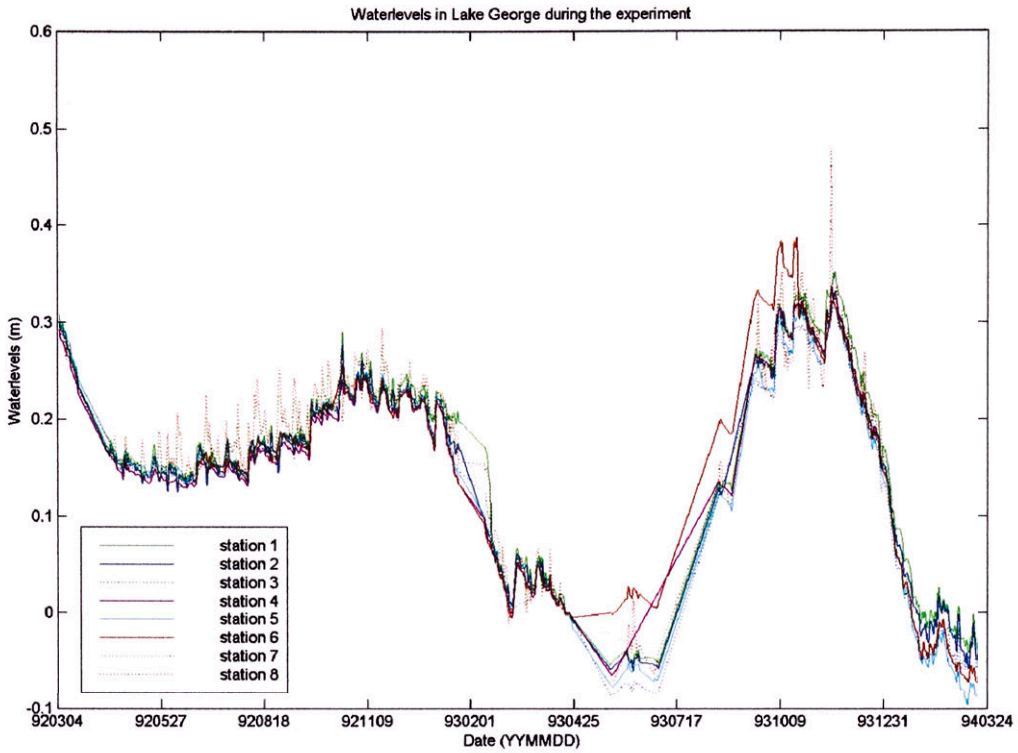

Figure 1.5 Levels measured during the Lake George Experiment. In the winter the rain filled the lake, while in the summer the water in the lake evaporated. Note that winter and summer in the southern hemisphere are around July and December respectively. The zero datum was the level of the lake at the time of measurement.

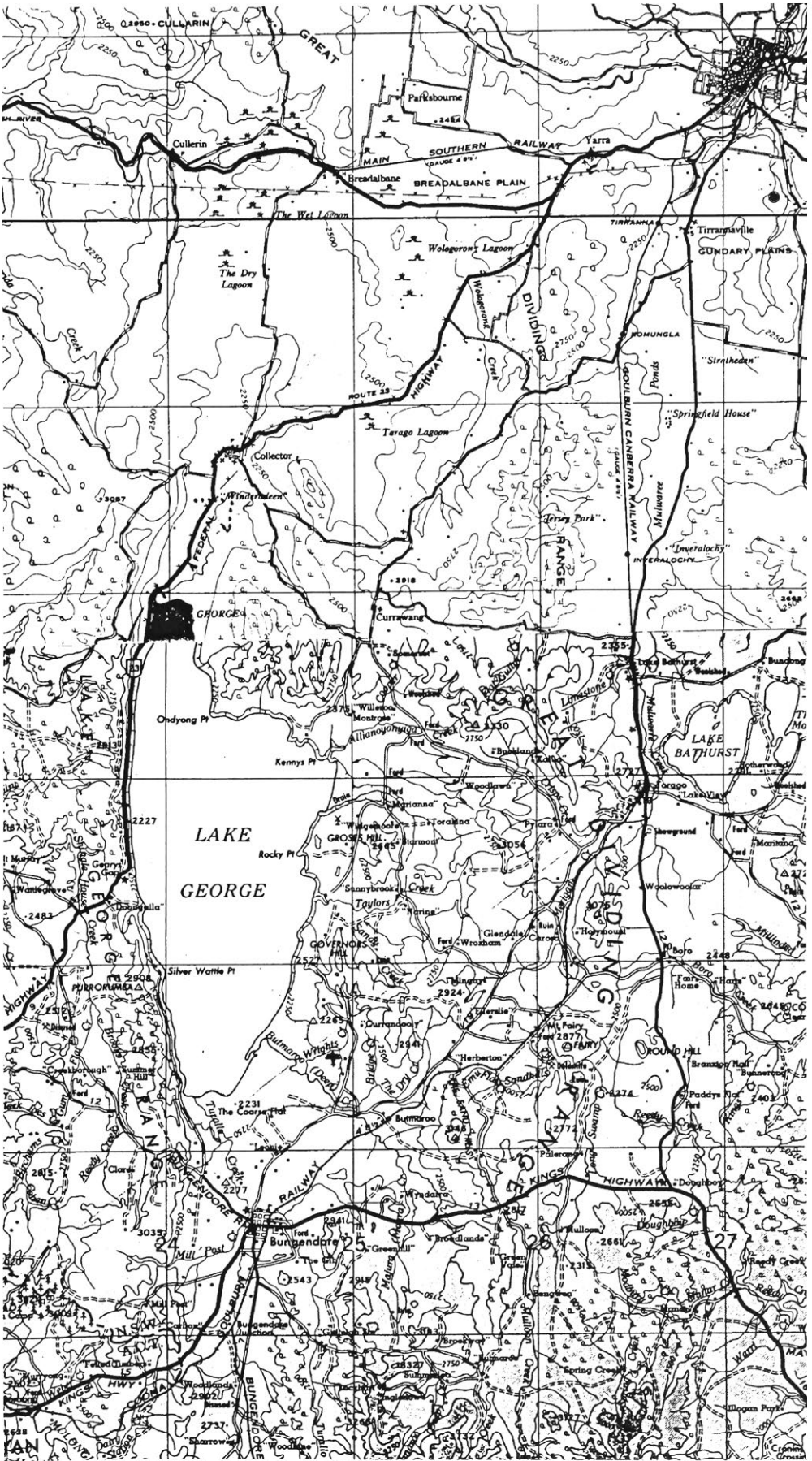

Figure 1.6 Detailed map of Lake George and surroundings

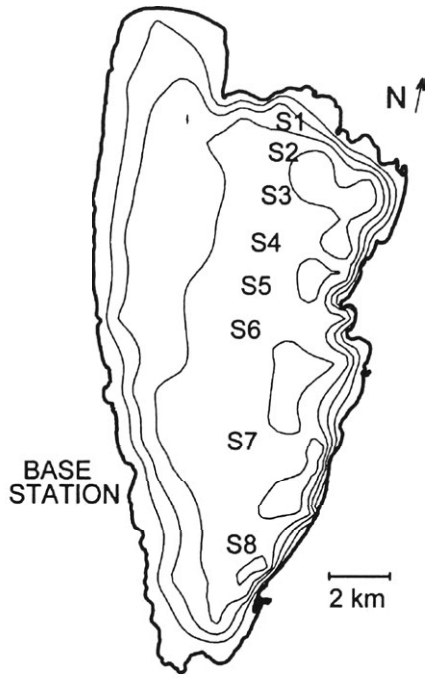

Figure 1.7 Bottom Contours of Lake George. Note the smoothness of the bottom. The deepest part of the lake was just over 2 metres deep during the experiment. The lake is nearly 24 kilometres long and 12 kilometres wide. The contours are every 0.5 metres

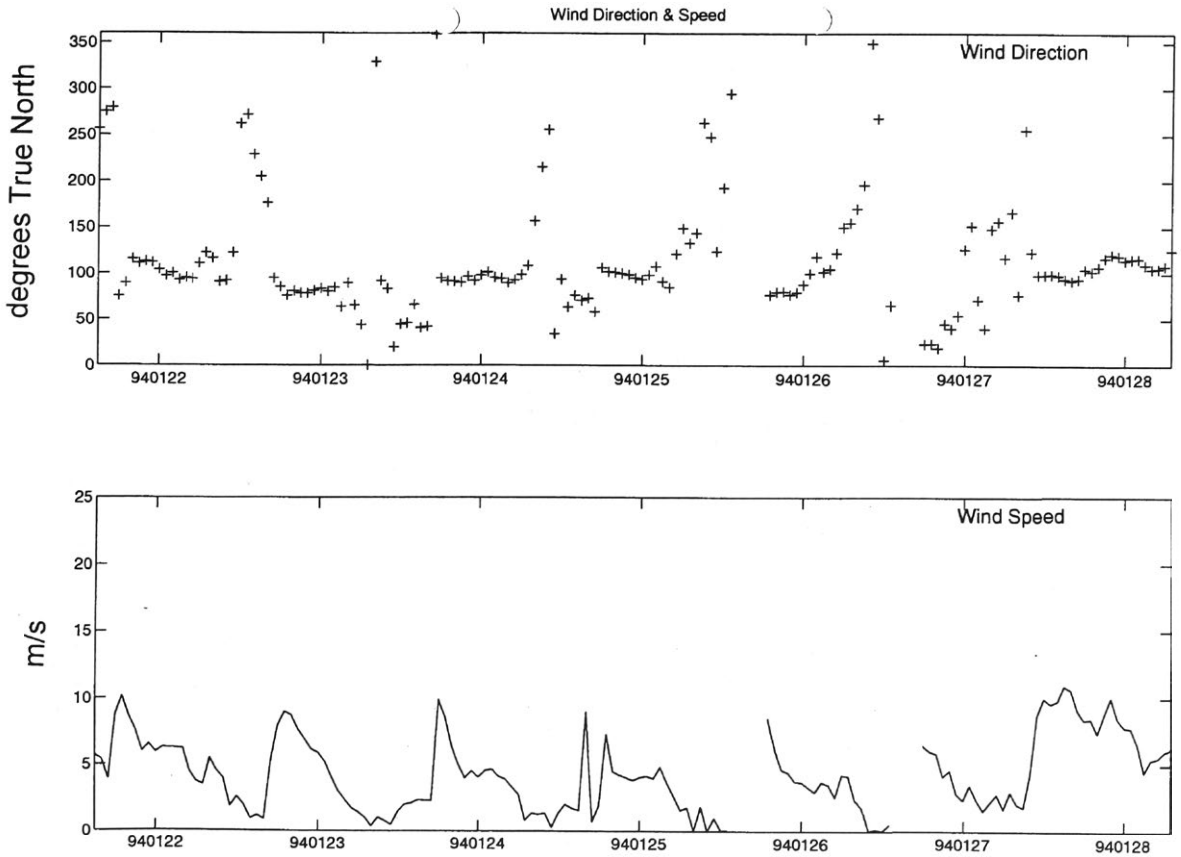

Figure 1.8 Wind Change in the afternoon at Lake George. Although Lake George is about 100 km inland and on a 500 metre high plateau, in the summer the sea breeze came between 4 and 5 o'clock in the afternoon. The dates are in the YYMMDD format. The y-axis on the wind direction graph is degrees true north and the y-axis on the wind speed graph is in metres/second.

Figure 1.9 Warning sign erected along the lake in the last part of the experiment. These were put up after the death of two fishermen, who drowned on the lake.

2.Description of the Lake George Experiment

2.Description of the Lake George Experiment

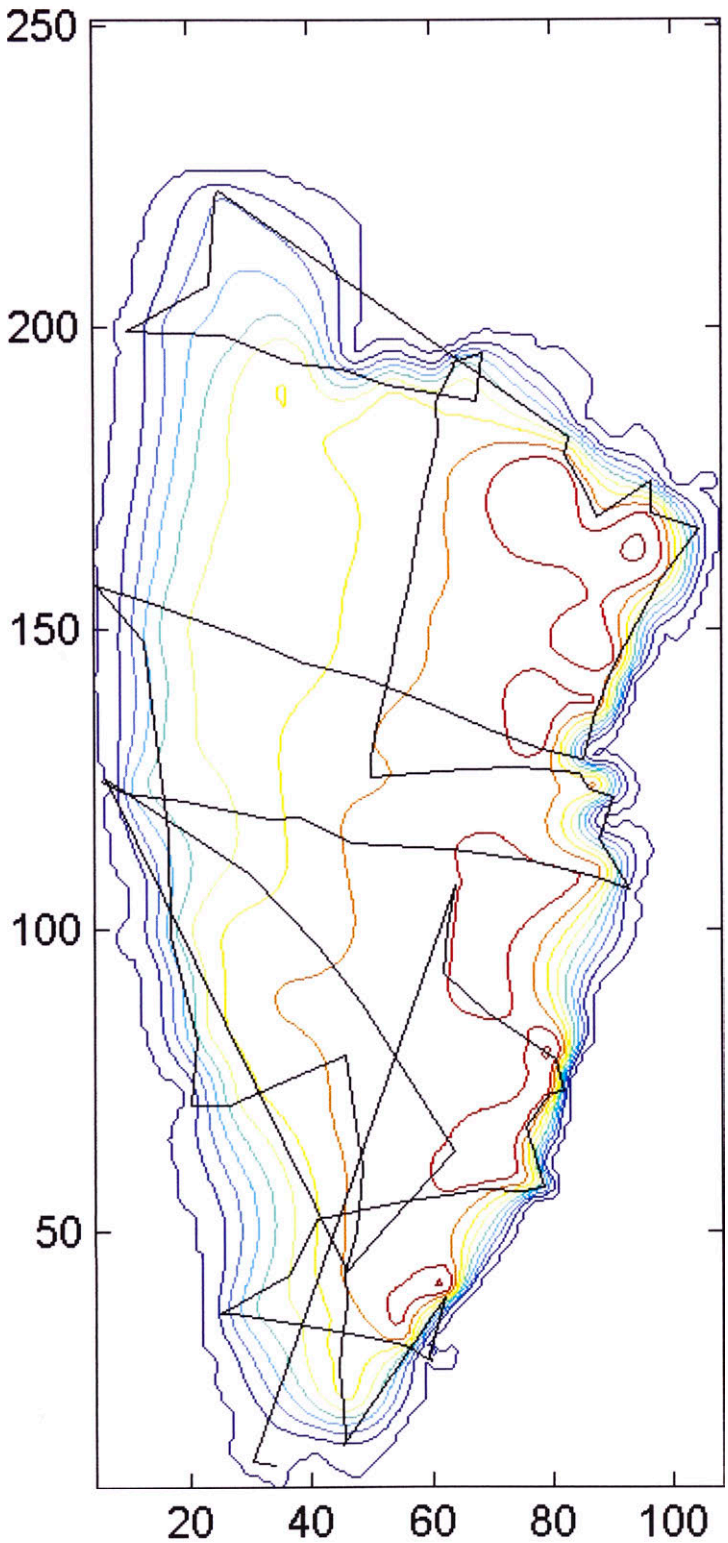

Figure 2.1 Outline of Lake George with the survey path. The black lines indicate the approximate path between two measurements. Other lines show the depth contours derived from the measurements.

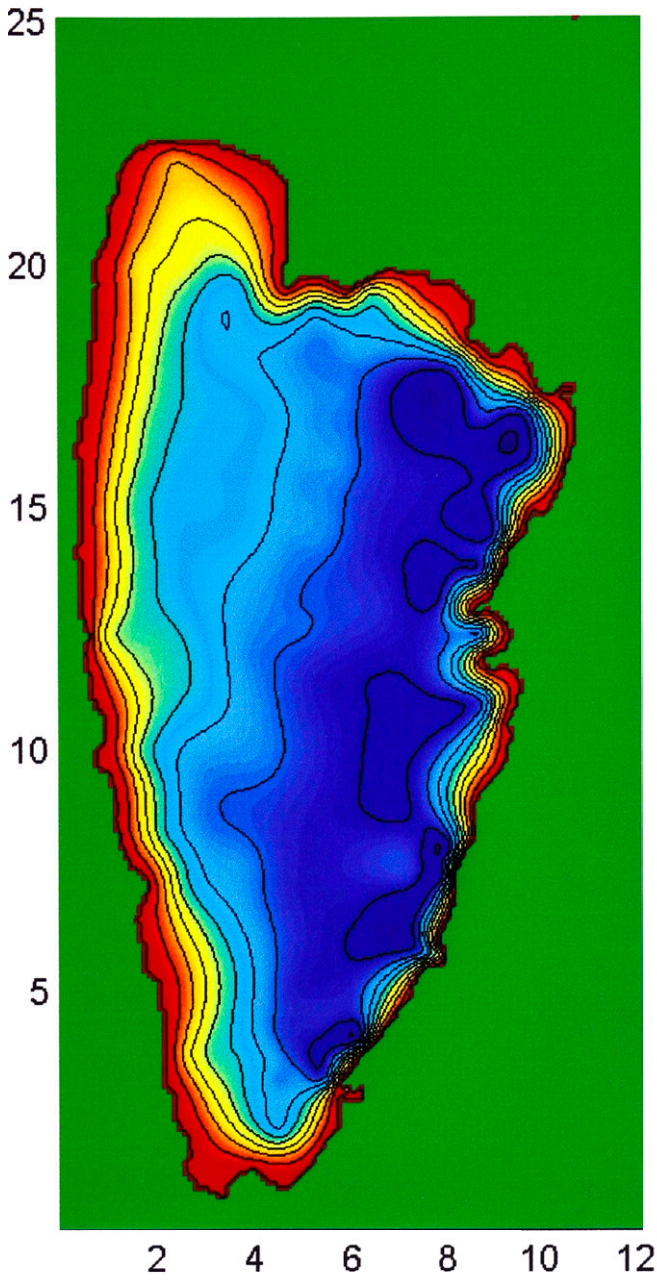

Figure 2.2 The bathymetry of Lake George. Contours every 0.2 metres. The datum is set to the level of the lake on the day of the survey. The axes are in units of kilometres.

Figure 2.3 The inflatable AVON with an inflatable keel instead of a wooden keel

Figure 2.4 The 4m aluminum fishing boat, called "tinny"

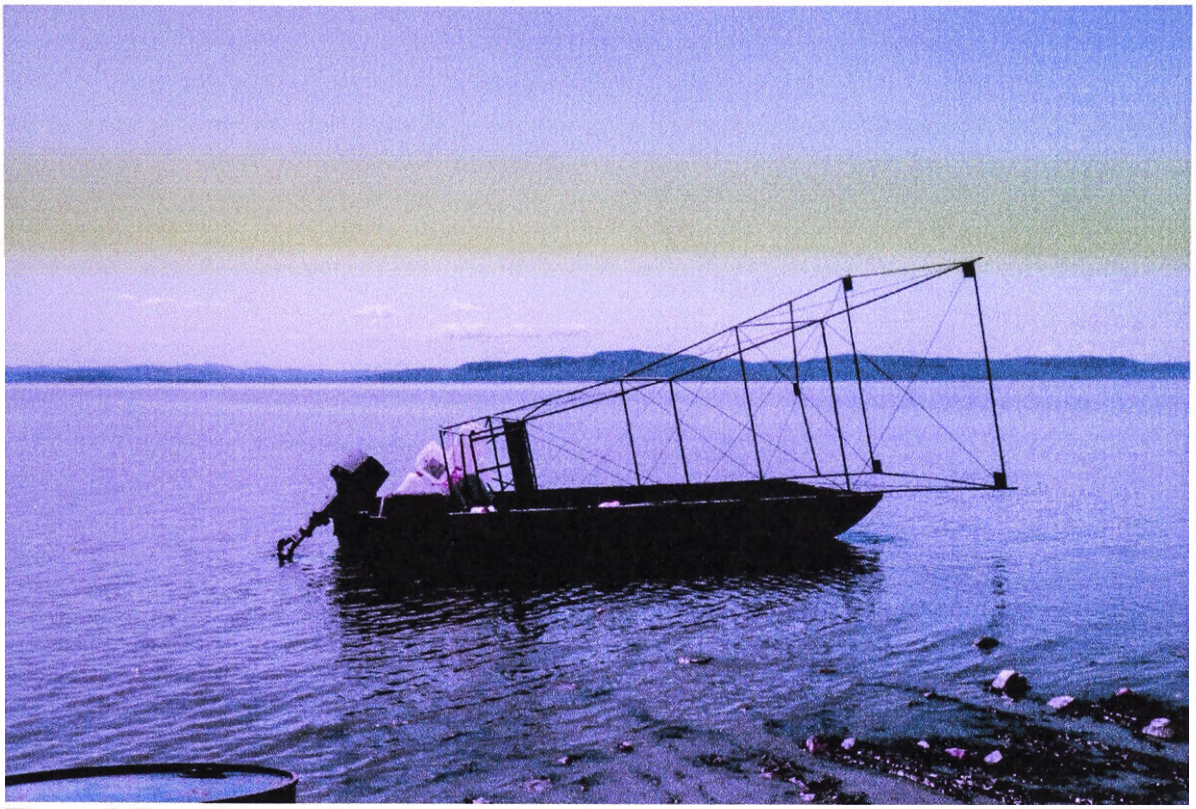

Figure 2.5 The assault craft of the Royal Australian Army.

Figure 2.6 The inflatable craft of the Royal Australian Navy. This boat was used to go out in rough weather. Unlike the first inflatable, it had a wooden keel.

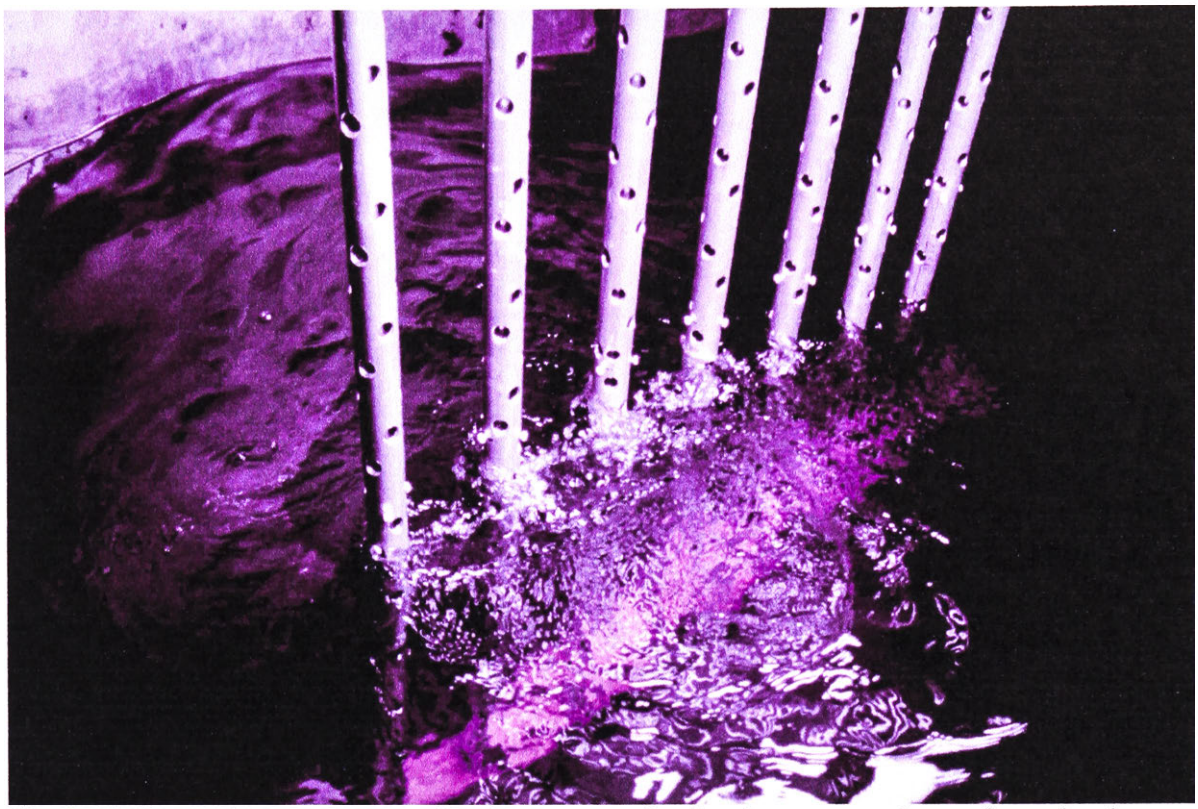

Figure 2.7 The wave measuring instrument finally chosen was the surface piercing transmission line gauges described by Zwarts (1974). This figure shows 7 Zwarts poles being tested in a flume.

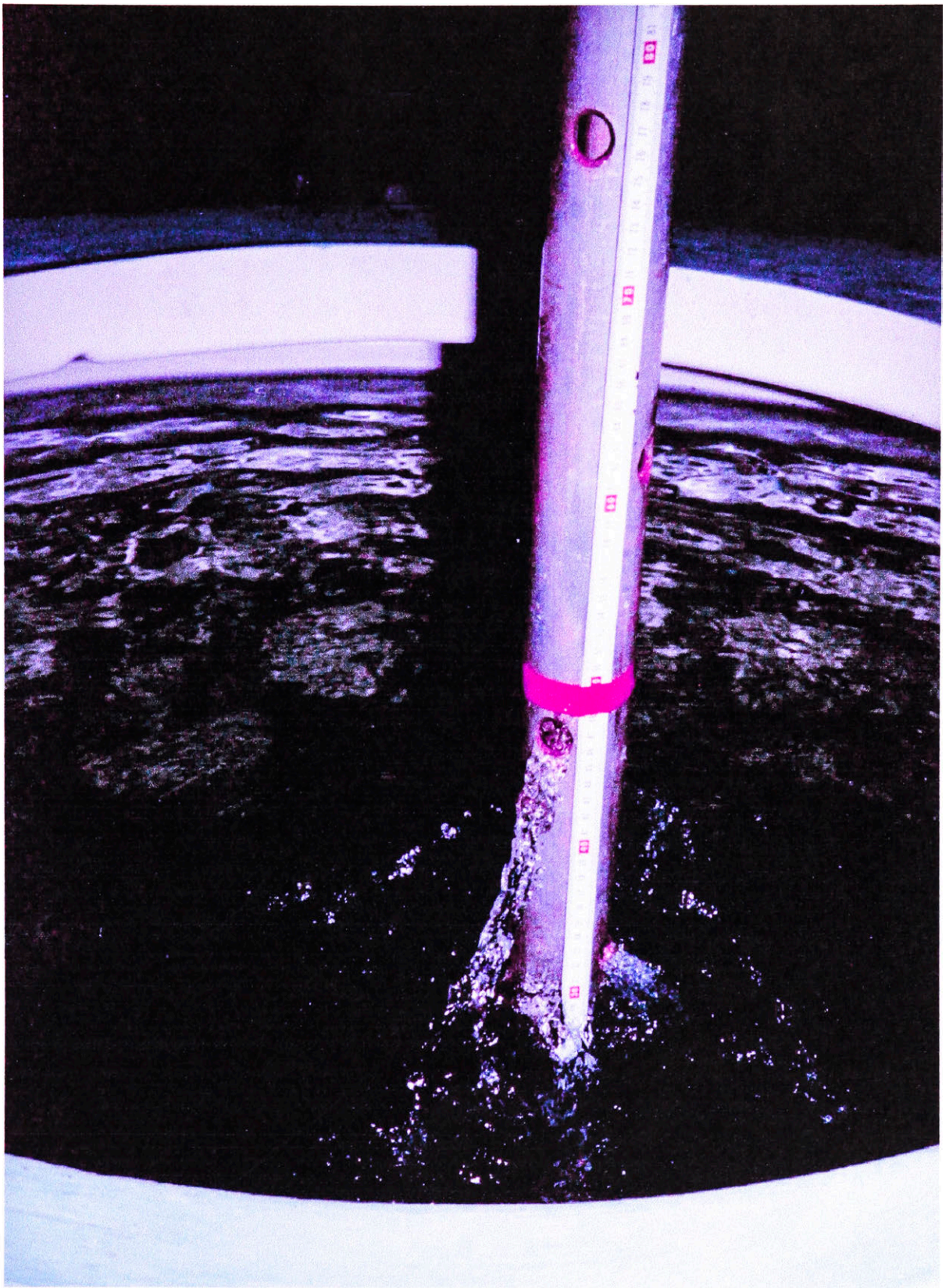

Figure 2.8 A Zwarts pole being tested to determine its dynamic response (transfer function). The Zwarts poles were constructed of two concentric aluminium tubes. The inner tube can be seen through the holes in the outer tube. In the experiment shown the pole was plunged in and out of a tank at a very high frequency with a unrealistically large amplitude. Therefore, the water level in the pole could not adjust fast enough to the water level outside the pole. This is clearly apparent as water is streaming from the holes.

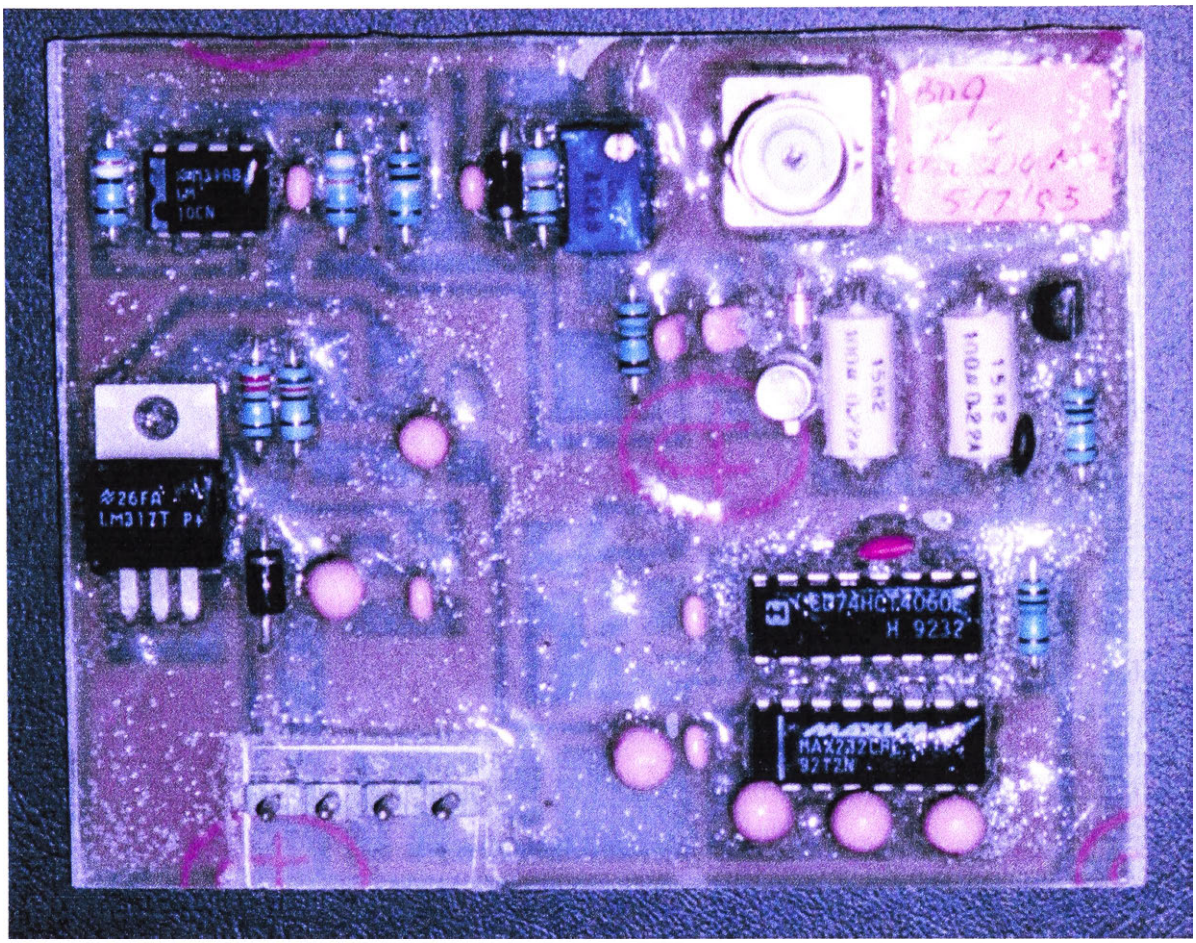

Figure 2.9 The electronics required to produce the standing (electrical) wave. These were skilfully designed and manufactured by the electronics section of the Department of Civil Engineering of the University of New South Wales, Canberra.

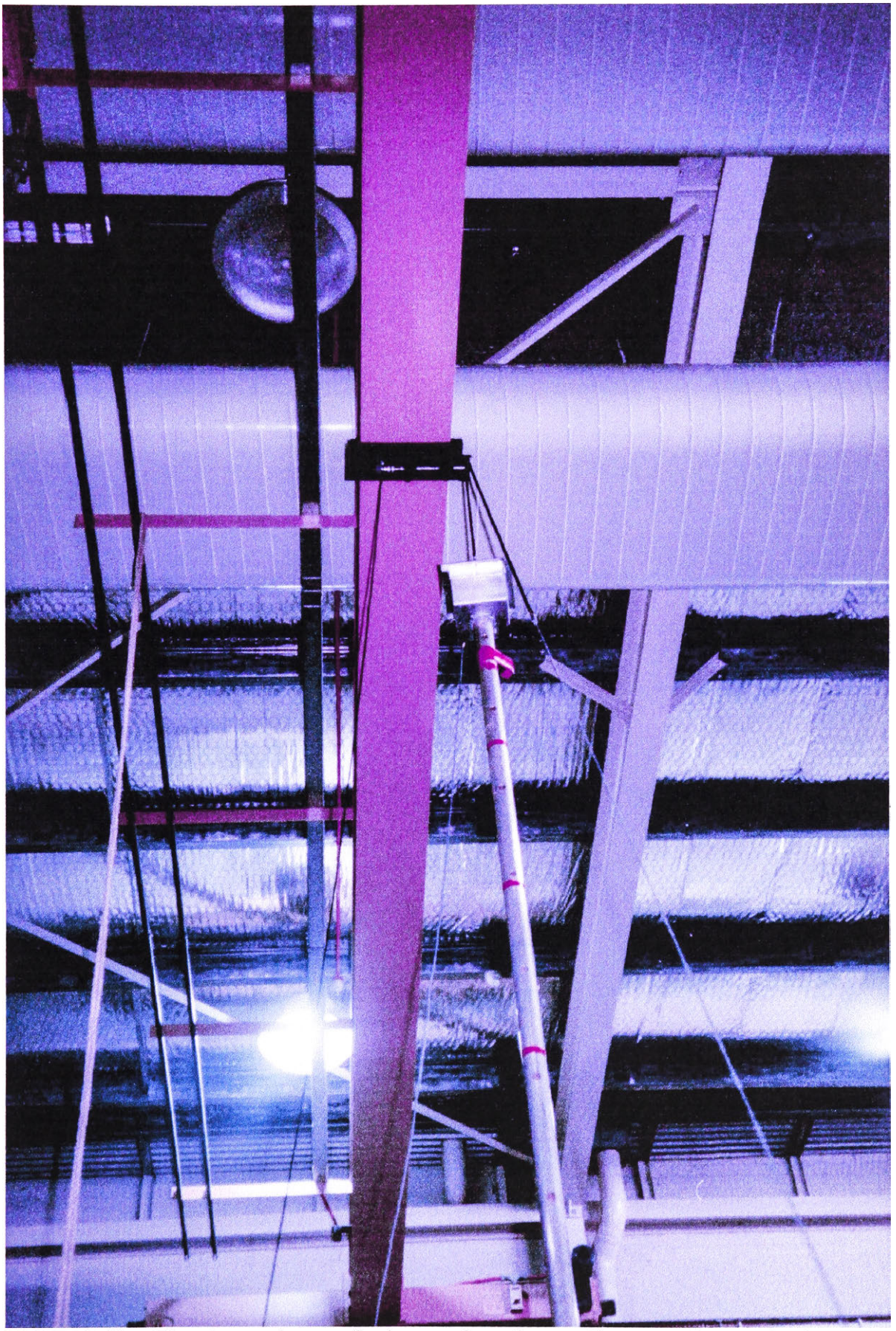

Figure 2.10 The electronics required to produce the standing wave is contained within a small waterproof enclosure fixed to the top of the pole.

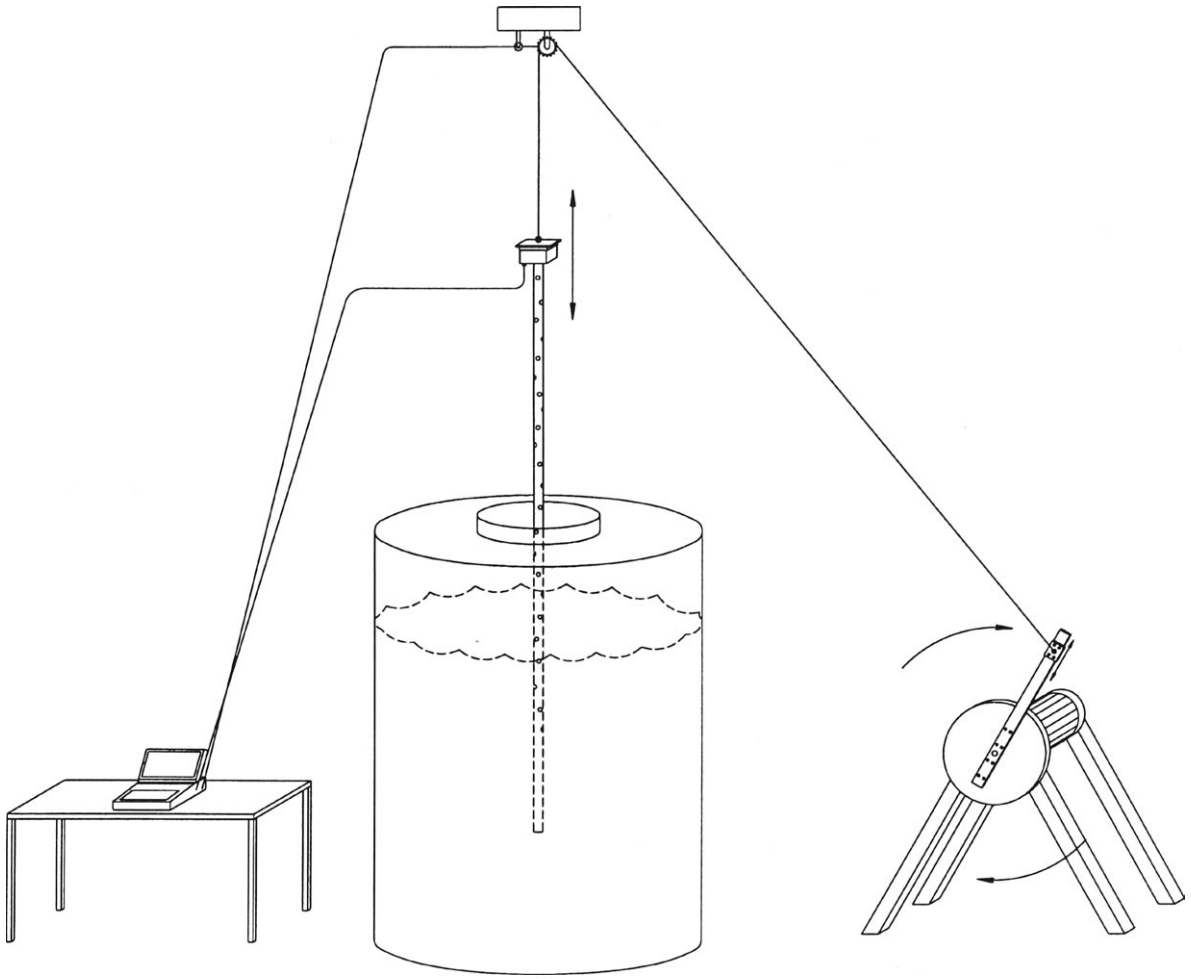

Figure 2.11 Schematic diagram of the system used to dynamically calibrate the Zwarts poles.

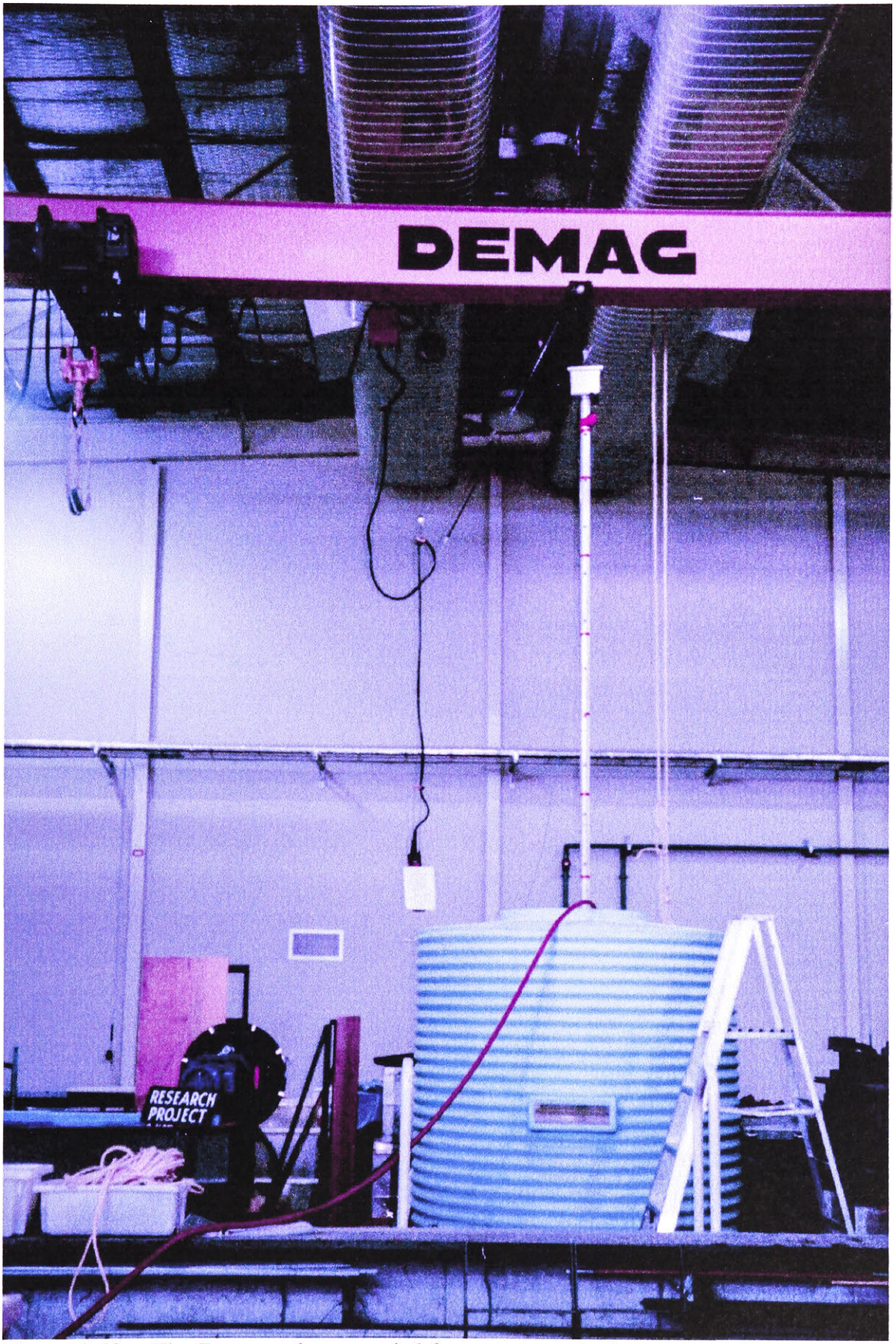

Figure 2.12 The Zwarts pole suspended from a cog on the beam above the water tank. Left of the water tank is the circular disk to which the arm of the electric motor was attached.

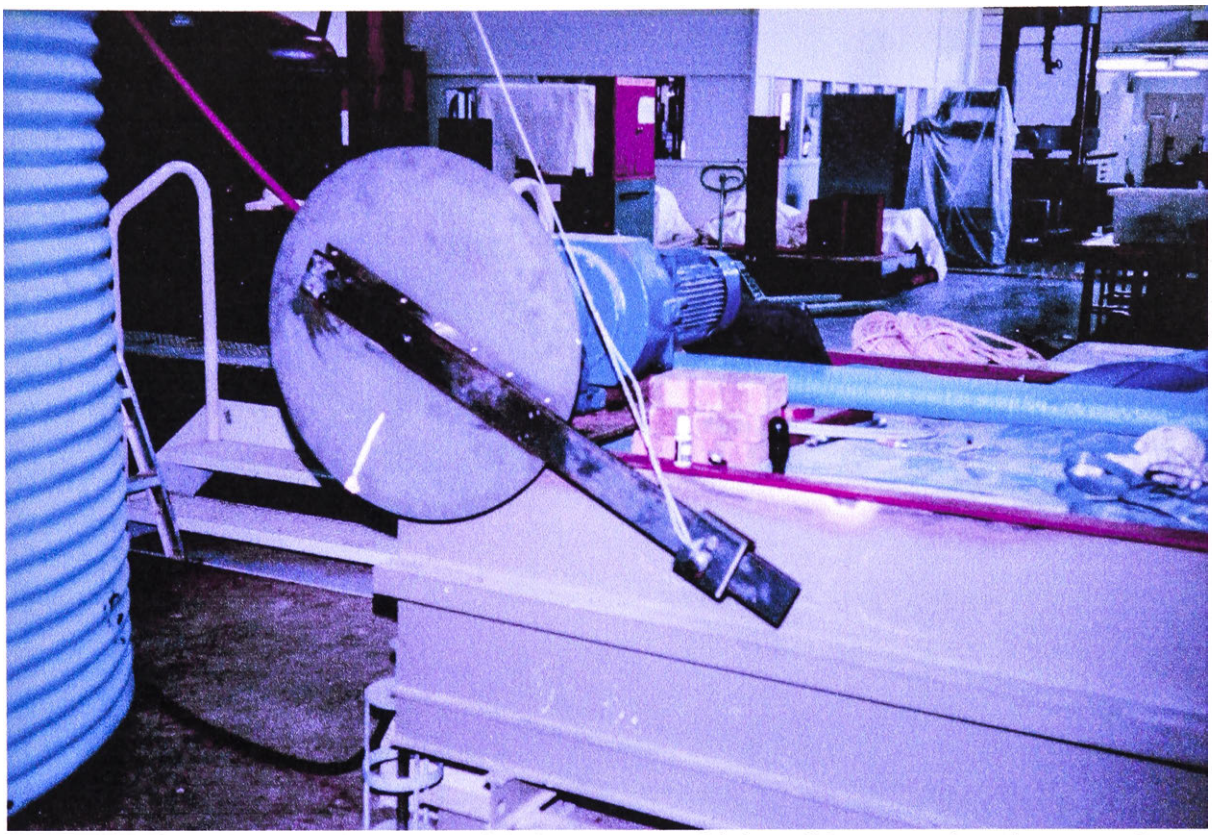

Figure 2.13 The electric motor with the arm on which a slider was placed to vary the amplitude of the raising and lowering of the Zwarts pole. The motor could be varied in speed to simulate different frequencies.

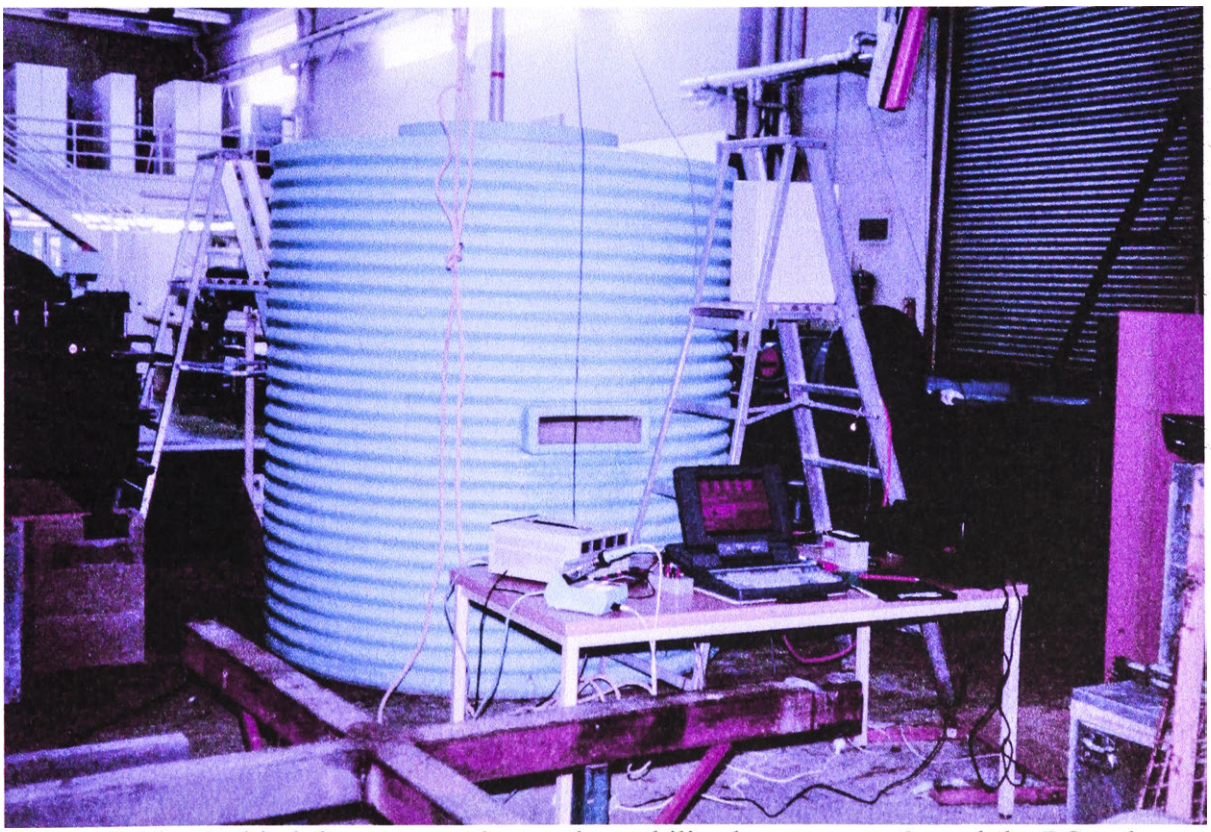

Figure 2.14 Behind the water tank was the stabilized power supply and the PC to log the signals from the variable resistor and the Zwarts pole.

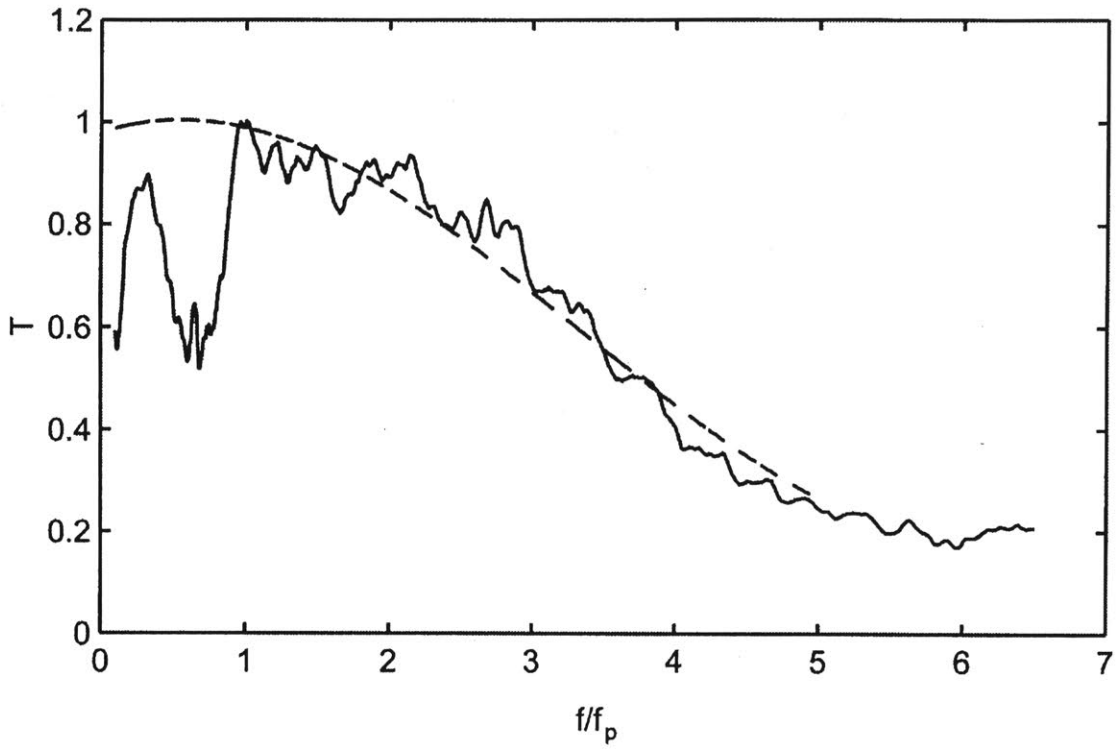

Figure 2.15 Transfer function for Zwarts poles determined from field comparison with resistance gauges. All spectra are cut off at $f/f_p = 5$ because of the limitation of the Zwarts poles frequency response. The transfer function below $f/f_p < 1$ is very sensitive to small changes due to the lack of energy in this part of the spectrum. Therefore it is assumed that the transfer function is equal to one in this region. The dashed line represents a polynomial fit to the experimental results.

Figure 2.16 Space frame tower shown before installation. About half the space frame would be submerged in the lake.

Figure 2.17 Hammering of one of the anchors into the lake bed. Note the guy wire still hanging lose.

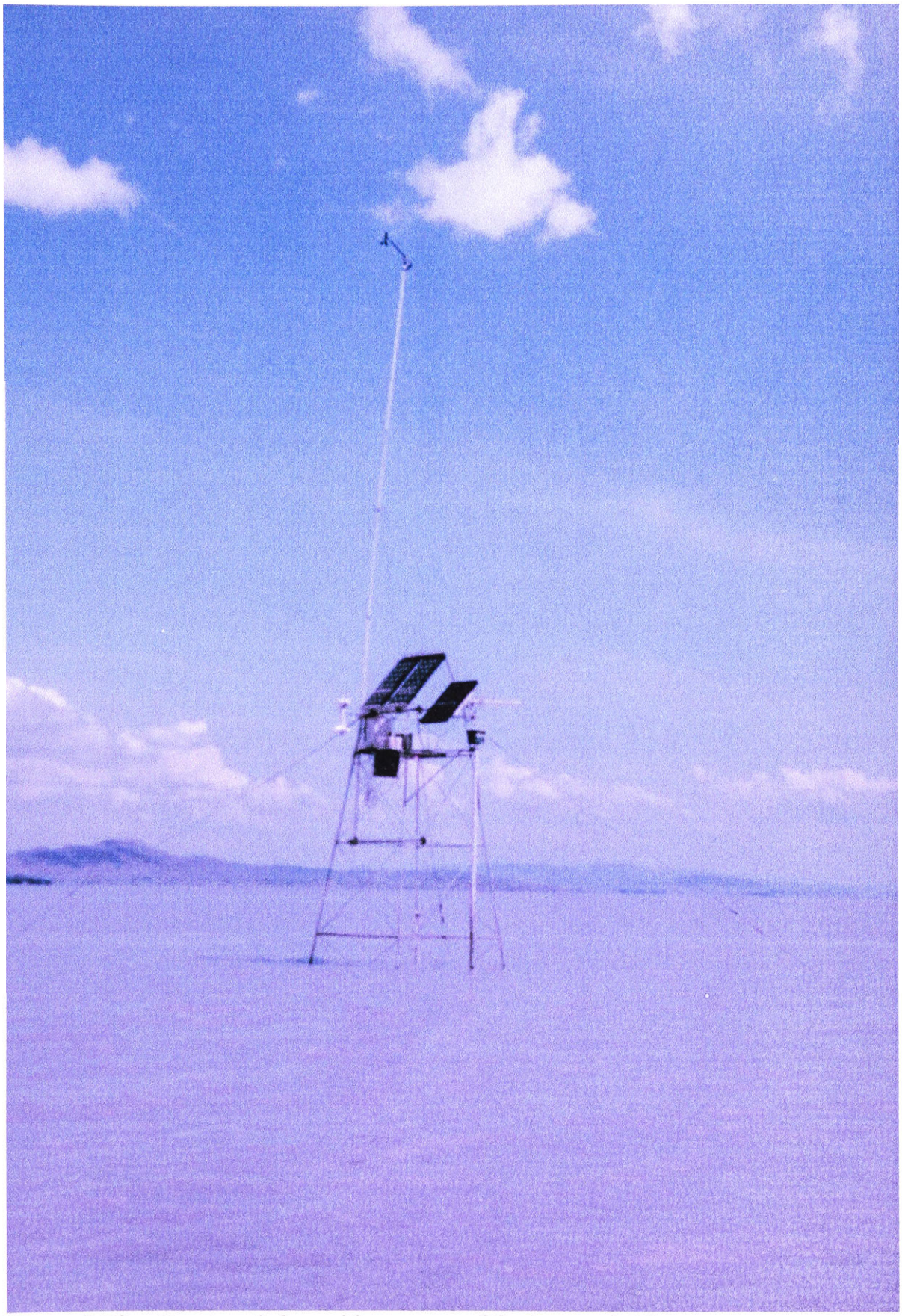

Figure 2.18 Zwarts pole in position on one of the towers. A 10 metre anemometer mast is also placed on this tower. All towers had solar panels that had to be cleared of bird droppings regularly.

Figure 2.19 Radio and Counter Card box on the tower.

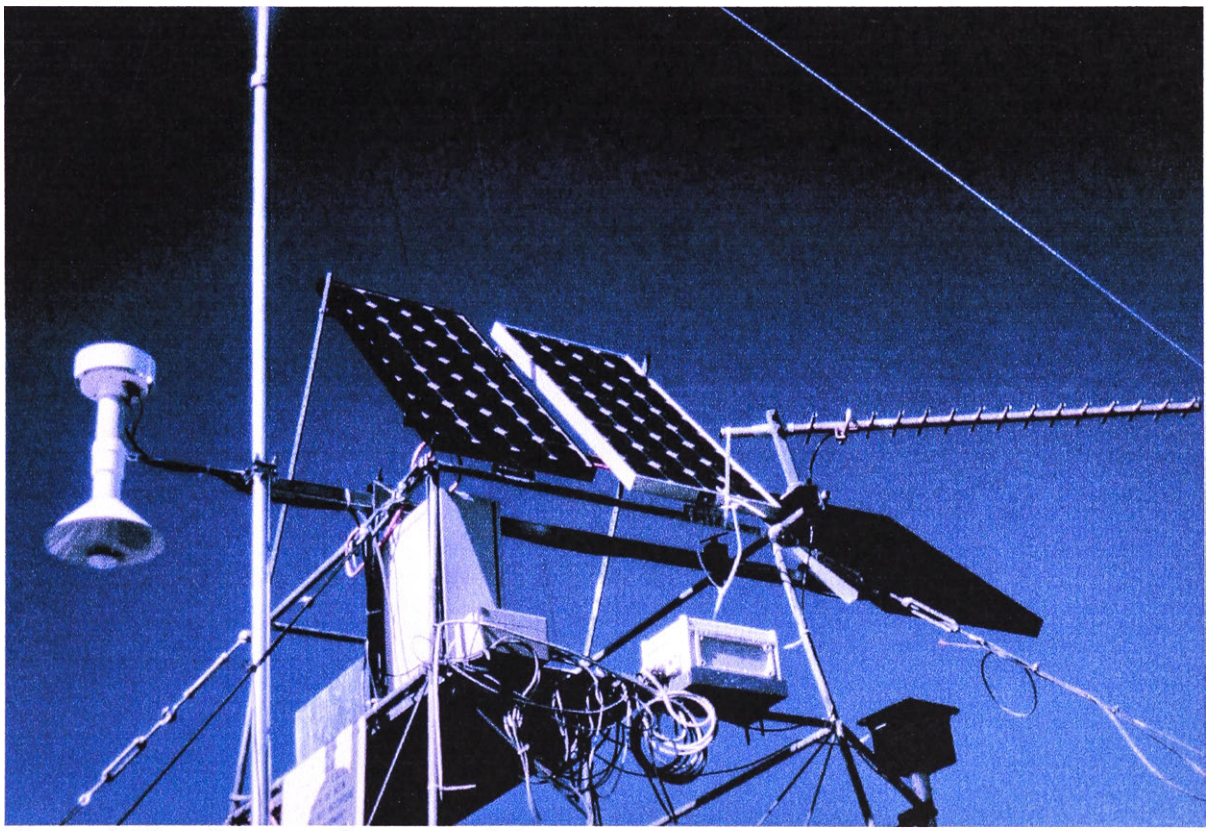

Figure 2.20 Solar panels on top of the tower to supply power for the electronics and radio.

Figure 2.21 The extra anemometer masts which were located at 4 stations.

Figure 2.22 One of the towers being deployed on the assault craft provided by the Royal Australian Army.

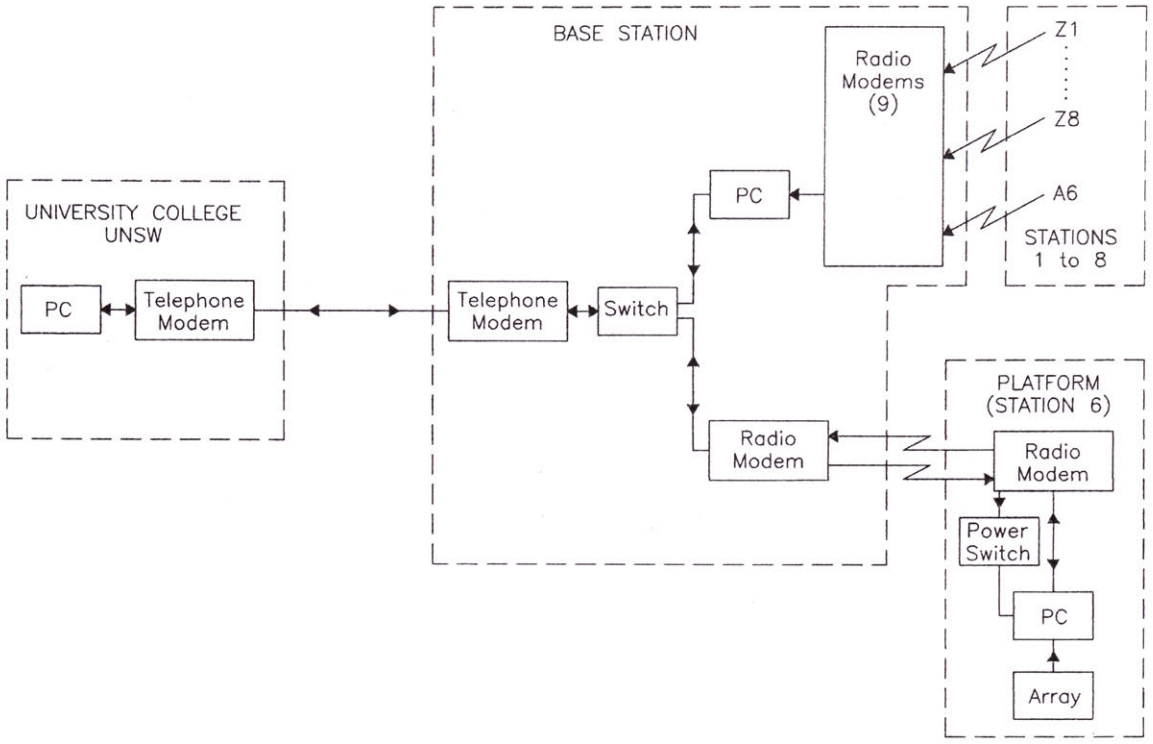

Figure 2.23 Schematics of the radio links at Lake George.

Figure 2.24 Platform at Station 6.

Figure 2.25 A sonic anemometer deployed at the end of the 4m long measurement bridge at the platform (station 6).

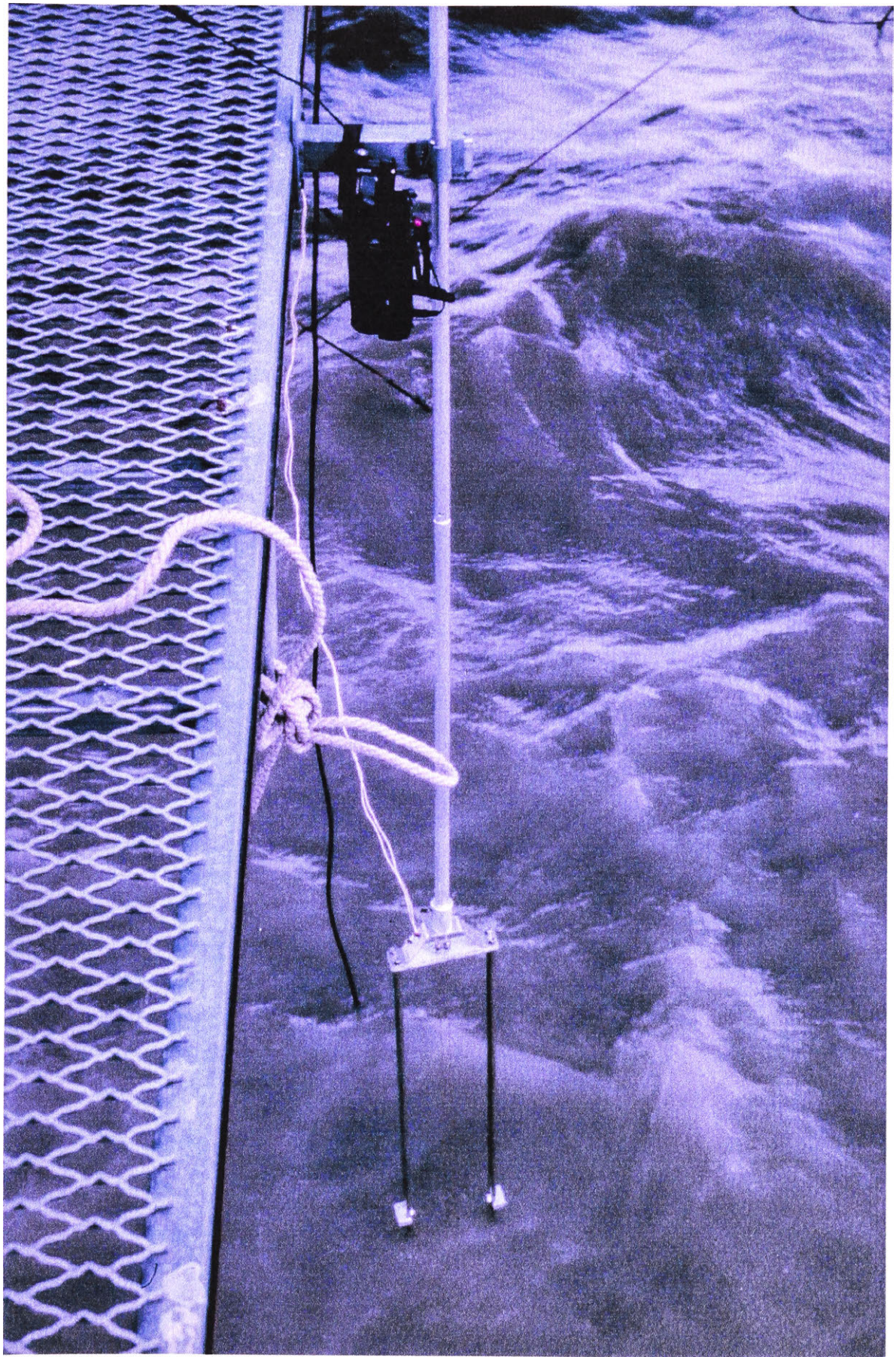

Figure 2.26 Video, wave measuring gauge, hydrophone (under water) taking measurements from the measurement bridge.

Figure 2.27 The base station on the western shore of the lake.

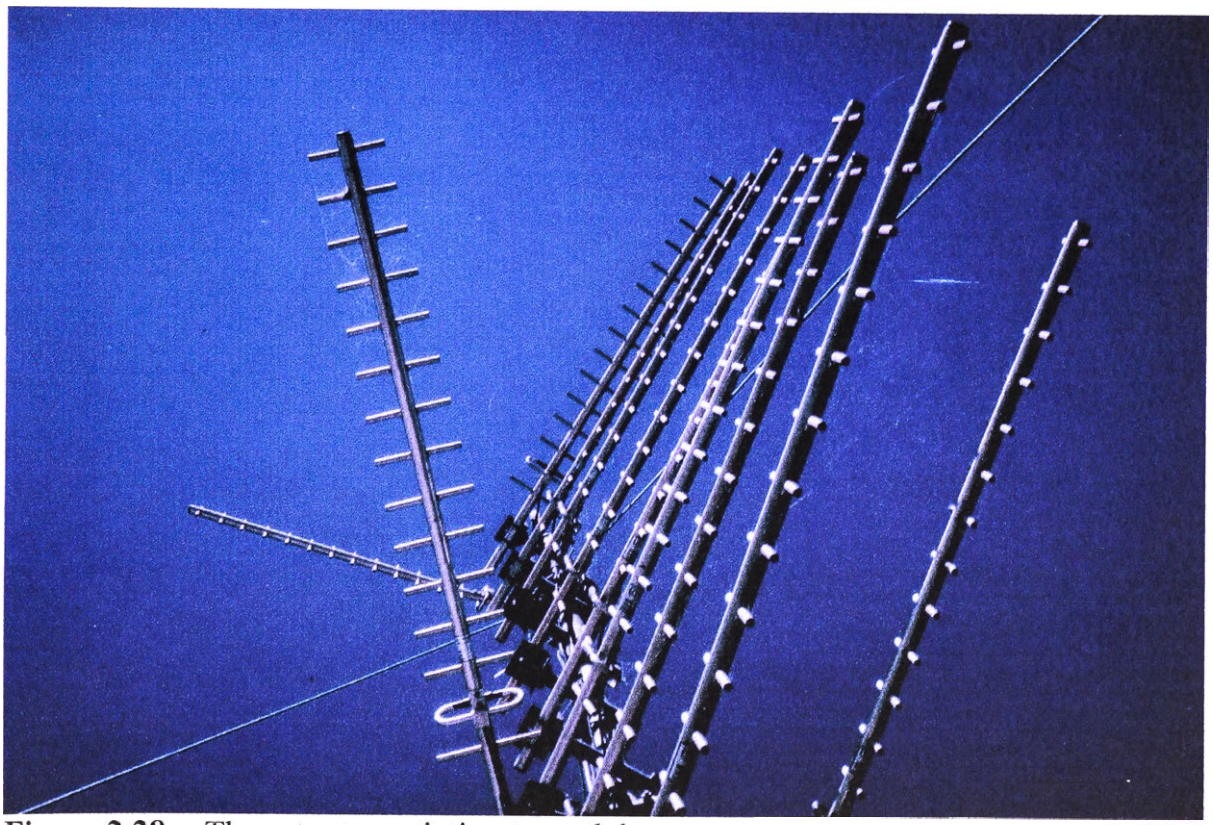

Figure 2.28 The antennas pointing toward the towers.

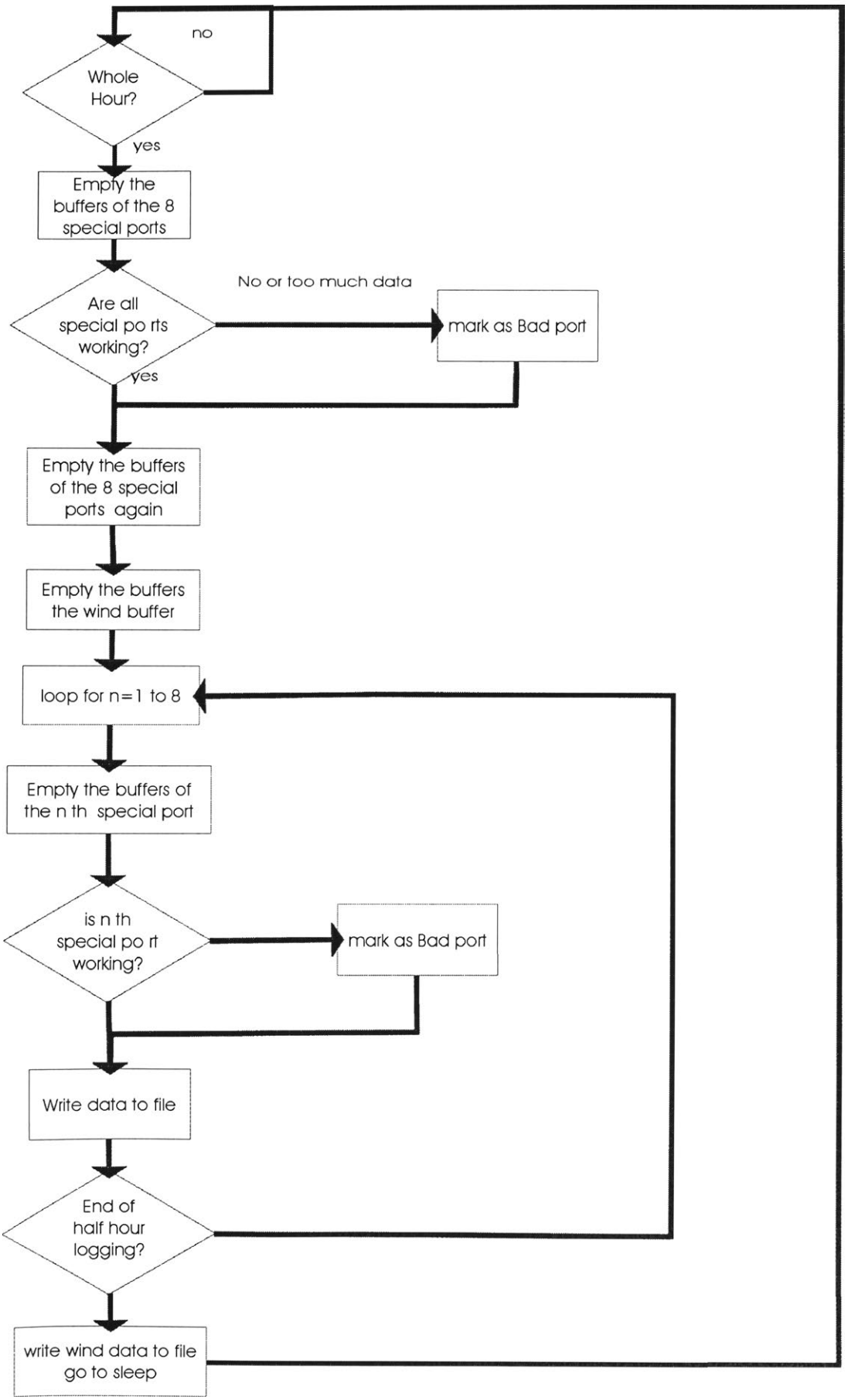

Figure 2.29 A flow chart of the data acquisition software.

Figure 2.30 Weekly down loading of the data onto a portable PC.

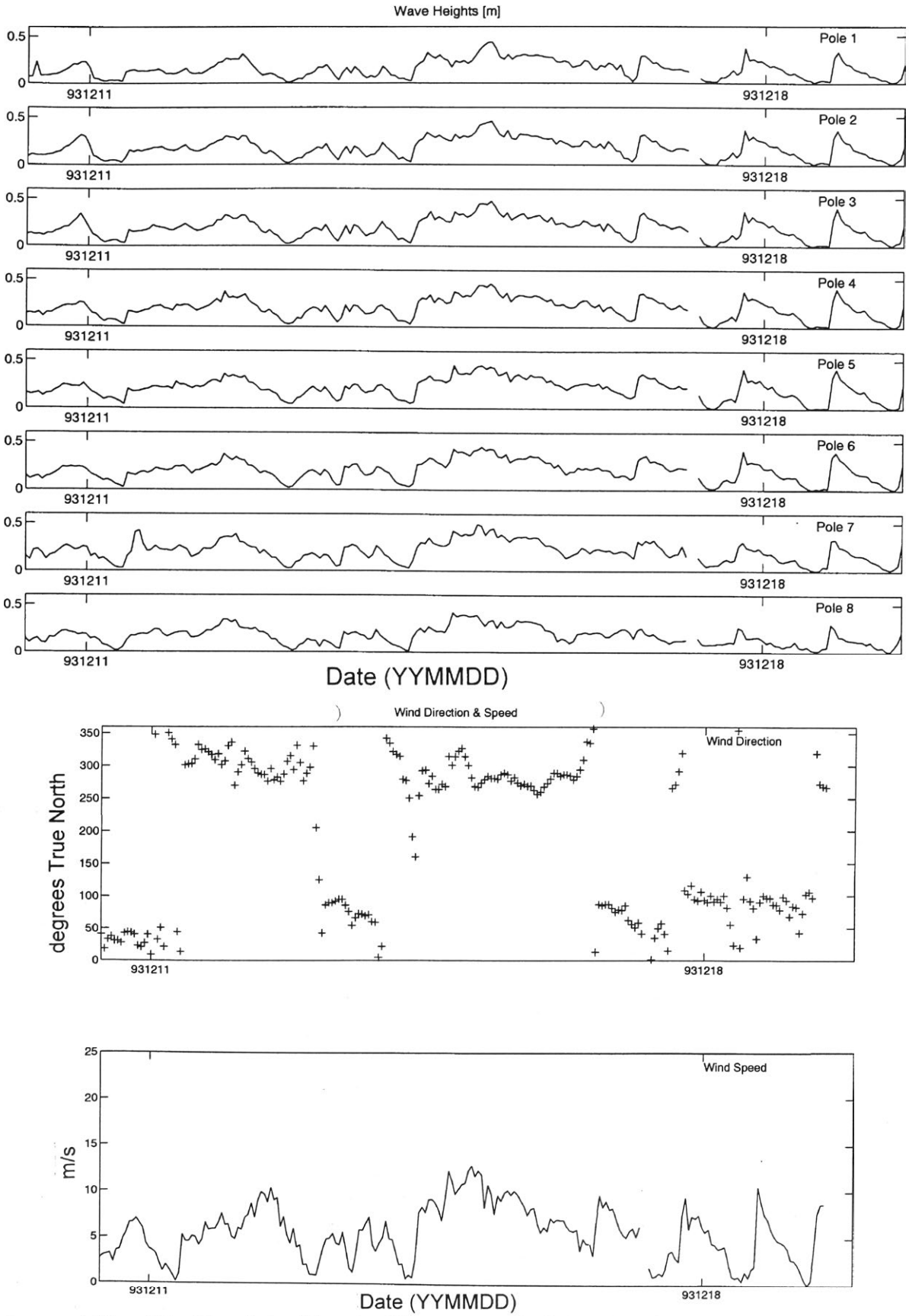

Figure 2.31 Weekly plot of the significant wave height, the wind speed and wind direction. This was done as a check that none of the stations were behaving abnormally.

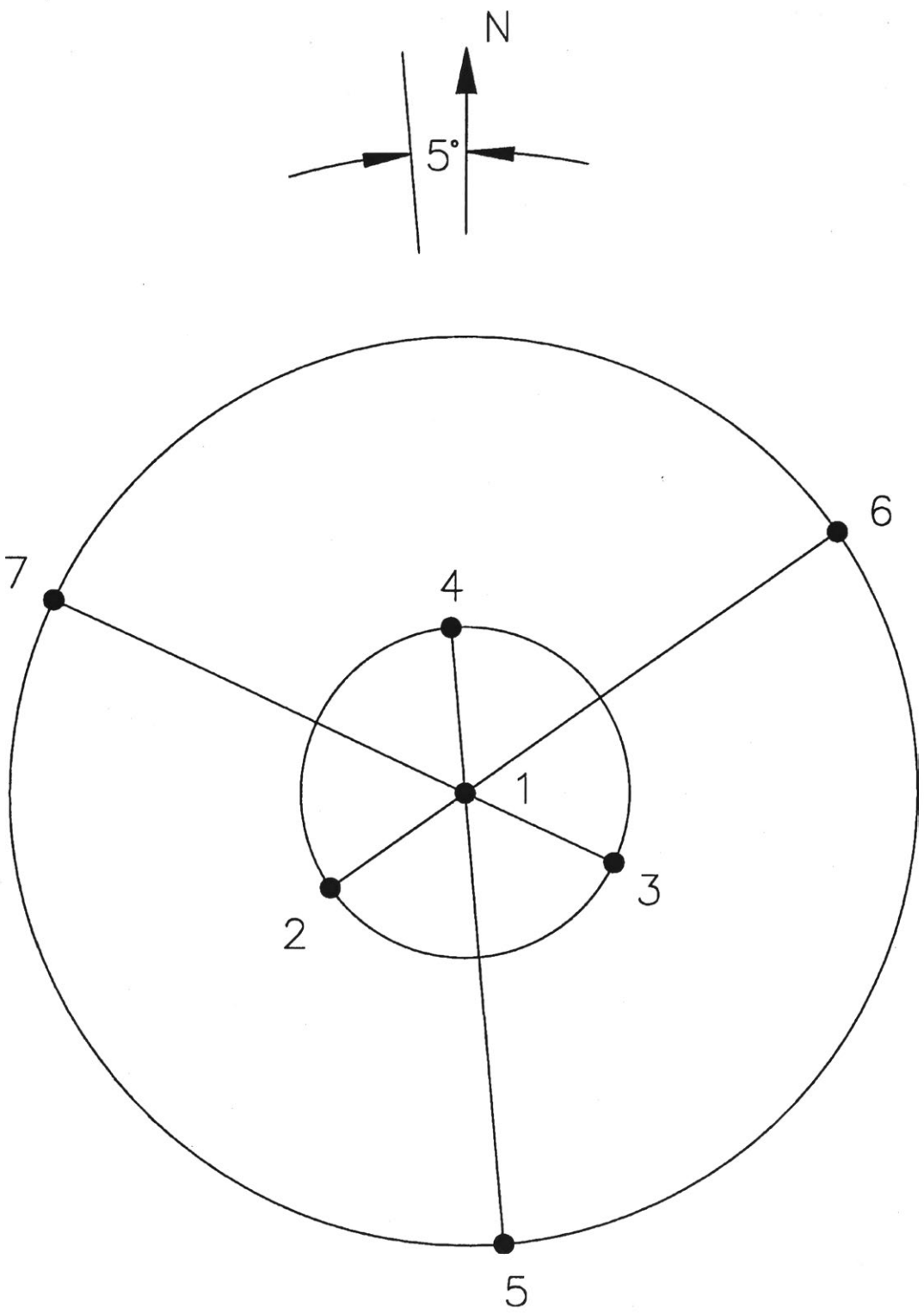

Figure 2.32 The arrangement of Zwarts poles in the spatial array. The poles are configured in the shape of a "Mercedes" star.

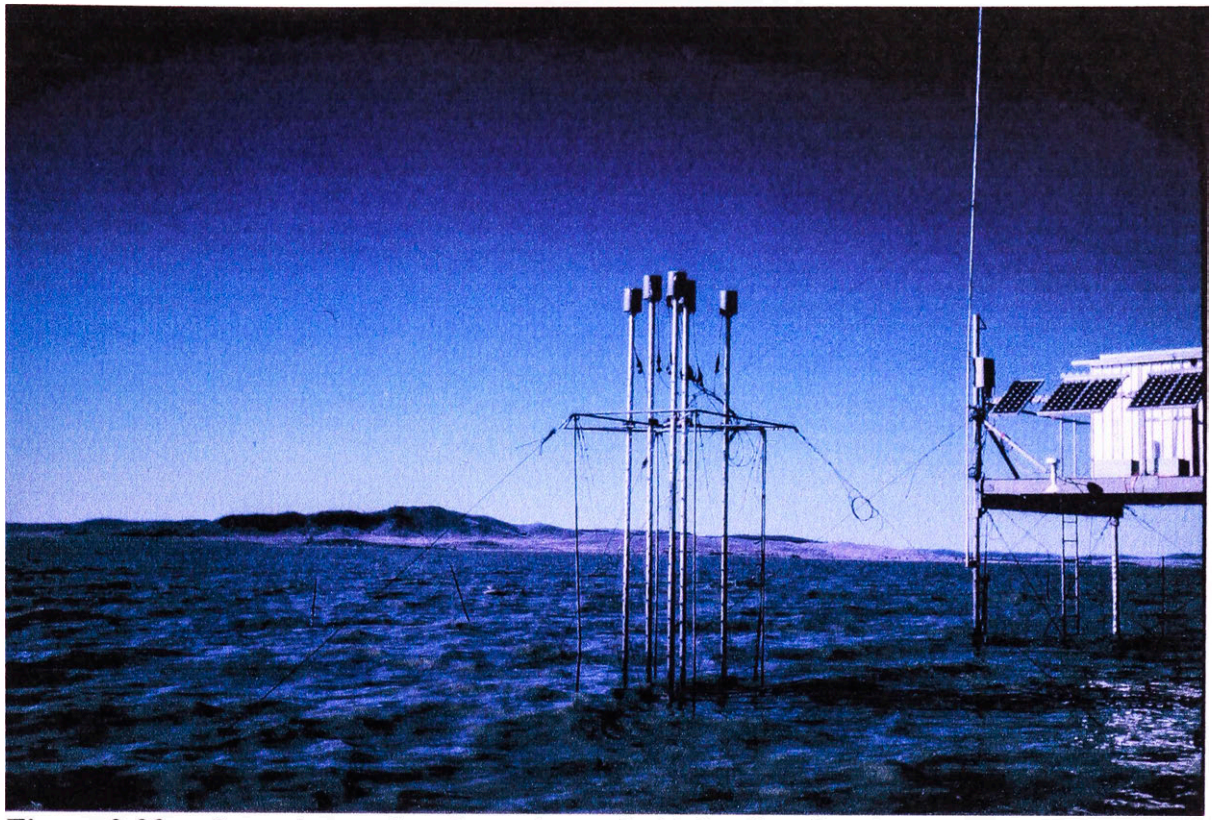

Figure 2.33 Guy wires and anchor wires to hold the directional array in place.

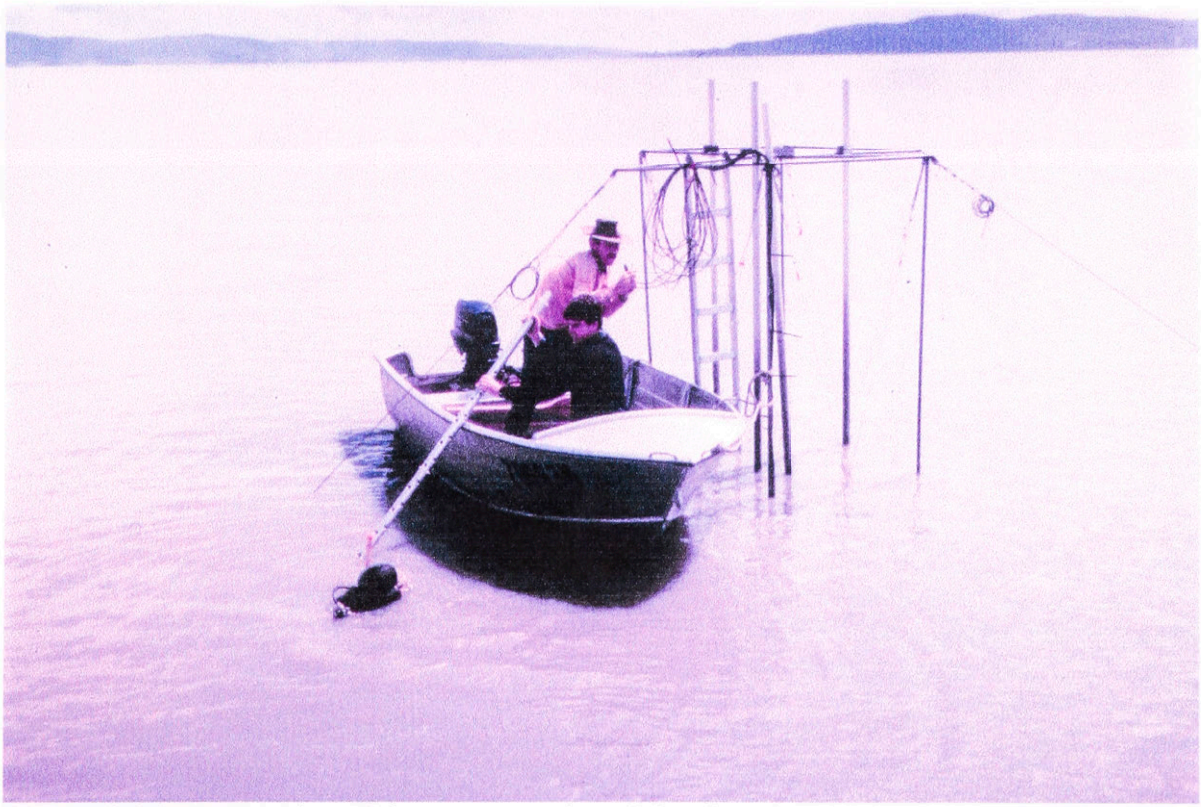

Figure 2.34 Mounting of the Zwarts poles of the directional array after cleaning. Note the diver in the water who is about to install the pole underwater.

3. Results from Lake George

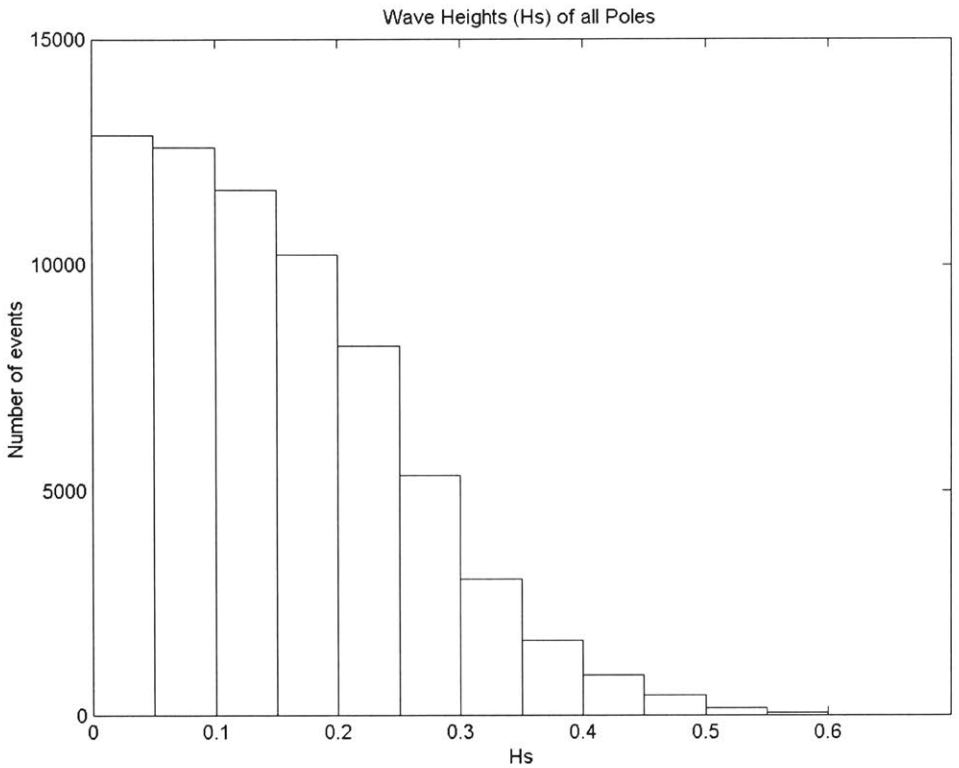

Figure 3.1 Distribution histogram for H_s (m) measured at all eight stations.

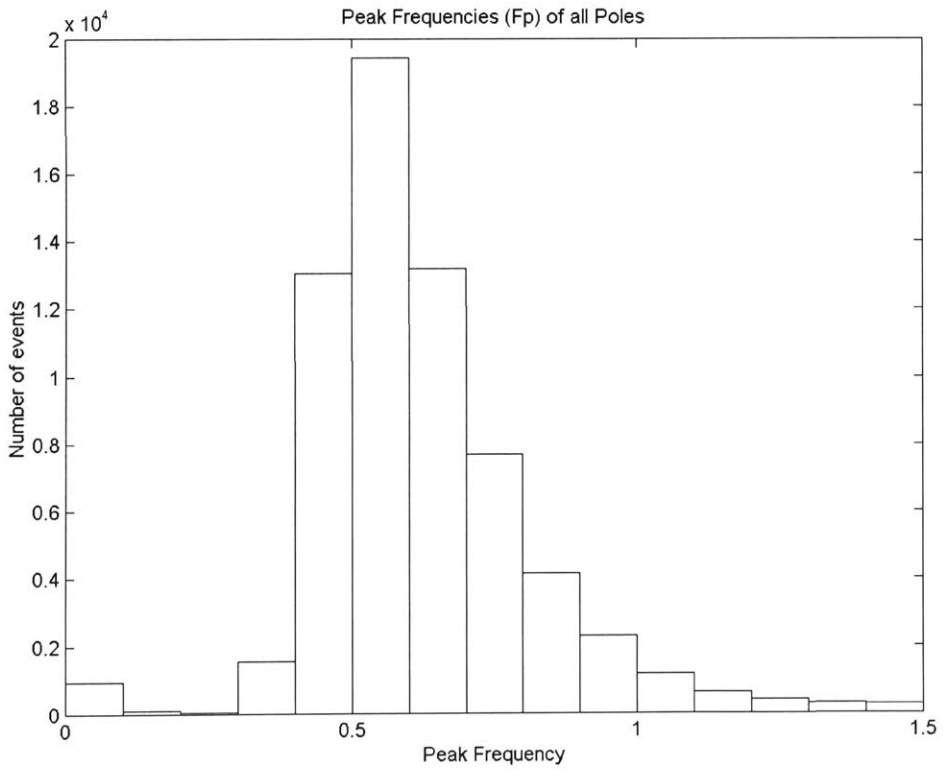

Figure 3.2 Distribution histogram for f_p (Hz) measured at all eight stations.

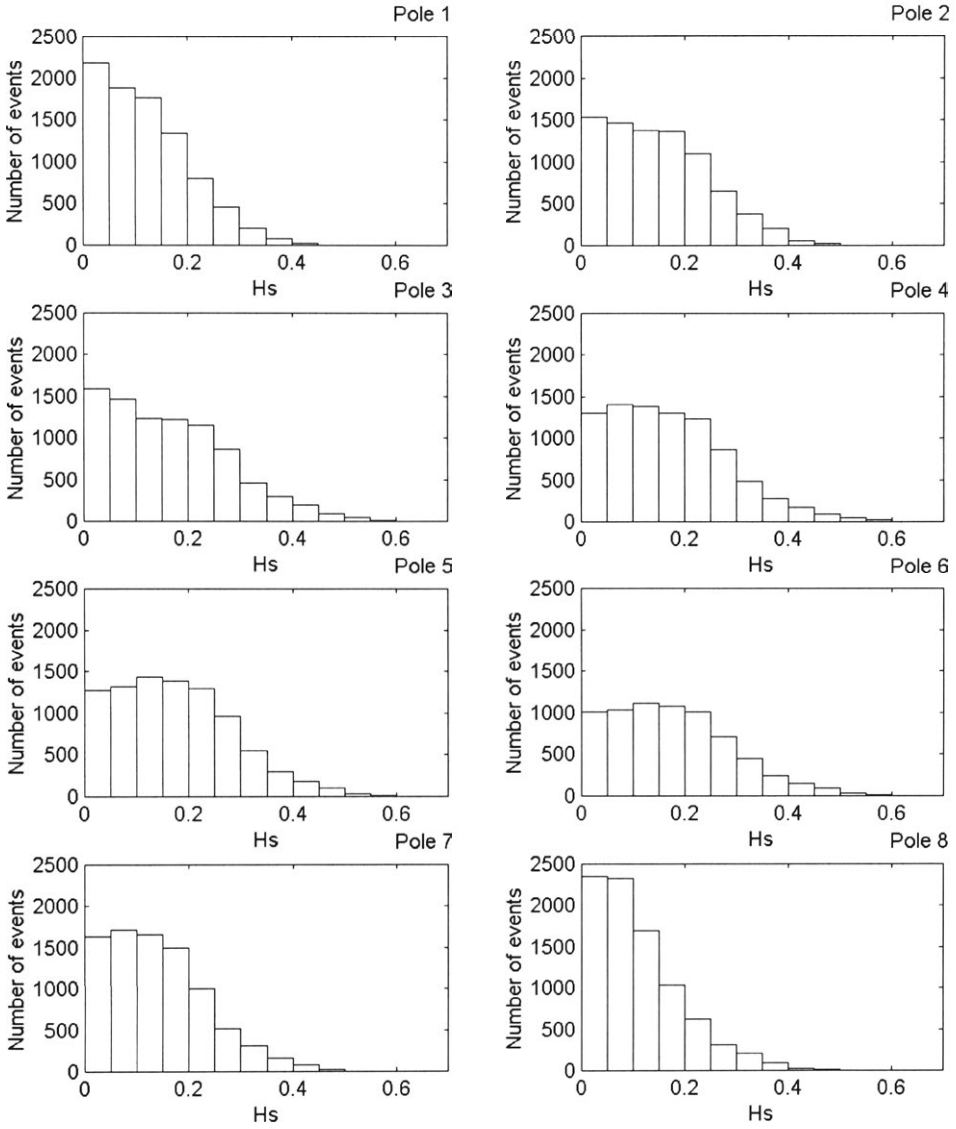

Figure 3.3 Histograms of significant wave height (H_s in metres) for each station. One interesting feature of these graphs is that the stations in the middle of the lake have higher wave heights on average, than the stations at the ends. This occurs since a significant proportion of the data are for east/west winds for which stations 1 and 8 have relatively short fetches.

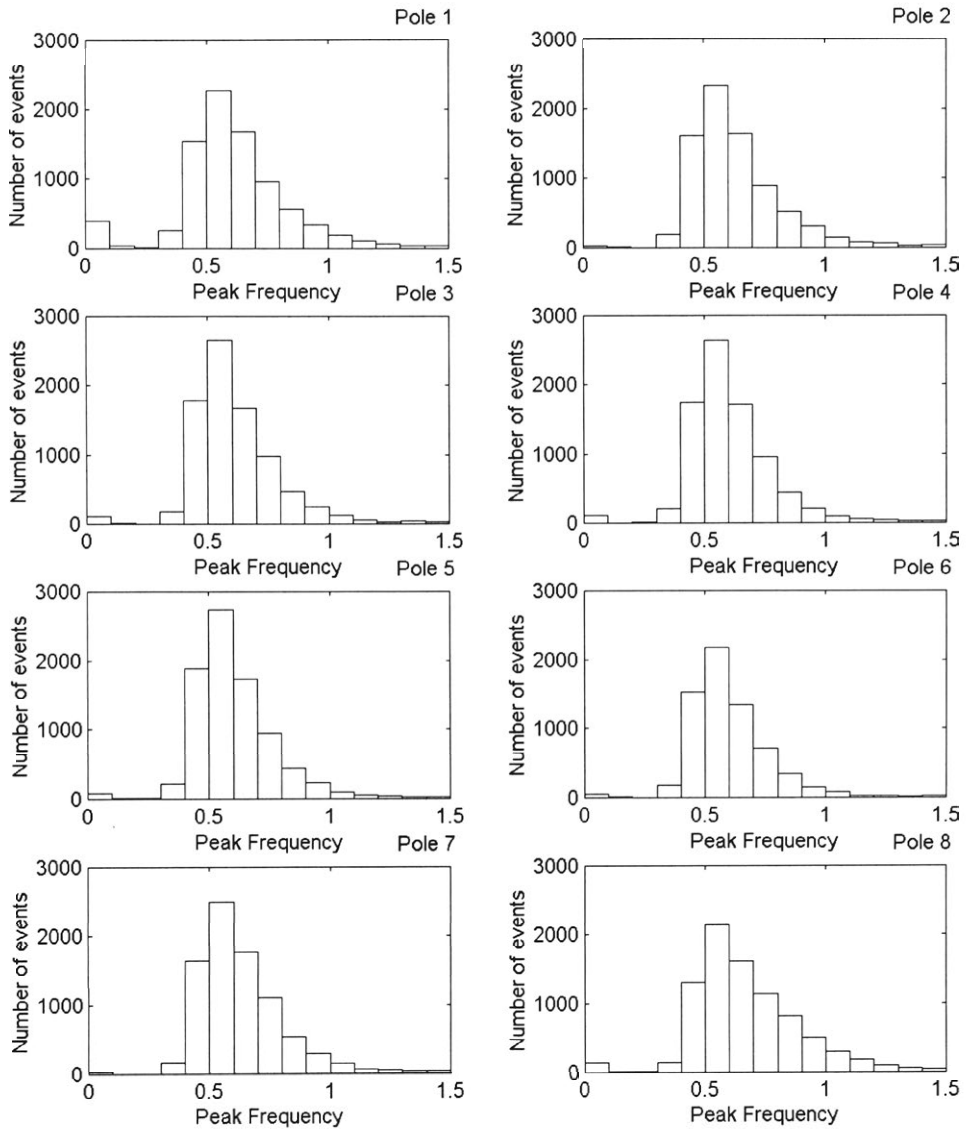

Figure 3.4 Histograms of peak frequency (f_p in Hertz) for each of the stations. Note, unlike the significant wave height there is no obvious trend with position.

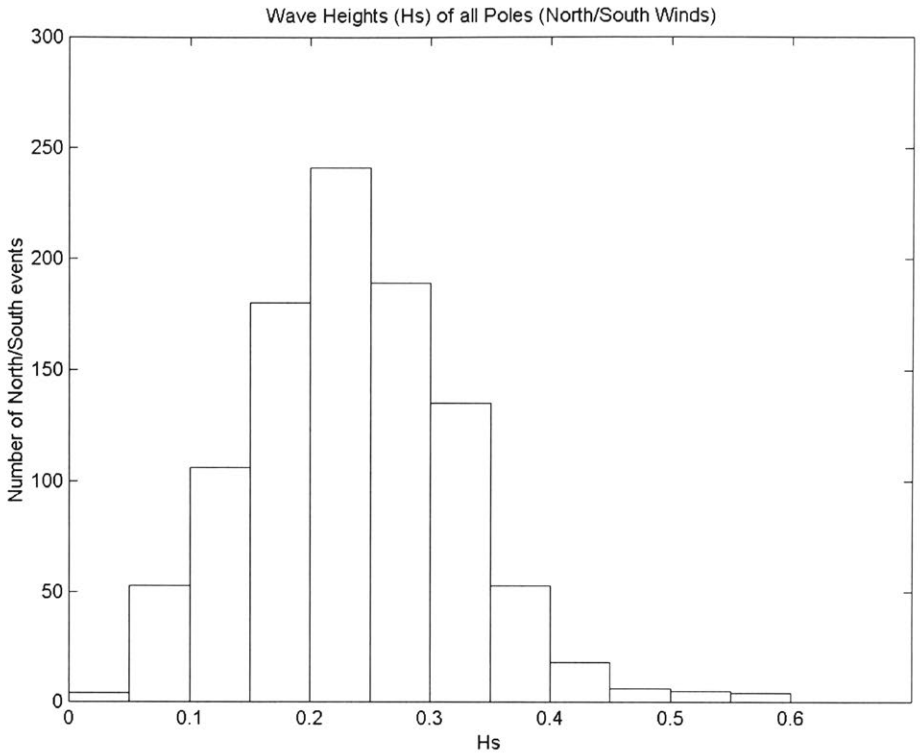

Figure 3.5 Histogram of significant wave height (H_s in metres) for the North South data from all stations.

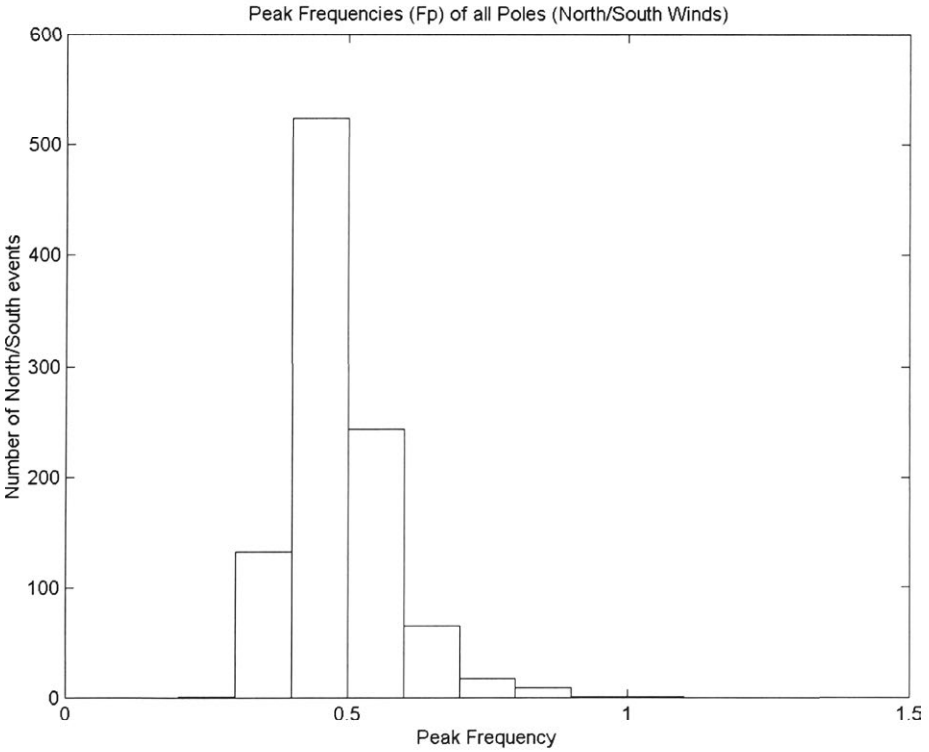

Figure 3.6 Histogram of peak frequency (f_p in Hertz) for the North South data from all eight stations.

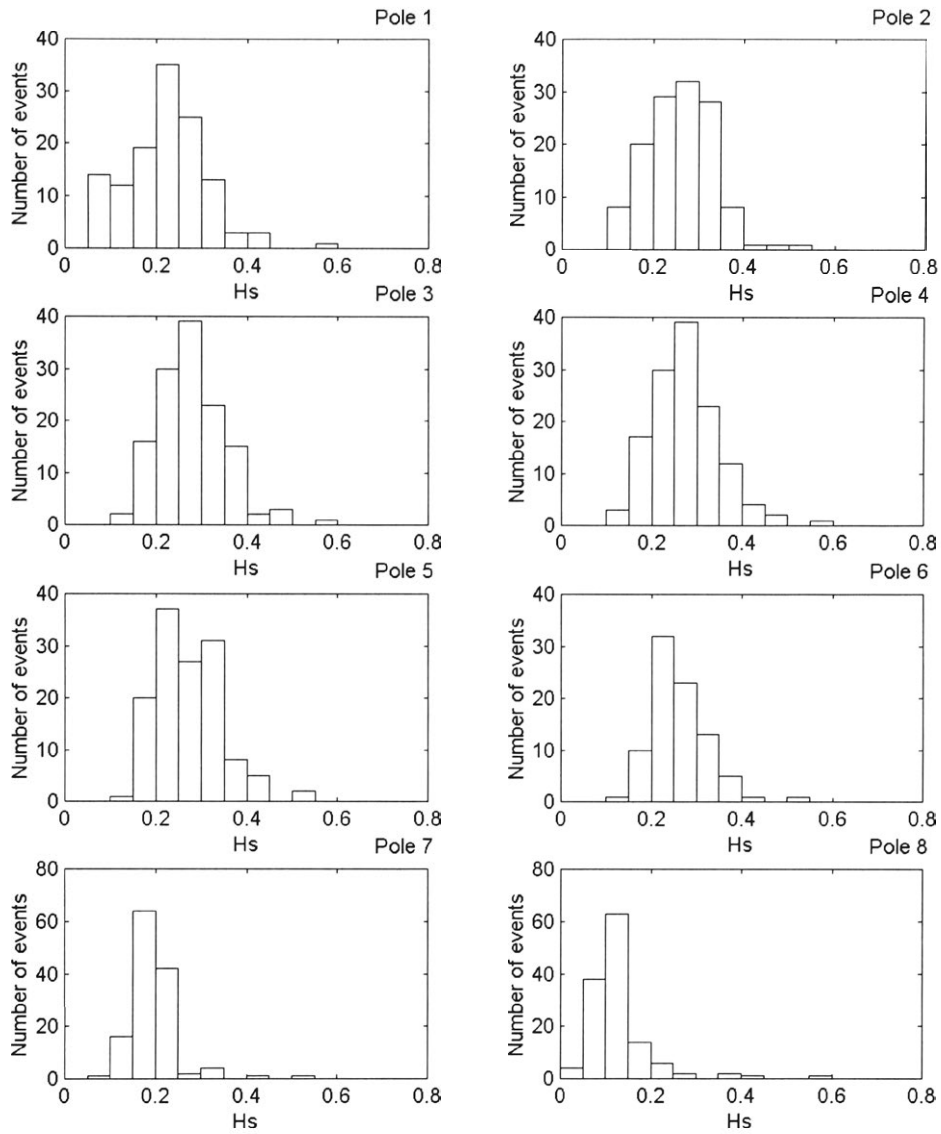

Figure 3.7 Histogram of significant wave height (H_s in metres) for the North South data from each of the eight stations. One interesting feature of these graphs is that the poles in the middle of the lake have higher waves on average than the poles at the ends. This occurs due to the increase in fetch along the array.

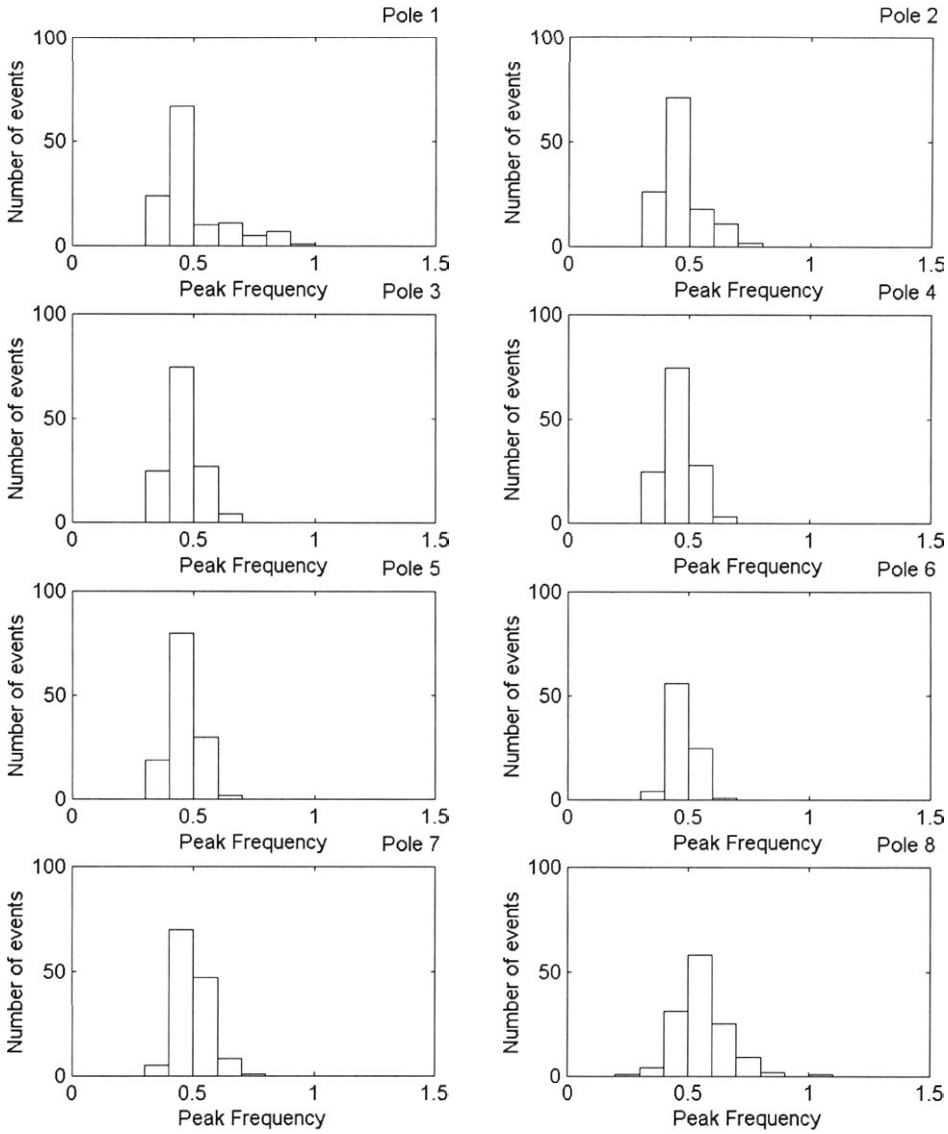

Figure 3.8 Histogram of peak frequency (f_p in Hertz) for the North South data for each of the eight stations.

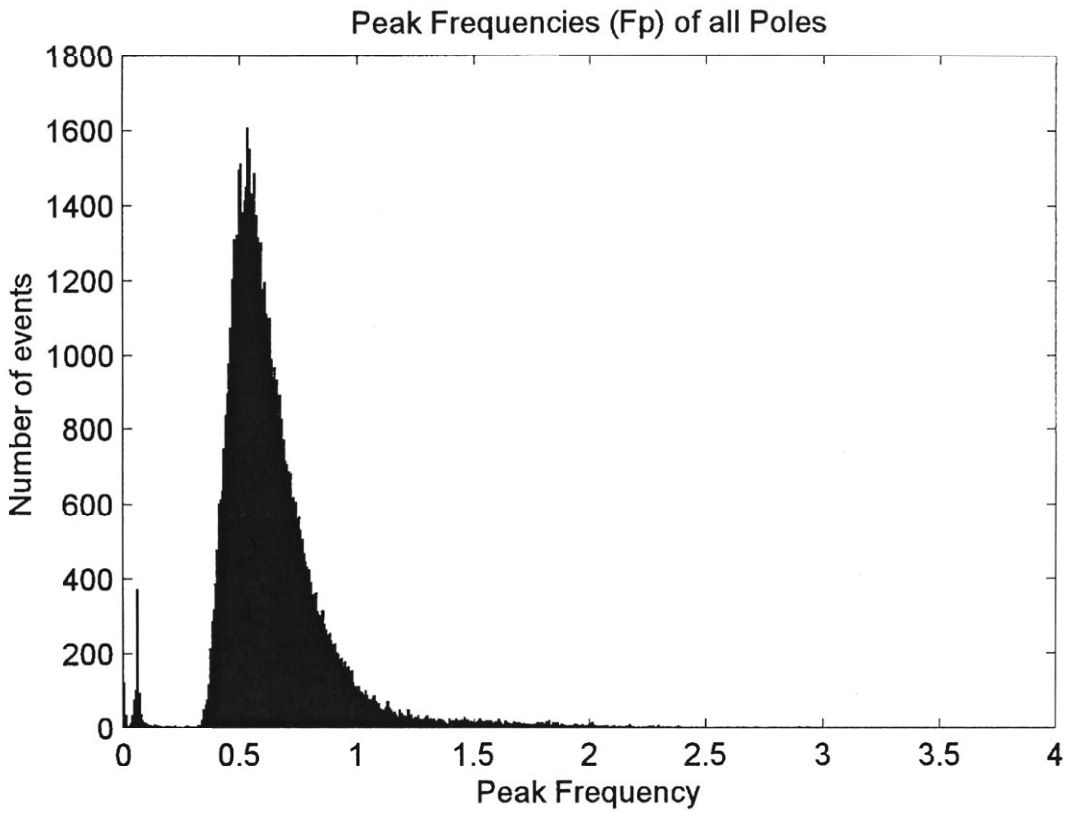

Figure 3.9 Histogram of peak frequency (f_p in Hertz) of all the data from the eight stations. A small bin size has been used to define the distribution shape.

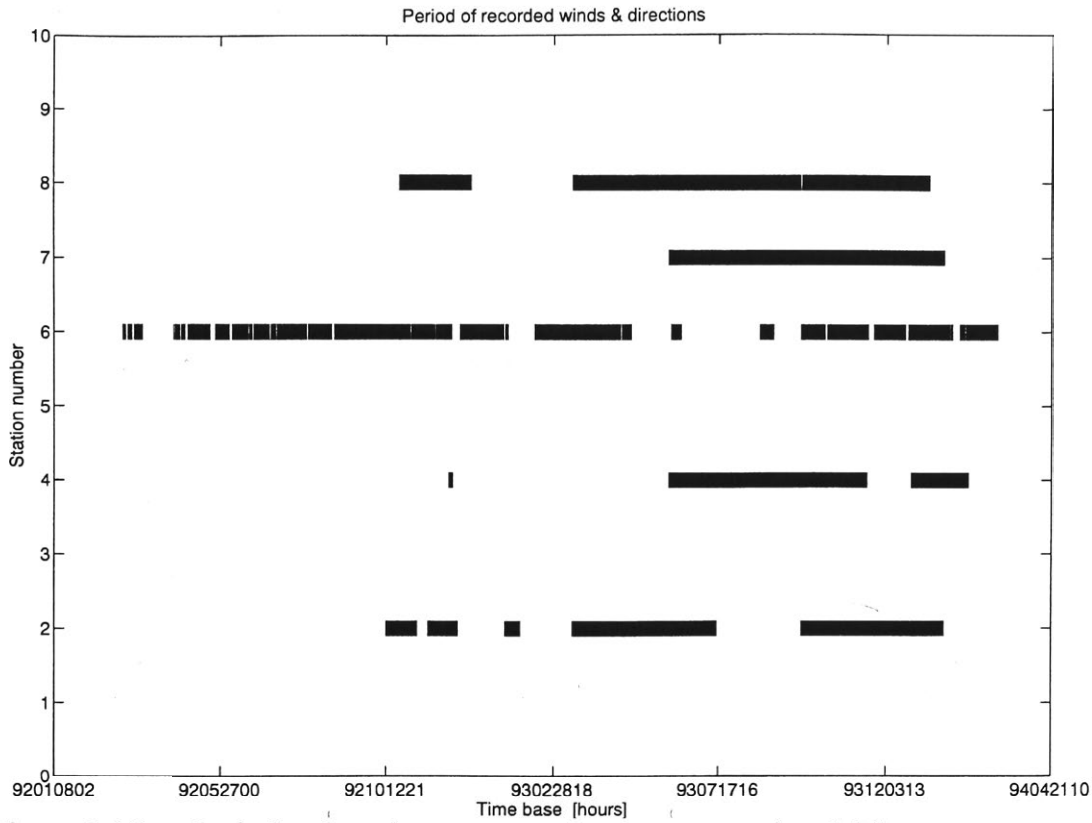

Figure 3.10 Periods when the anemometers were operational. The anemometers were placed on stations 2, 4, 6, 7, and 8. The number of occasions when all anemometers were working is small.

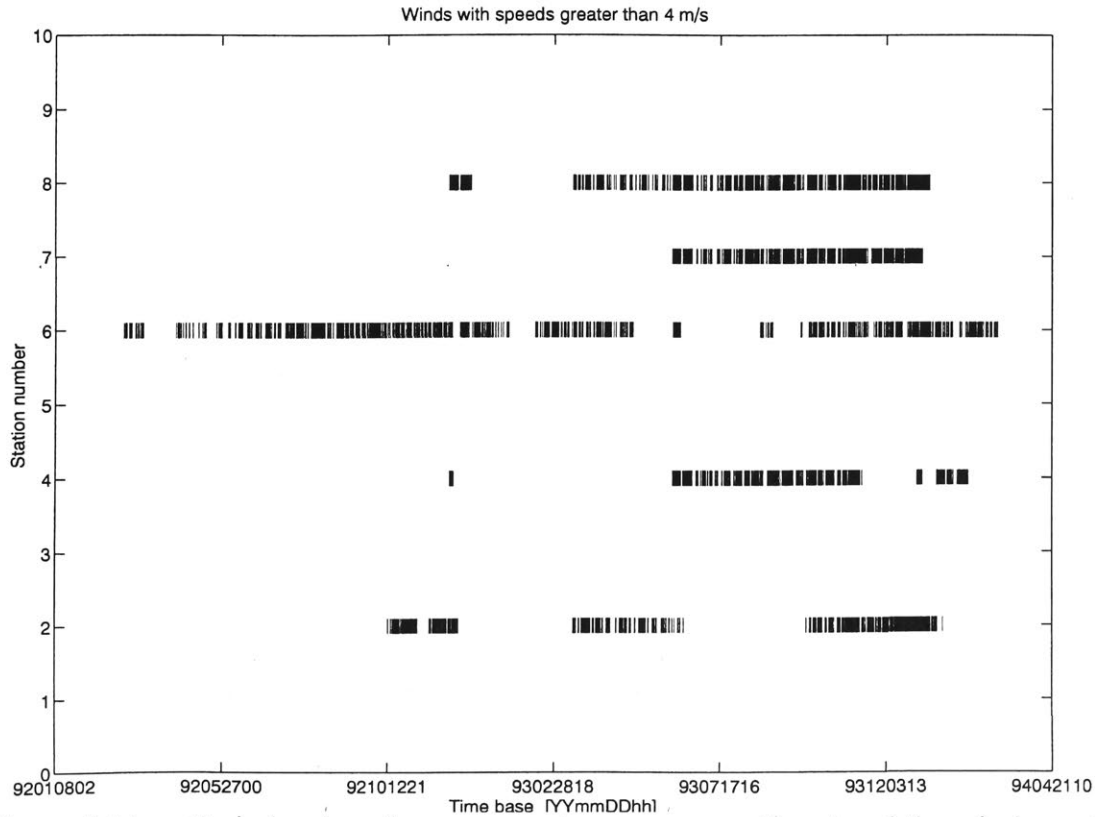

Figure 3.11 Periods when the anemometers were operational and the wind speed was over 4 m/s.

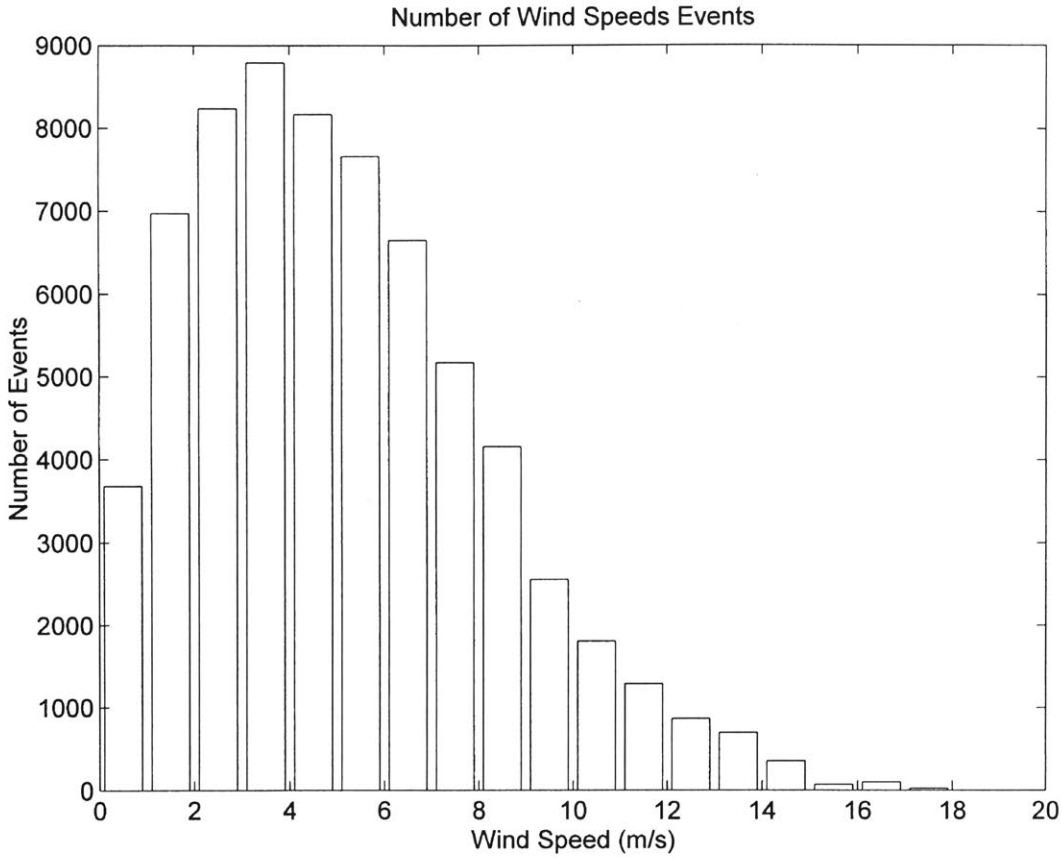

Figure 3.12 Histogram of wind speed for all the data from Lake George.

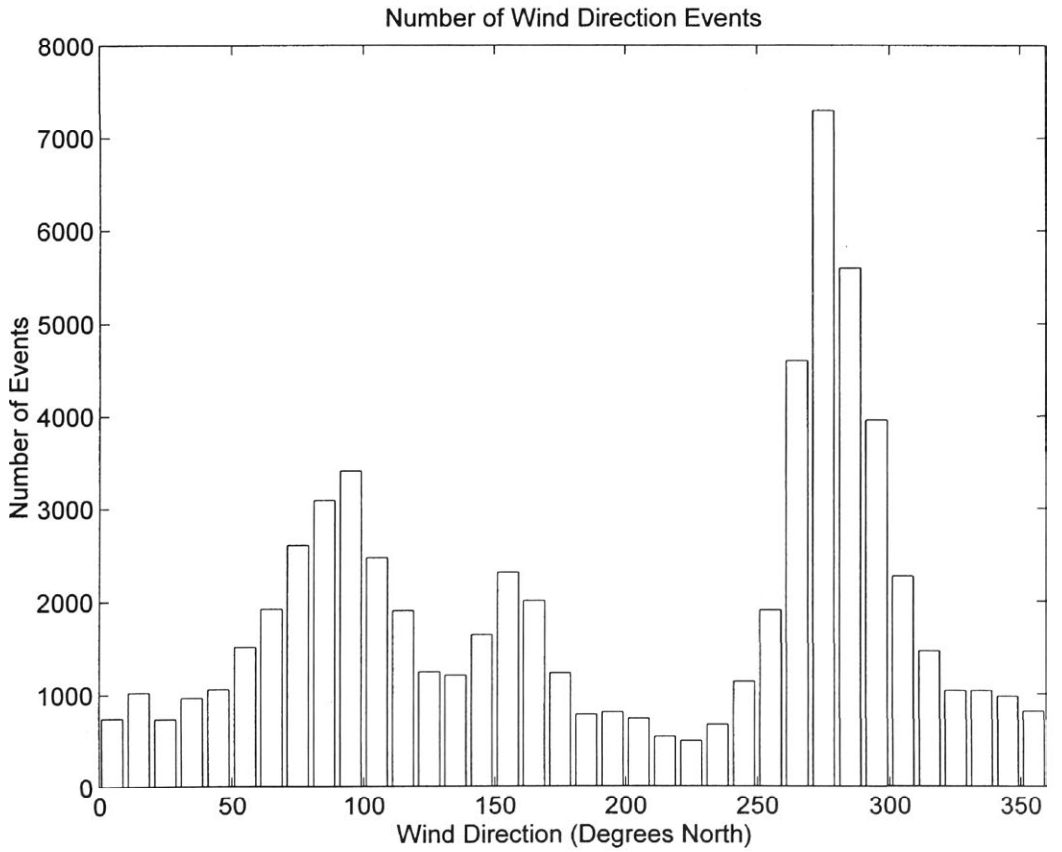

Figure 3.13 Histogram of the wind directions for all the Lake George data. As can be seen, the main wind directions were easterly and westerly.

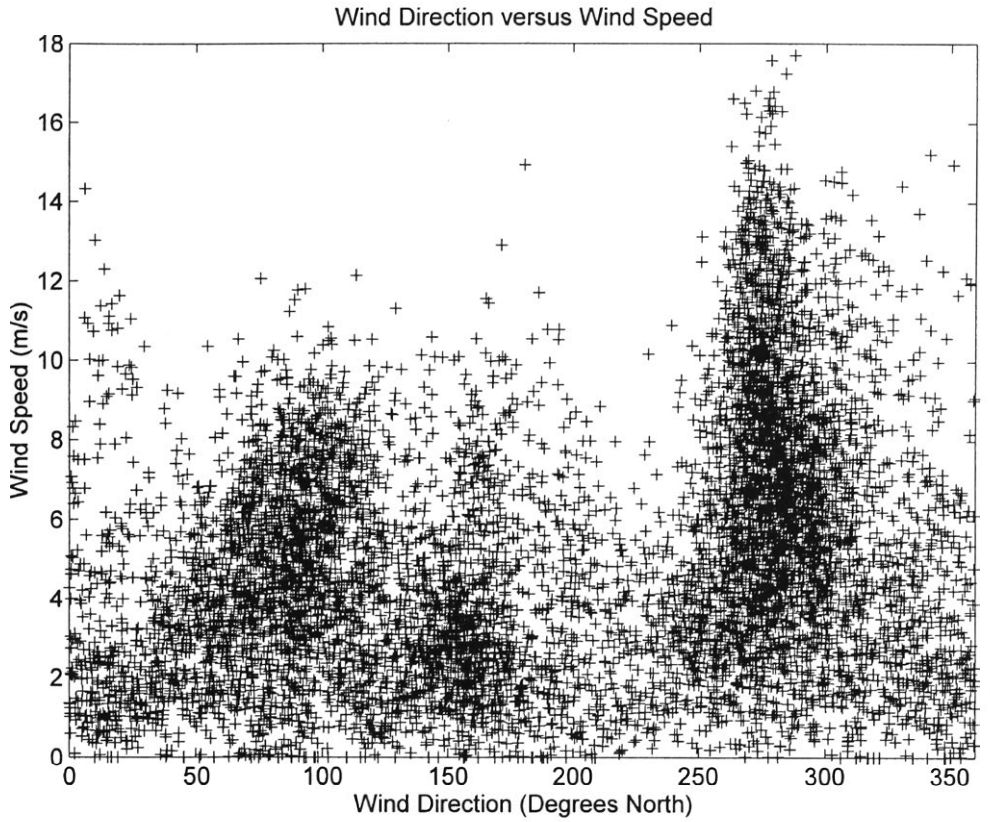

Figure 3.14 A scattergram of the wind speed and wind direction. In theory it is possible that the main wind direction and the higher wind speed directions are not the same. But at Lake George this was not the case.

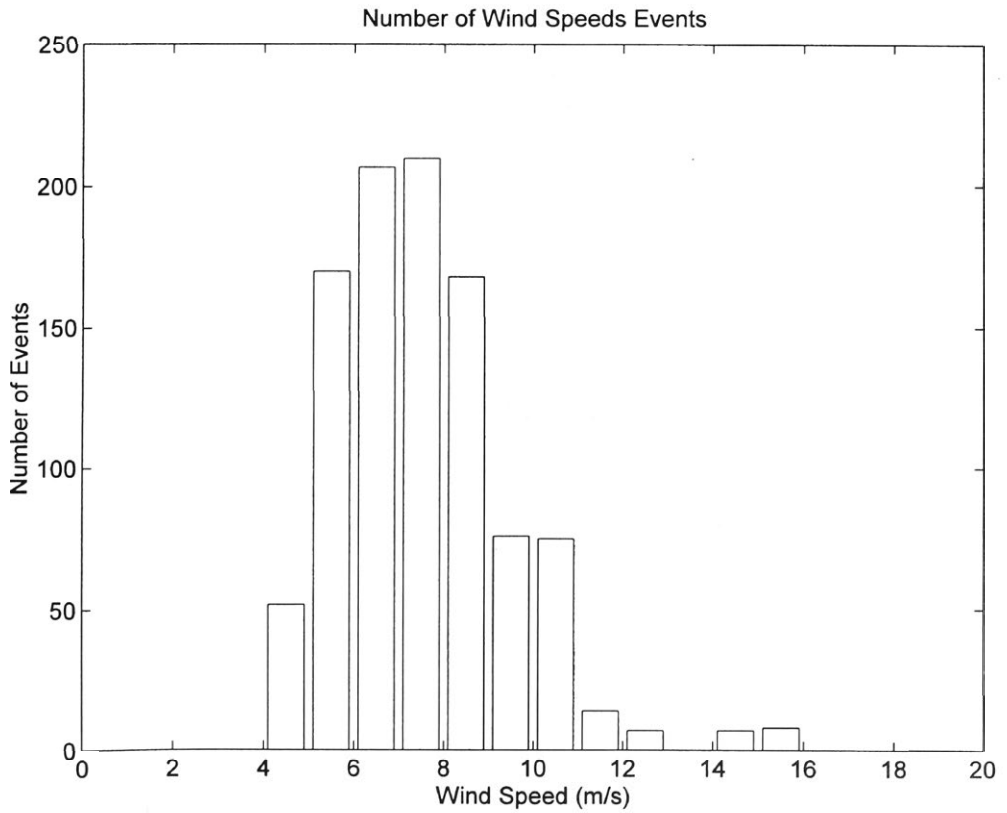

Figure 3.15 Wind speed histogram for the North South data set. Wind speeds less than 4 m/s were filtered out of the North South data set.

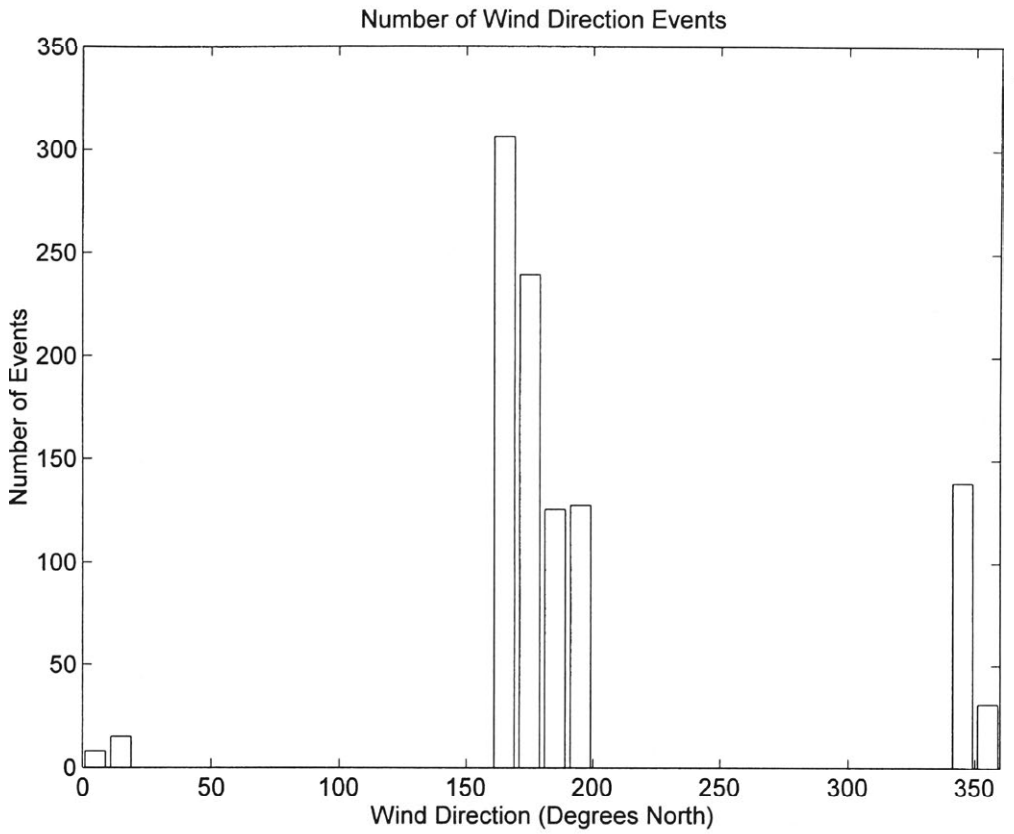

Figure 3.16 Histogram of wind direction for the North-South data set.

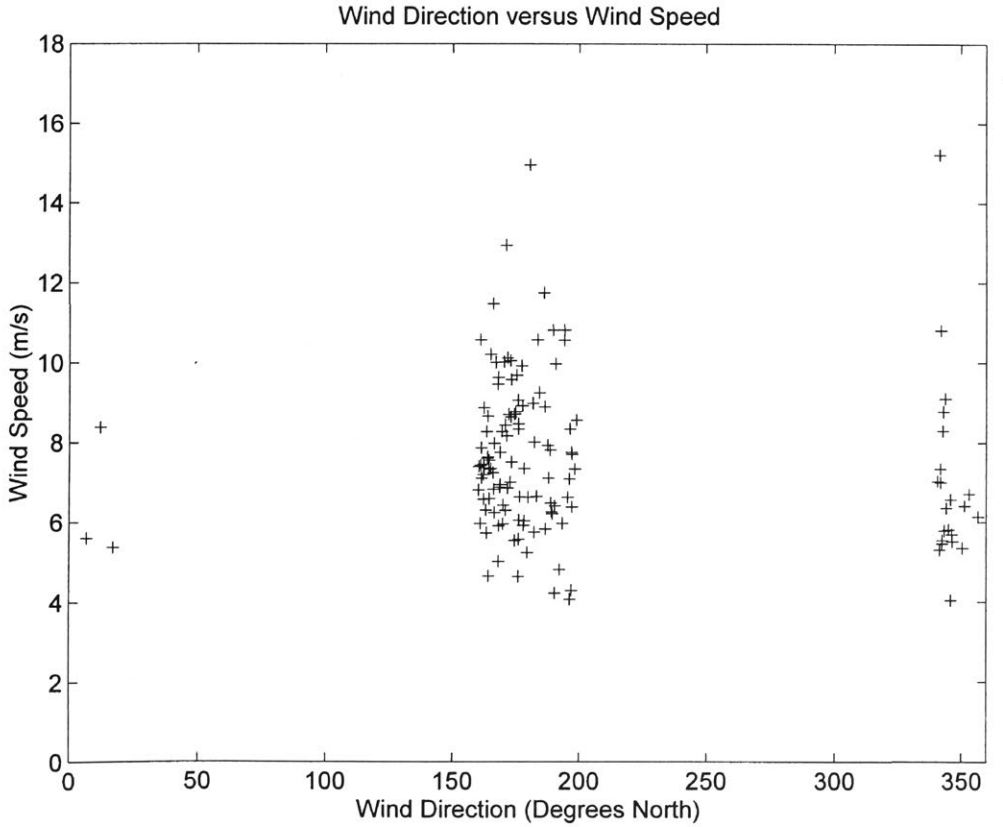

Figure 3.17 Scattergram of wind speed and wind direction for the North South data. Note that wind speeds lower that 4 m/s are omitted.

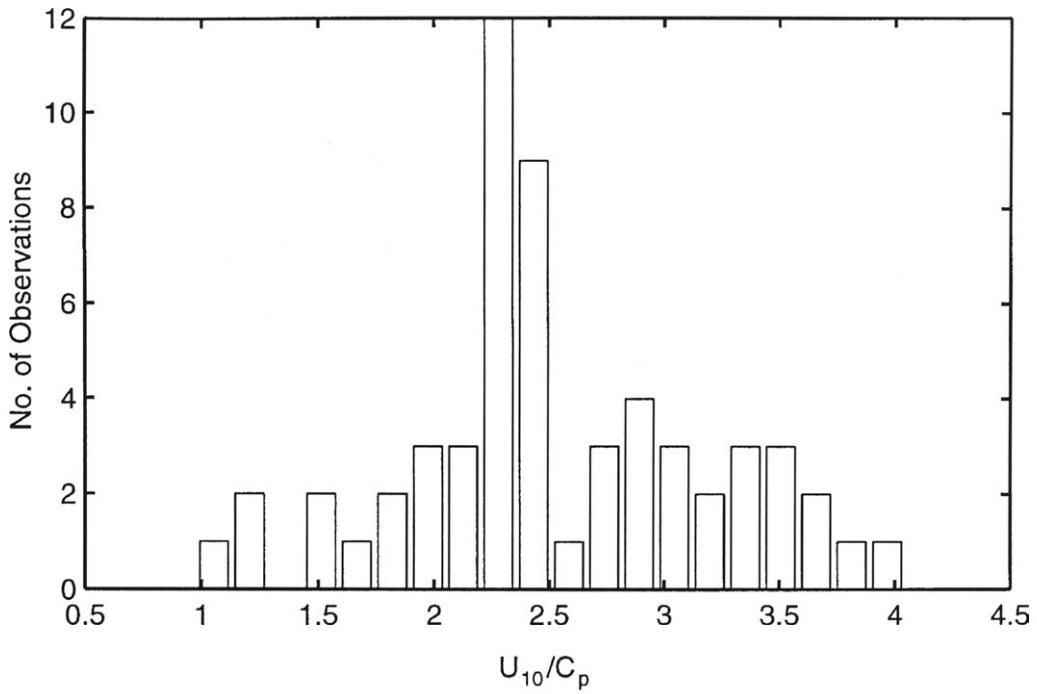

Figure 3.18 Distribution of the inverse wave age (U_{10}/C_p) for the 58 directional records taken at Lake George were the wind was from the east or west. The distribution ranges from fully developed spectra ($U_{10}/C_p = 1$) to young seas ($U_{10}/C_p = 4$).

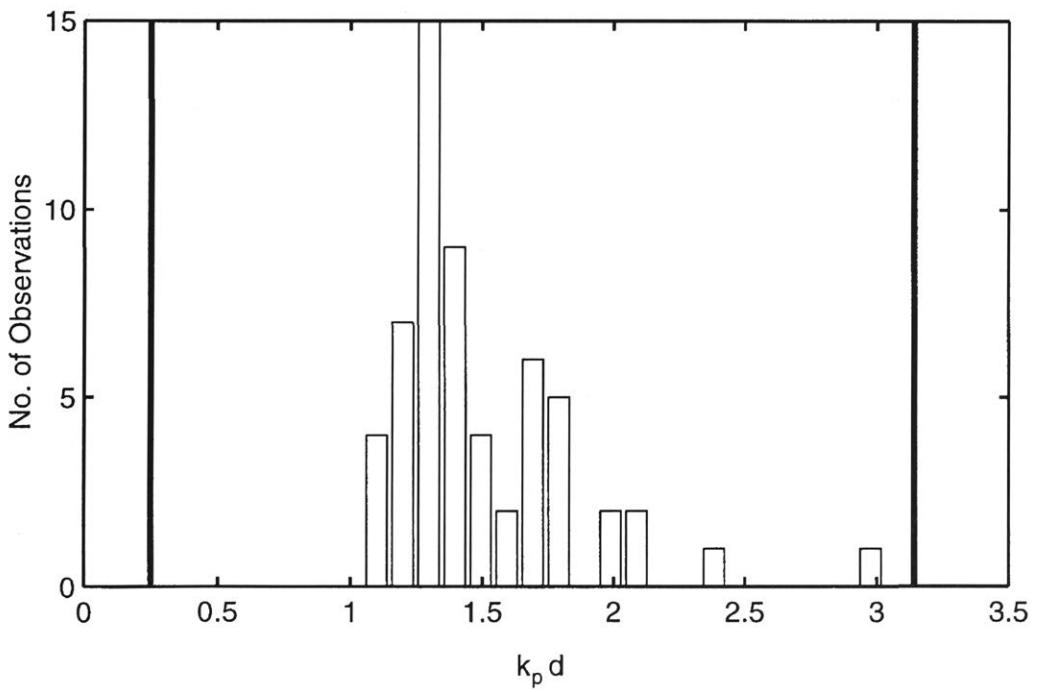

Figure 3.19 Distribution of the non-dimensional depth parameters $k_p d$. Two thick lines on the graph indicate shallow water ($k_p d < 0.25$) and deep water ($k_p d > \pi$). As can be seen, the 58 directional spectra measured at Lake George are in transitional water depth, which indicates that the waves are influenced by the finite depth.

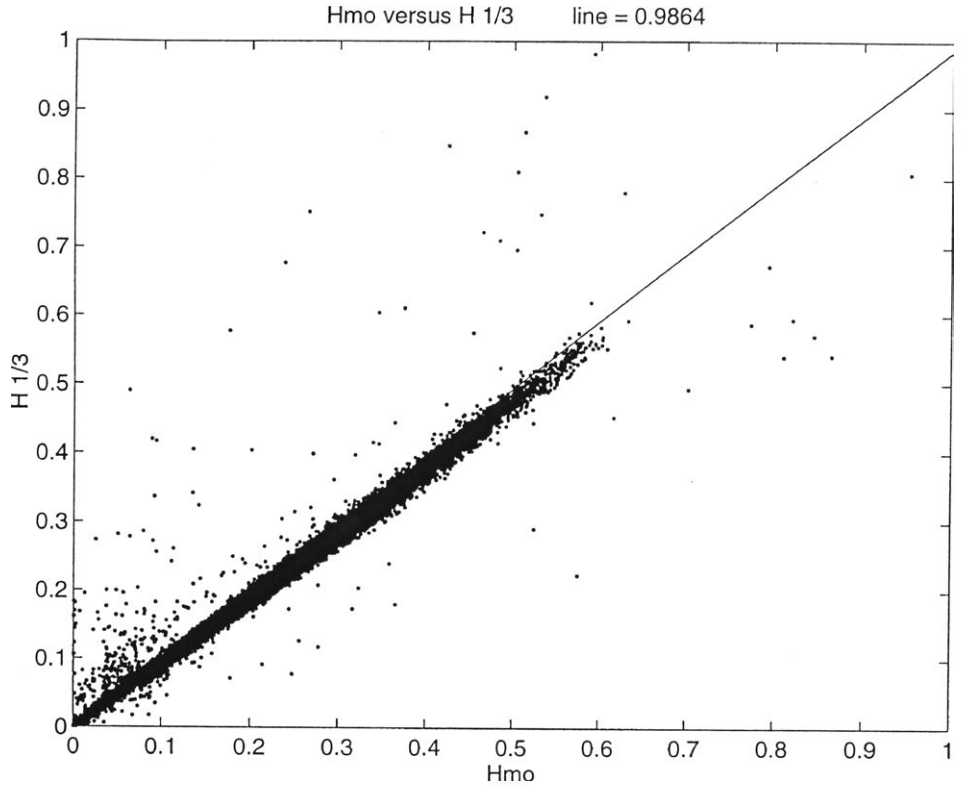

Figure 3.20 Scattergram of $H_{1/3}$ and H_{mo} (both in metres). $H_{1/3}$ is lower than H_{mo} by about 1.5 % for large waves. The water depth is approximately 1.9 metres. The data shown is from the full data set.

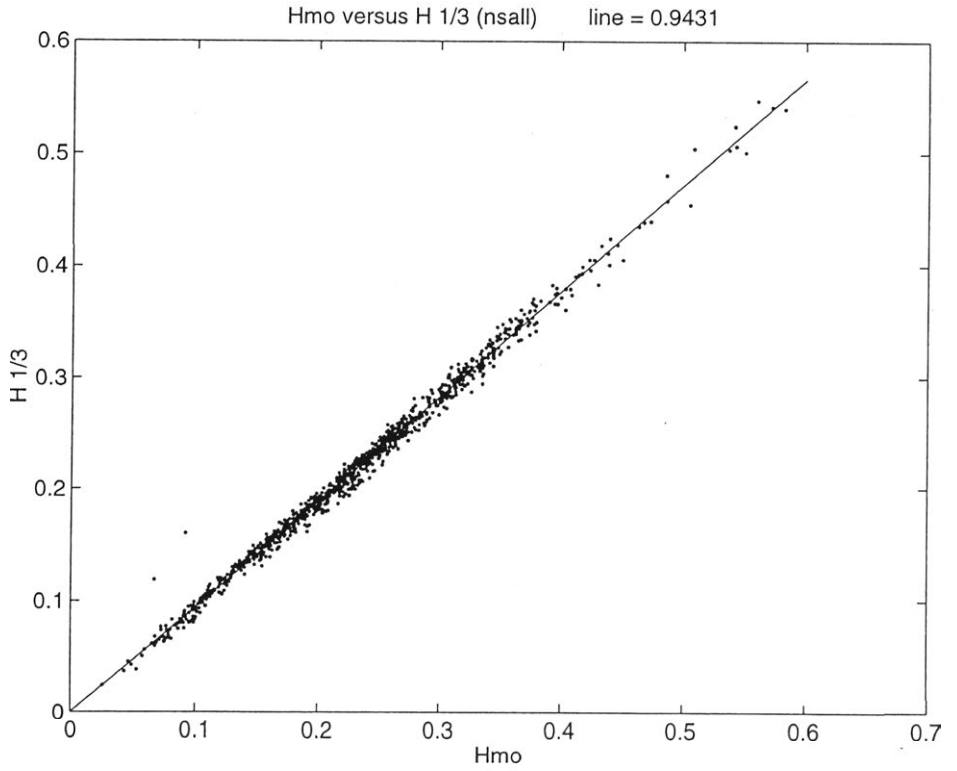

Figure 3.21 Scattergram of $H_{1/3}$ and H_{mo} (both in metres) for North South data. $H_{1/3}$ is lower than H_{mo} by about 4-6 % for large waves. The water depth is approximately 1.9 metres.

4. Growth Curves for Shallow Water

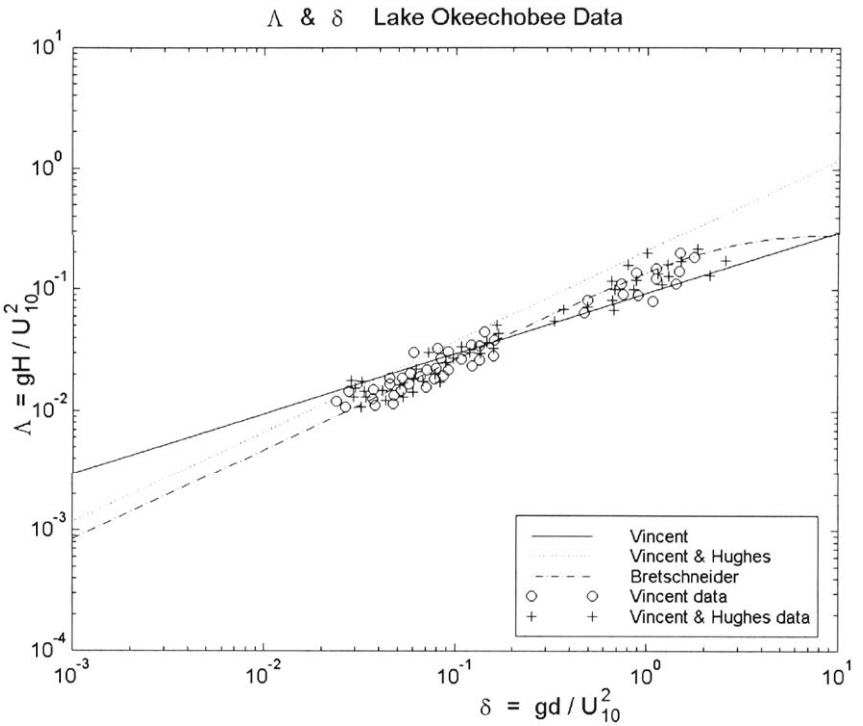

Figure 4.1 Lake Okeechobee data from Vincent (1985) (o) and Vincent and Hughes (1985)(+). The line "Vincent" is from Vincent (1985) where $H \sim d^{0.5}$, and "Vincent & Hughes" is from Vincent and Hughes (1985) where $H \sim d^{0.75}$. The last line is from Bretschneiders empirical results where $H \sim d^{0.75}$. Note the plateau Bretschneiders curve reaches at large δ.

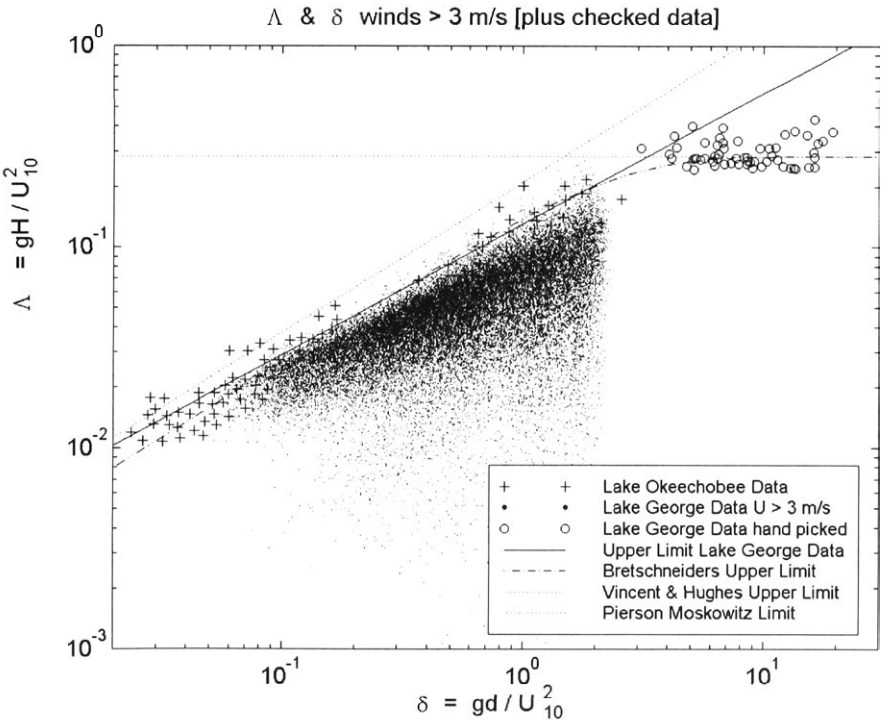

Figure 4.2 Dimensionless wave height (Λ) versus dimensionless depth (δ). All the data from Lake George with wind speeds greater than 3 m/s and handpicked data under 3 m/s are shown. The data from Lake Okeechobee are shown by crosses. Note the different upper limits from the two data. sets

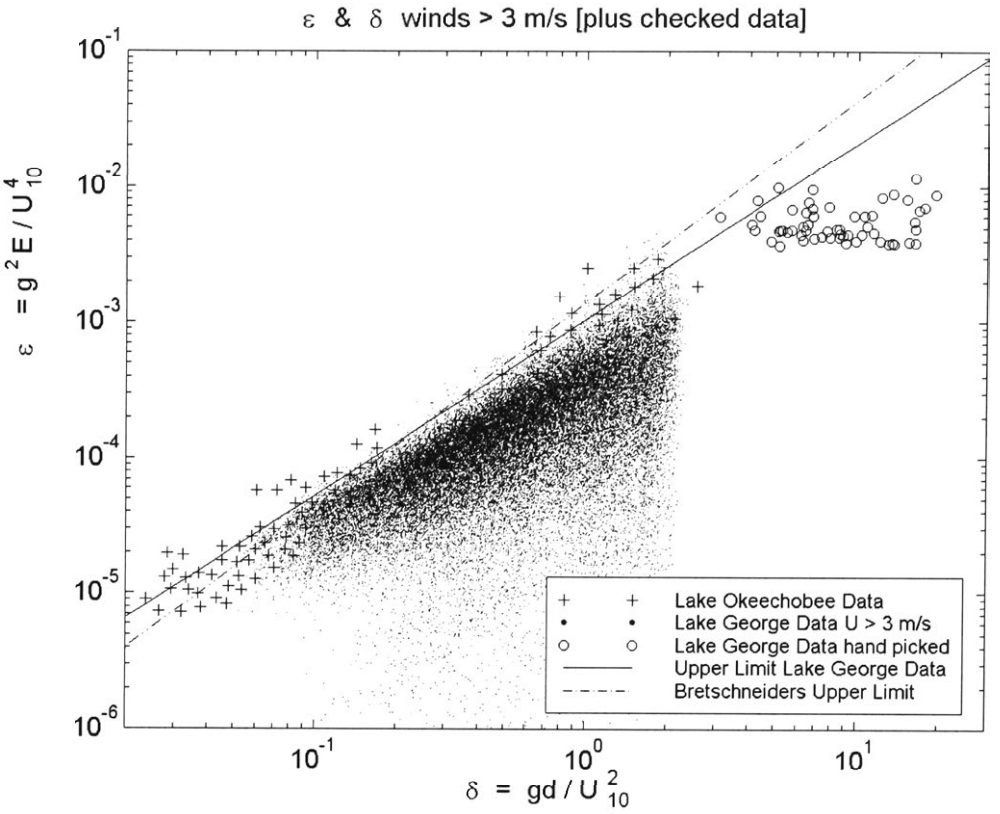

Figure 4.3 Dimensionless energy versus dimensionless depth. All the data with wind speed greater than 3 m/s and the handpicked data for winds less than 3 m/s are shown.

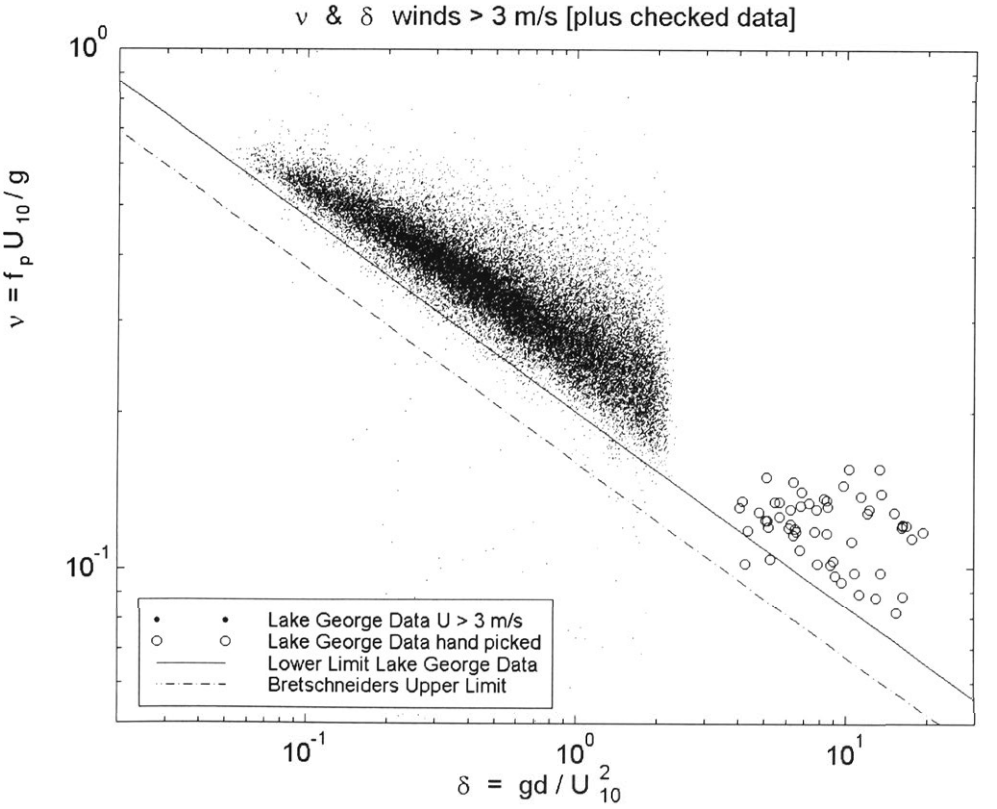

Figure 4.4 Dimensionless frequency versus dimensionless depth. All the data with wind speed greater than 3 m/s and the handpicked data for winds less than 3 m/s are shown.

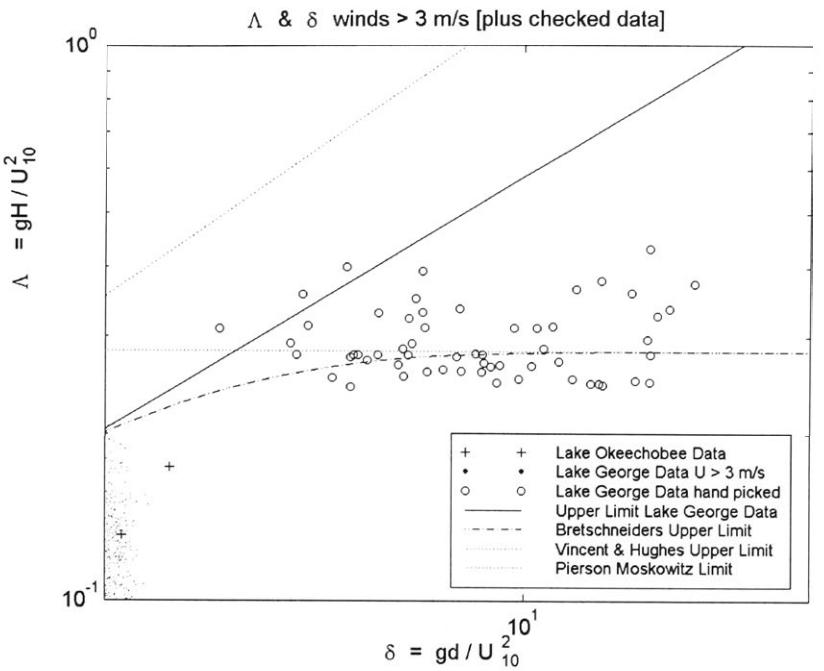

Figure 4.5 Dimensionless wave height (Λ) versus dimensionless depth (δ) for large dimensionless depth (δ > 1). Also shown are the data from Lake Okeechobee. The data appear to asymptote close to the Pierson-Moskowitz limit.

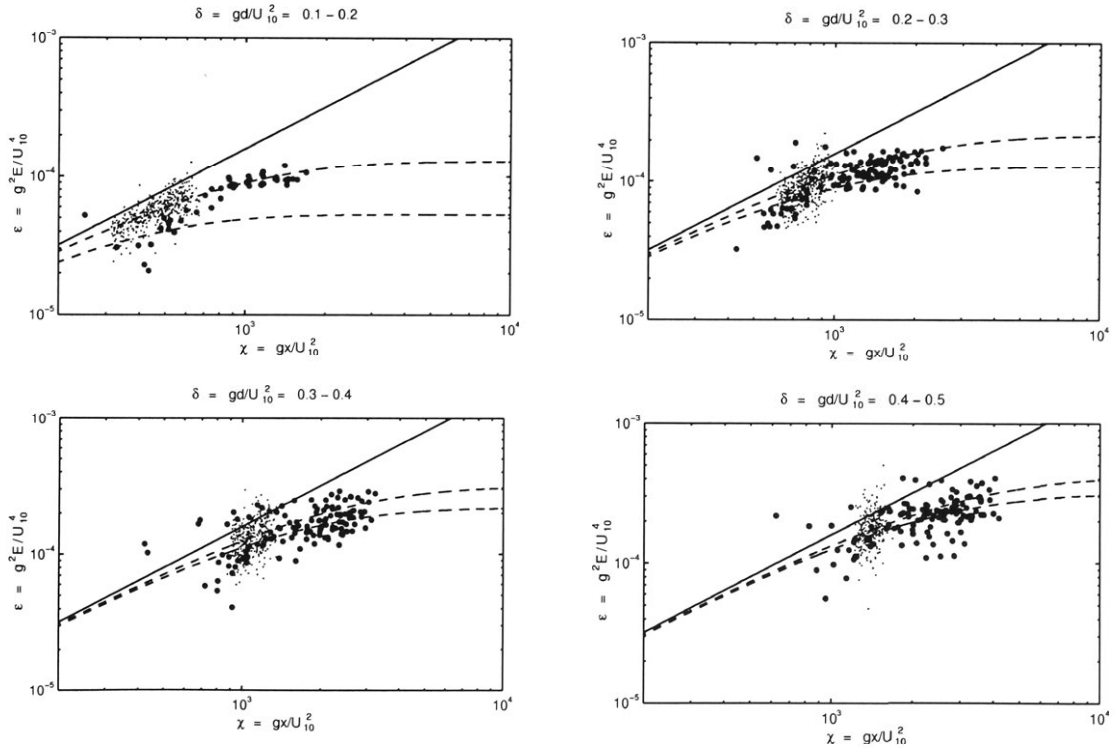

Figure 4.6 Dimensionless energy (ε) versus dimensionless fetch (χ). The data are split over 4 graphs with different dimensionless depth (a) $0.1 < \delta < 0.2$, (b) $0.2 < \delta < 0.3$, (c) $0.3 < \delta < 0.4$, (d) $0.4 < \delta < 0.5$. The dashed lines are the upper and lower dimensionless depth limits. The large dots are the North South data. The smaller dots are the East West data which are not corrected for the boundary layer effect. The solid line is the deep water JONSWAP result.

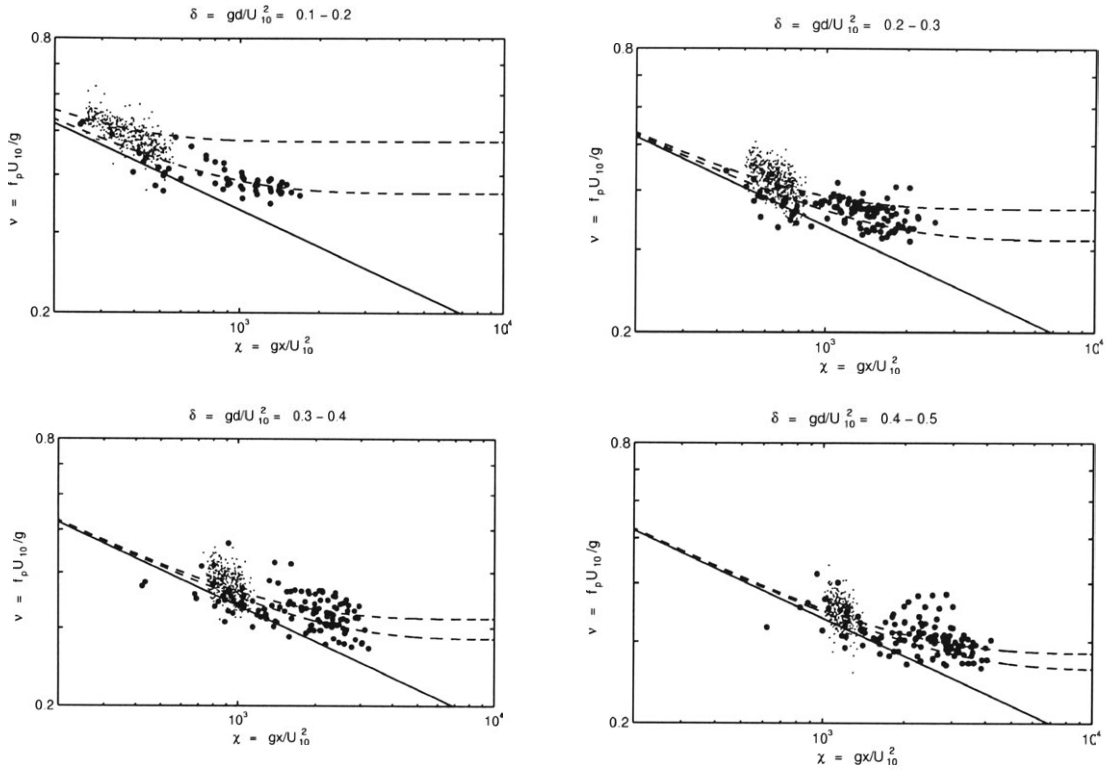

Figure 4.7 Dimensionless frequency (ν) versus dimensionless fetch (χ). The data are split over 4 graphs with different dimensionless depth (a) $0.1 < \delta < 0.2$, (b) $0.2 < \delta < 0.3$, (c) $0.3 < \delta < 0.4$, (d) $0.4 < \delta < 0.5$. The dashed lines are the upper and lower dimensionless depth limits. The large dots are the North South data. The smaller dots are the East West data which are not corrected for the boundary layer effect. The solid line is the deep water result of Kahma & Calkoen.

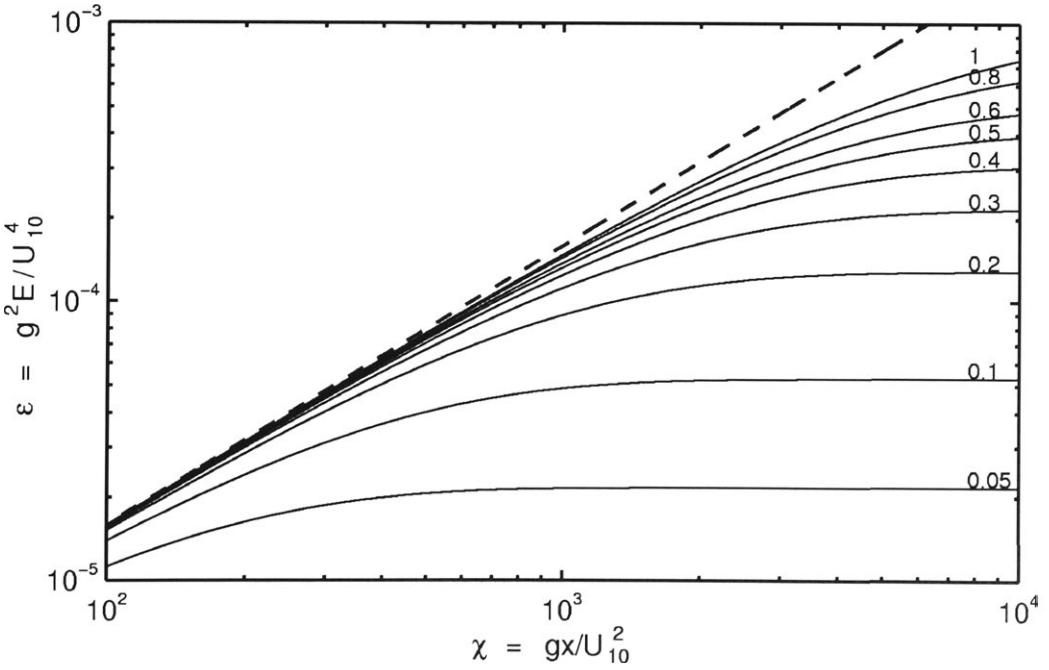

Figure 4.8 Non-dimensional energy (ε) versus non-dimensional fetch (χ). Each curve is for a specific non-dimensional depth (shown on the right-hand side).

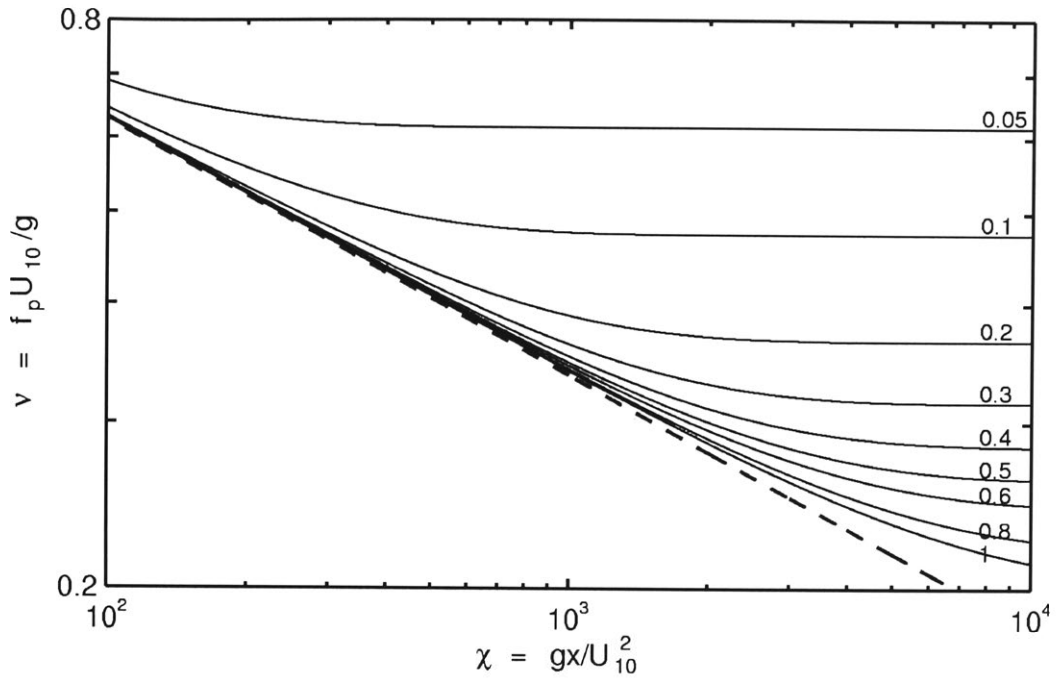

Figure 4.9 Non-dimensional frequency (ν) versus non-dimensional fetch (χ). Each curve is for a specific non-dimensional depth (shown on the right-hand side).

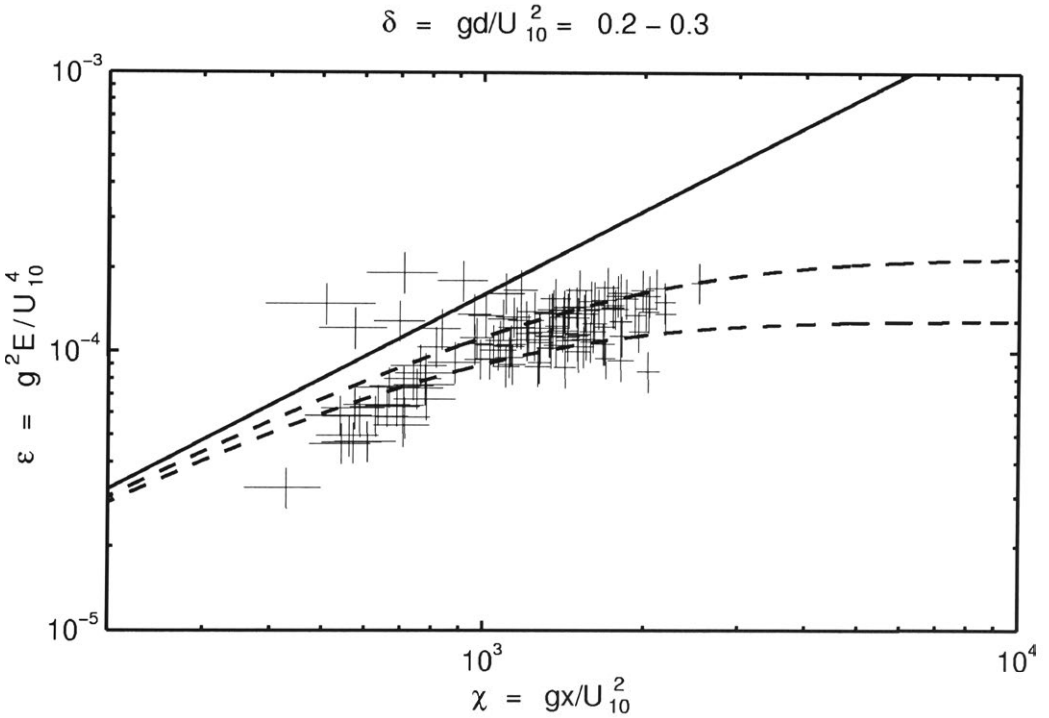

Figure 4.10 Dimensionless energy (ε) versus dimensionless fetch (χ). The data are shown for the dimensionless depth $0.2 < \delta < 0.3$. The dashed lines are the upper and lower dimensionless depth limits. Only the North South data are used in this analysis. The length of the crosses represent 95% confidence limits.

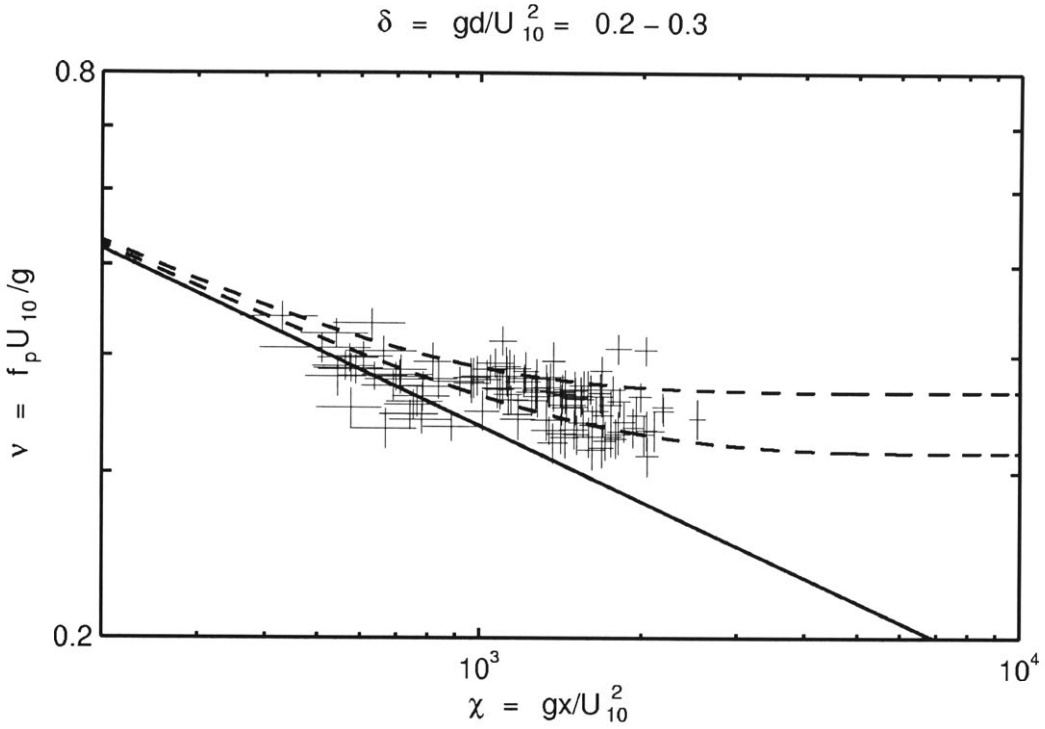

Figure 4.11 Dimensionless frequency (ν) versus dimensionless fetch (χ). The data are shown for the dimensionless depth $0.2 < \delta < 0.3$. The dashed lines are the upper and lower dimensionless depth limits. Only the North South data are used in this analysis. The length of the crosses represent 95% confidence limits.

5. One Dimensional Spectra

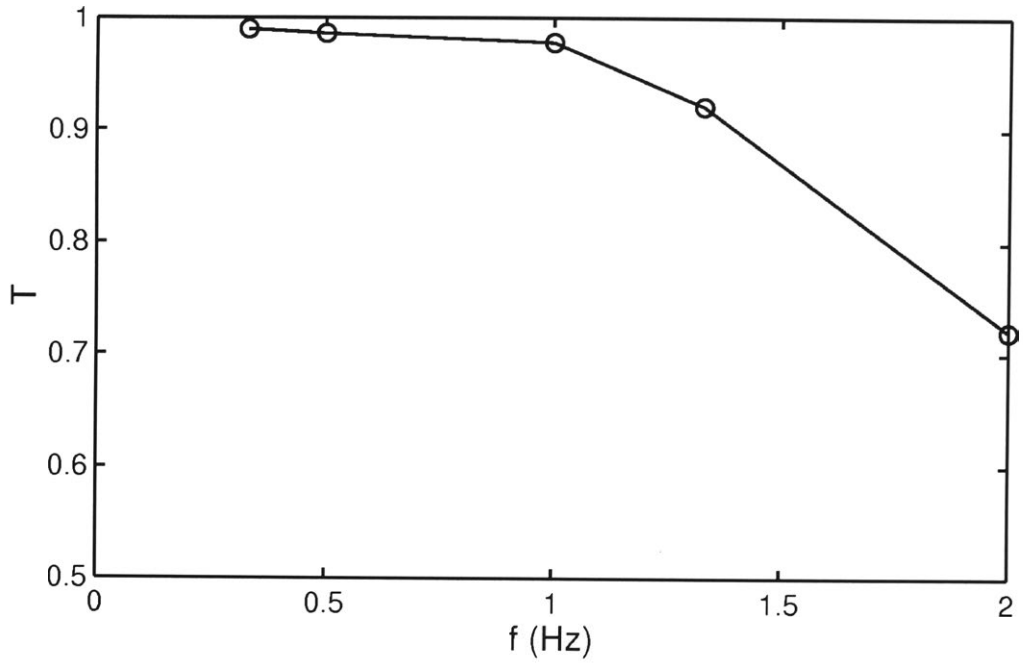

Figure 5.1 Frequency response of the Zwarts Poles from laboratory test.

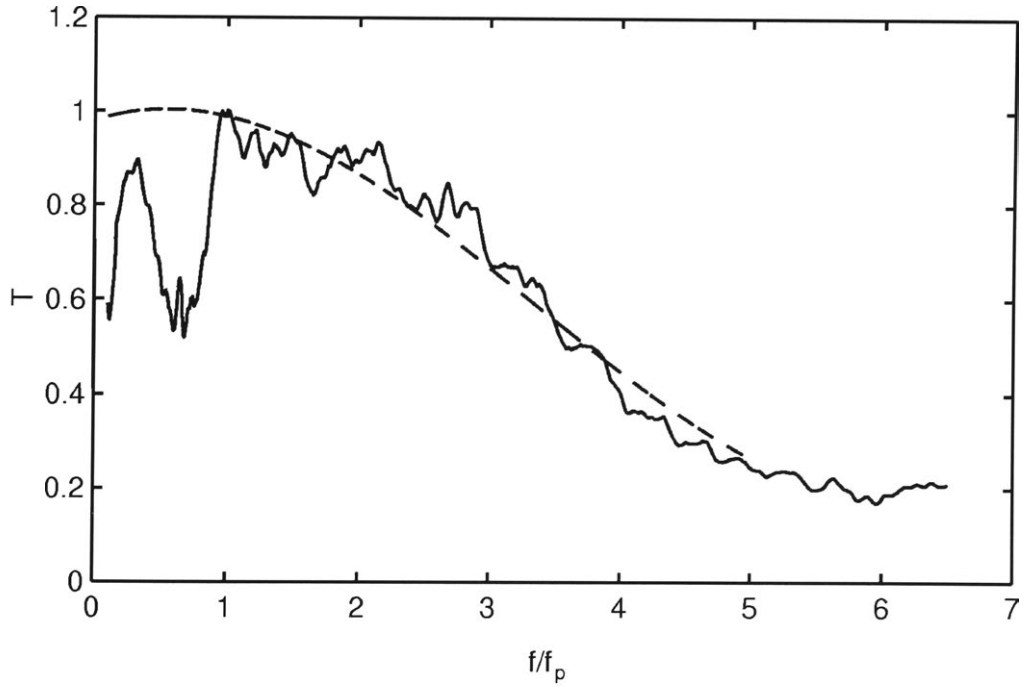

Figure 5.2 Transfer function of the Zwarts Poles developed from in situ comparison with resistance gauges.

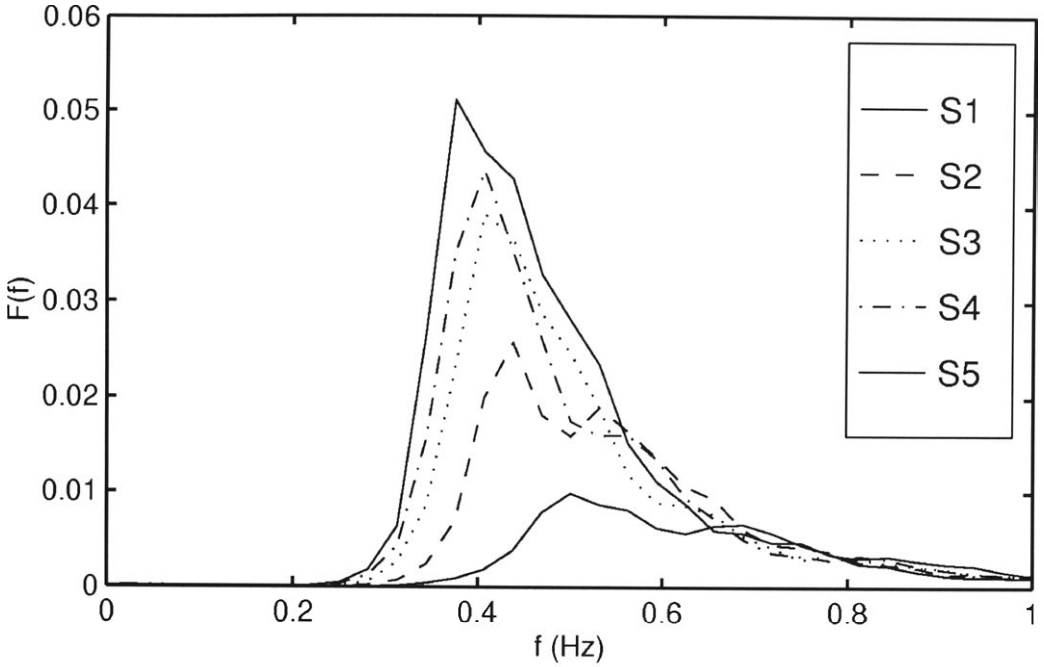

Figure 5.3 Example of the 1-Dimensional Spectra from stations 1-5, U_{10} = 10.8 m/s.

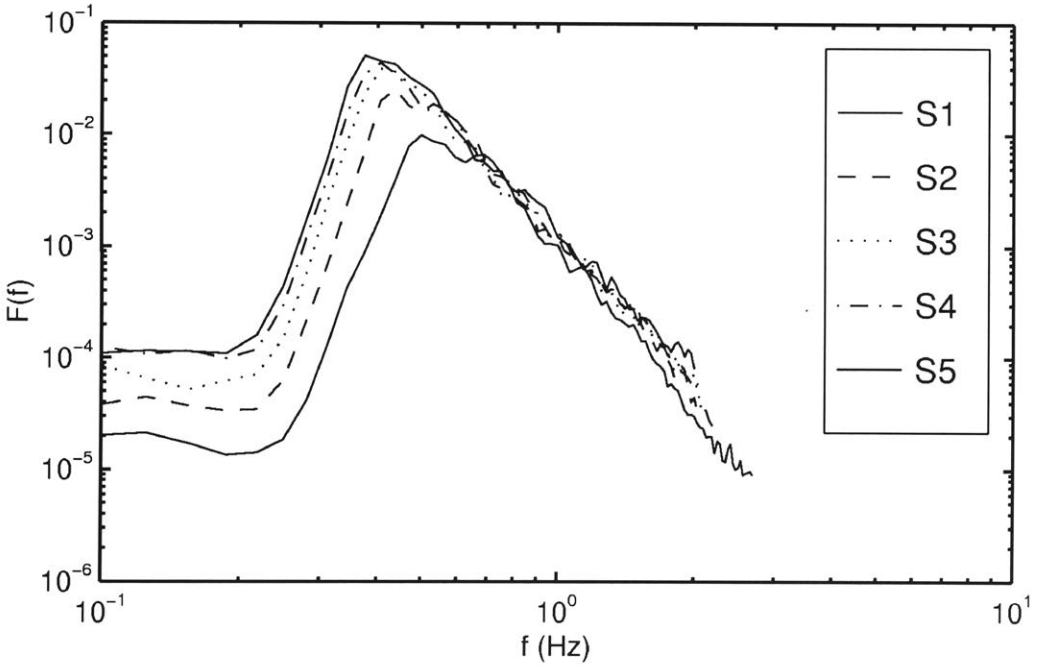

Figure 5.4 Example of the 1-Dimensional Spectra from stations 1-5, displayed on a logarithmic scale, U_{10} = 10.8 m/s.

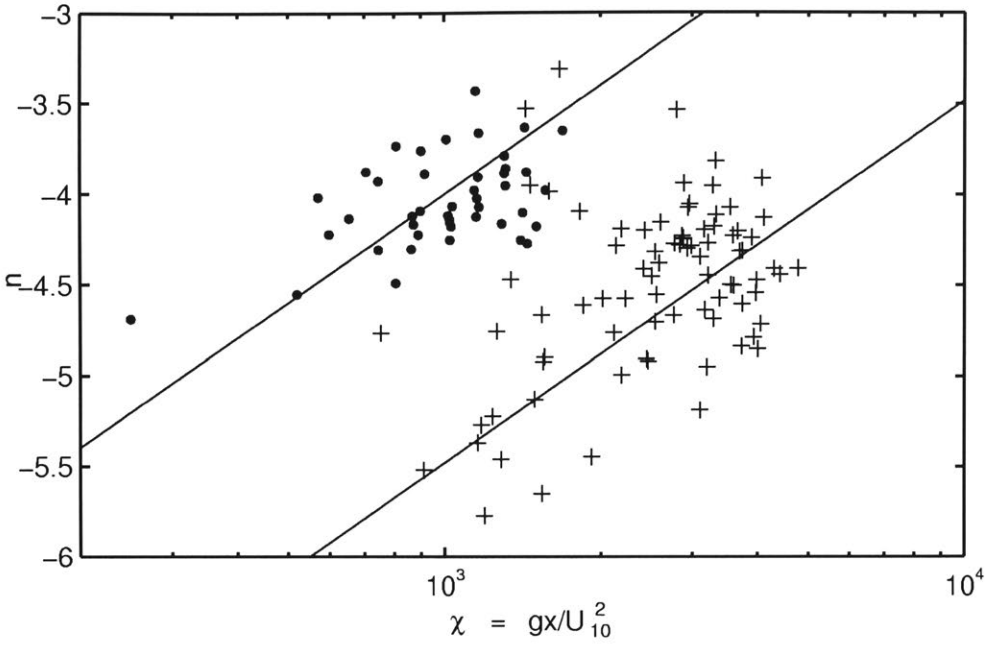

Figure 5.5 Values of the high frequency spectral exponent, n as a function of χ. Two ranges are shown here $\delta = 0.1$ to 0.2 (dots) and $\delta = 0.5$ to 0.6 (crosses). The solid lines are placed to show the trend in n for both values of δ.

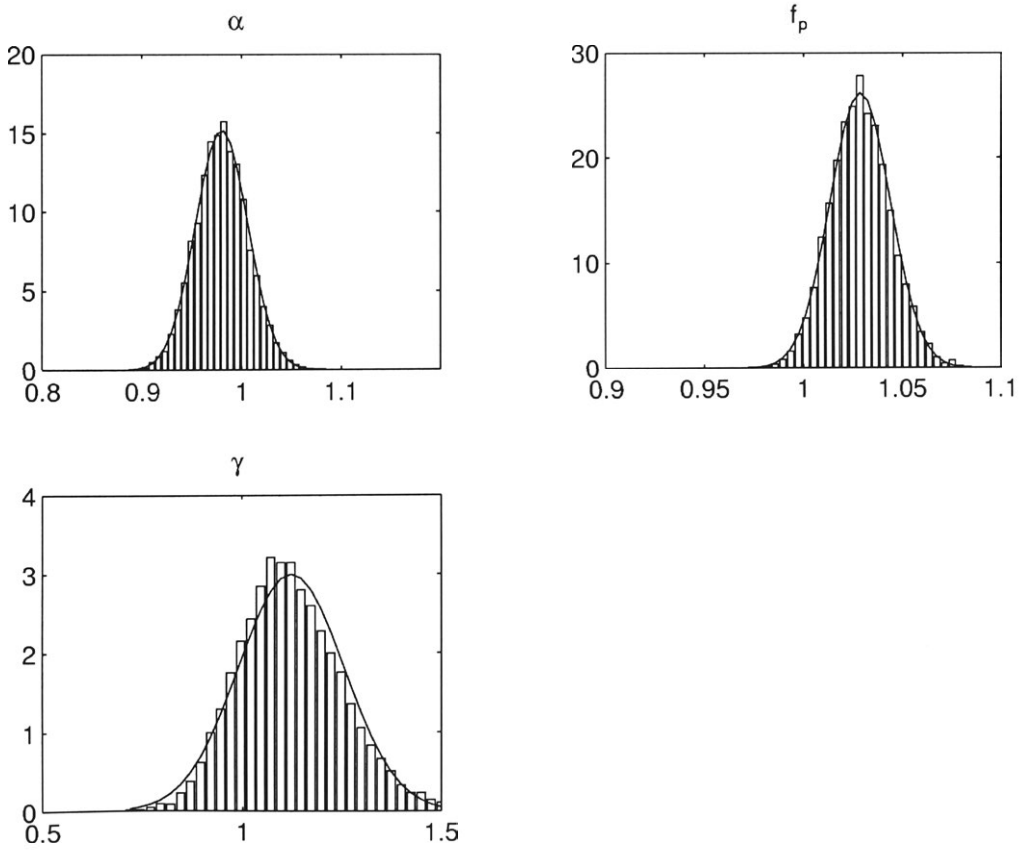

Figure 5.6 Results of the Monte Carlo Simulation in which the spectral parameters were individualy fitted to the spectrum. The parameter σ was held constant in this simulation and therefore only the results of α, f_p, and γ are given here.

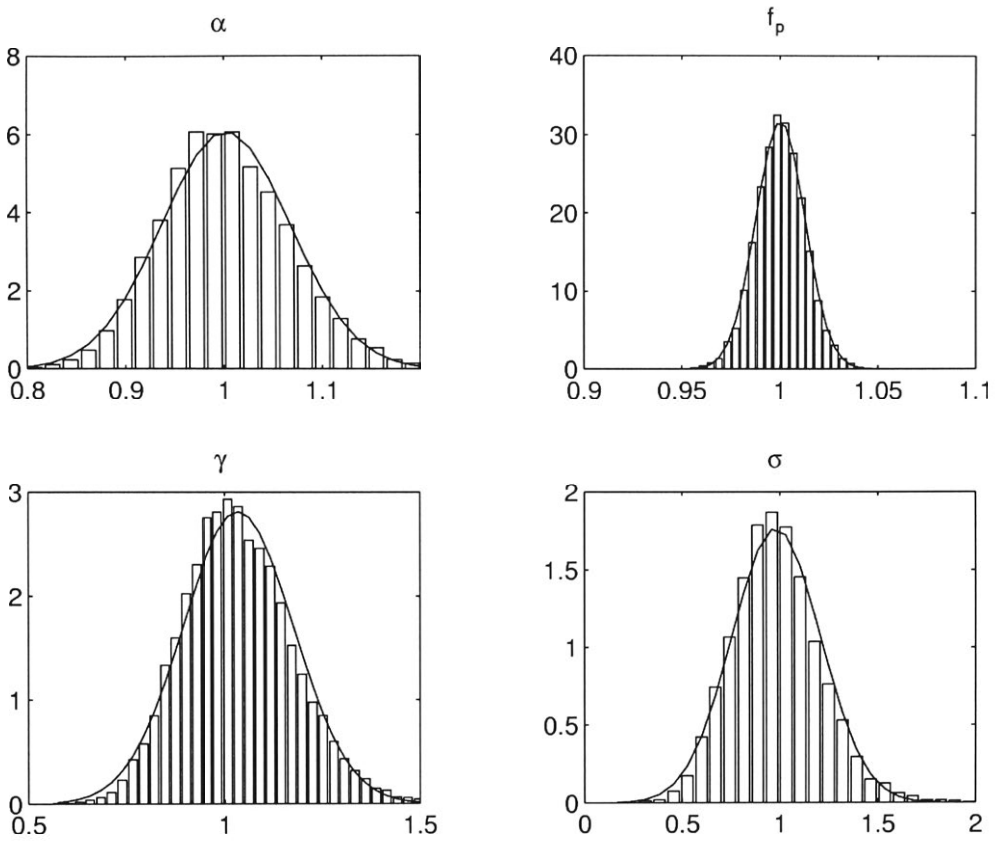

Figure 5.7 Results of the Monte Carlo Simulation with the simultaneous multi-parameter fitting technique. The results of the parameter σ, α, f_p, and γ are given here.

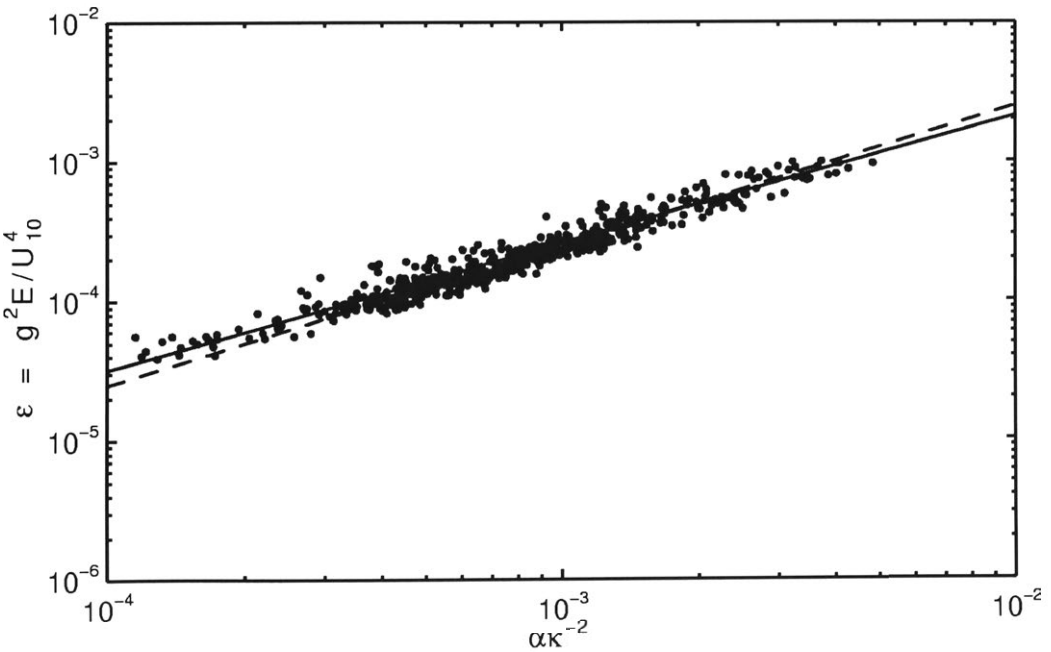

Figure 5.8 Non-dimensional energy (ε) as a function of $\alpha\kappa^{-2}$. The solid line is the least squares fit to the data and the dashed line is the TMA solution.

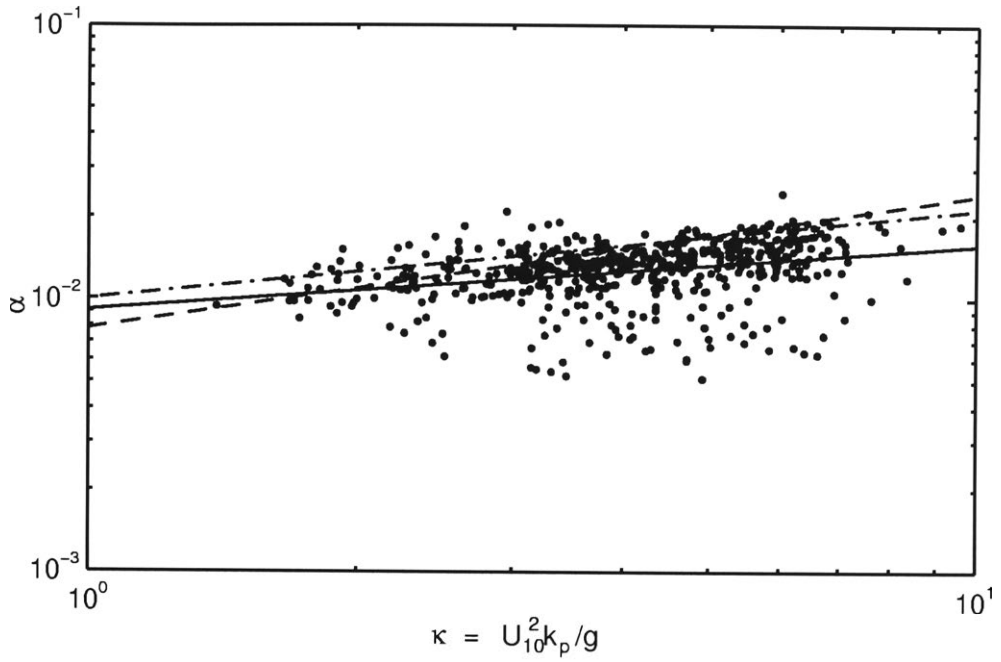

Figure 5.9 The spectral parameter α as a function of the non-dimensional wave number (κ). The solid line is a least squares fit to the data.
Also shown are the TMA (dash dash) and JONSWAP (dot dash) relationships.

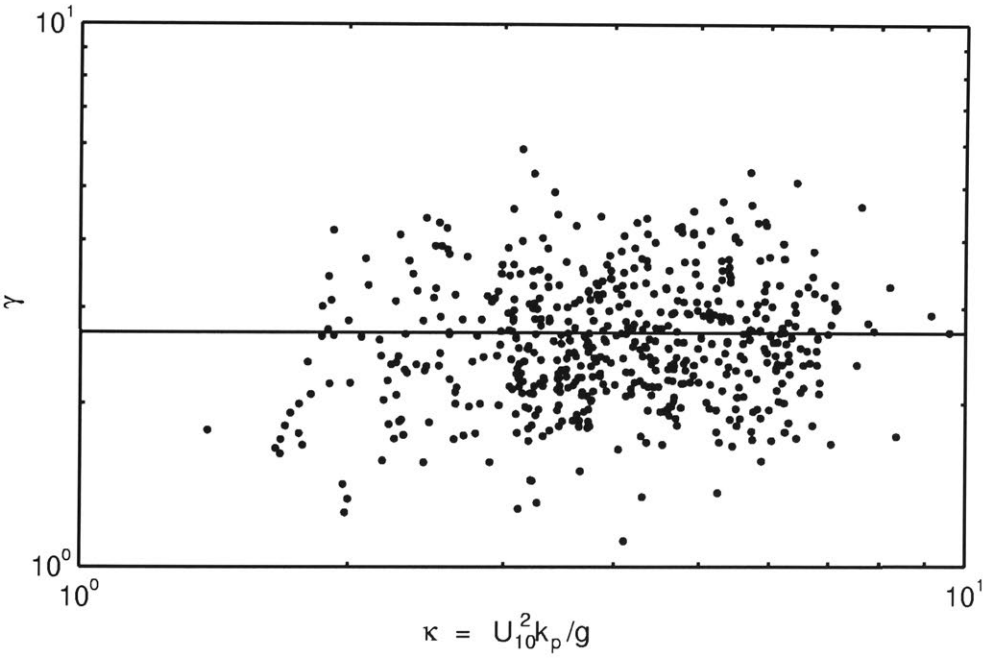

Figure 5.10 The peak enhancement (γ) as a function of the non-dimensional wave number (κ). The solid line is the mean value of $\gamma = 2.70$.

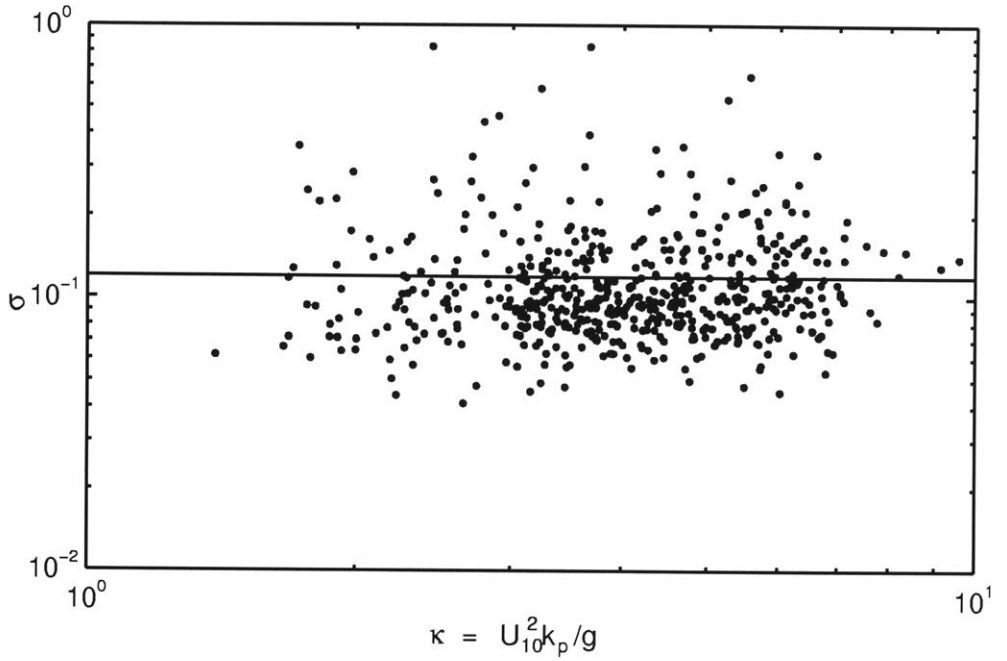

Figure 5.11 The spectral parameter σ as a function of the non-dimensional wave number (κ). The solid line is the mean value $\sigma = 0.12$.

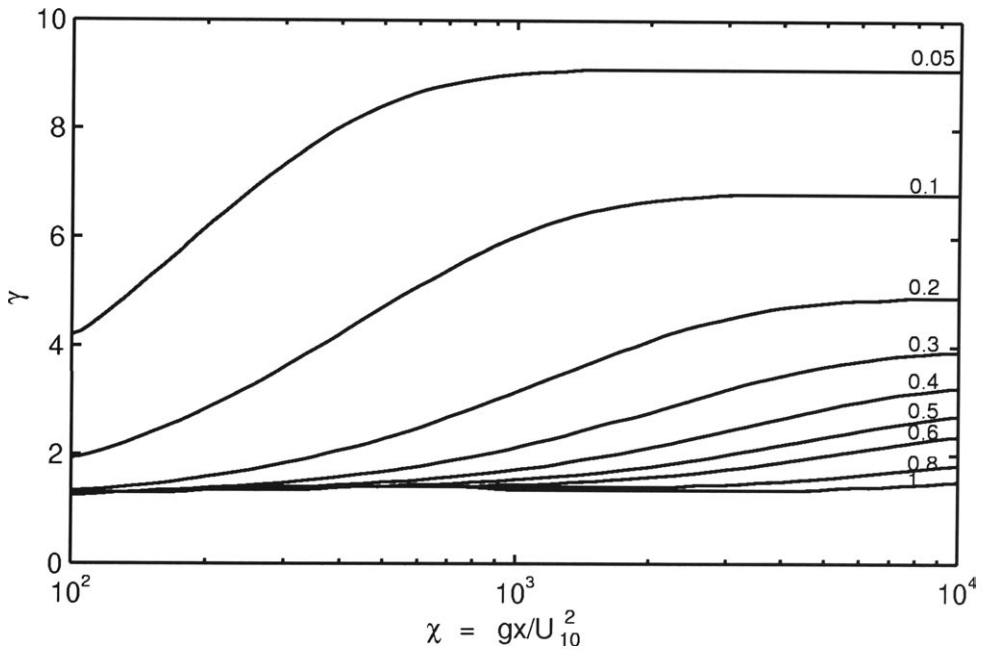

Figure 5.12 The peak enhancement factor (γ) as a function of the non-dimensional fetch (χ) for various non-dimensional depths (δ). The values for the non-dimensional depth (δ) are shown on the right side of the figure.

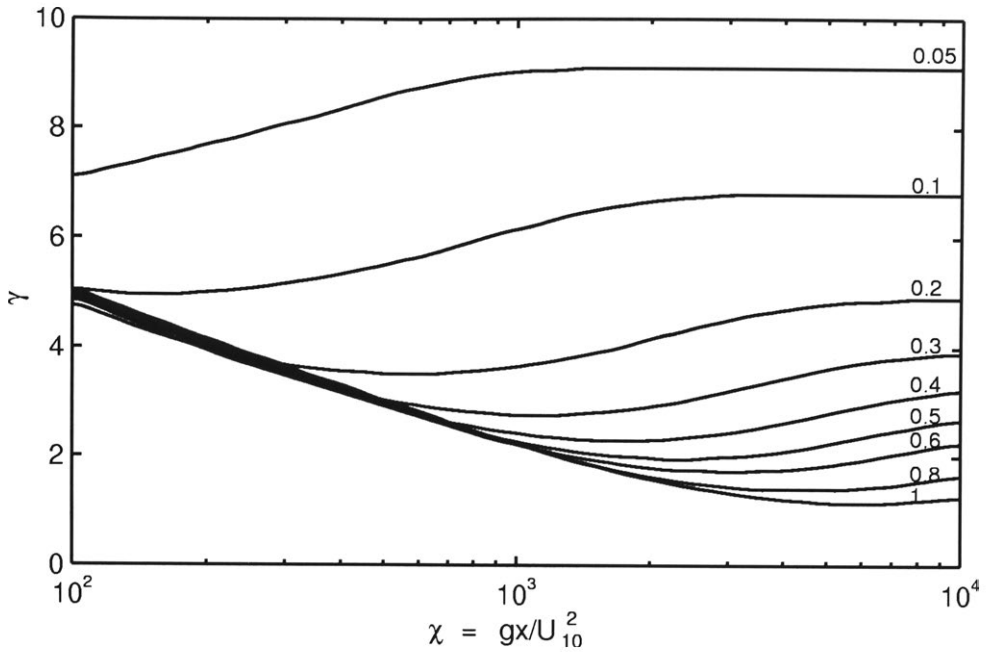

Figure 5.13 The peak enhancement factor (γ) as a function of the non-dimensional fetch (χ) for various non-dimensional depths (δ). The JONSWAP results were used in this graph as an asymptote for the non-dimensional peak frequency (ν). The values for the non-dimensional depth (δ) are shown on the right side of the figure.

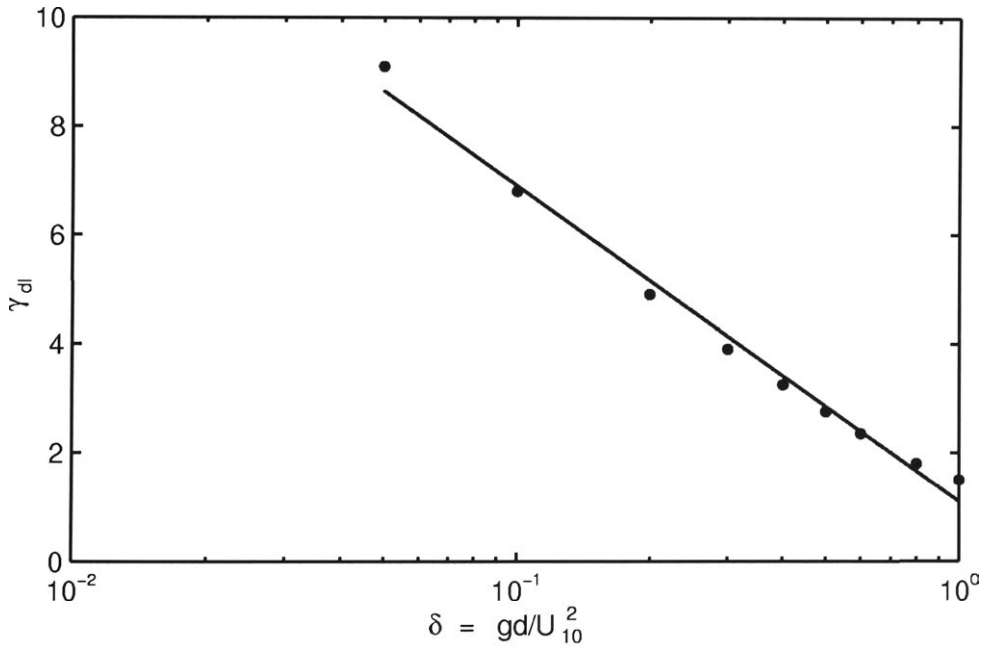

Figure 5.14 The peak enhancement factor (γ) as a function of the non-dimensional depth (δ) where non-dimensional fetch (χ) is very large (thus depth limited and not fetch limited "seas"). The line is a least squares fit to the data.

6. Directional Wave Spectra

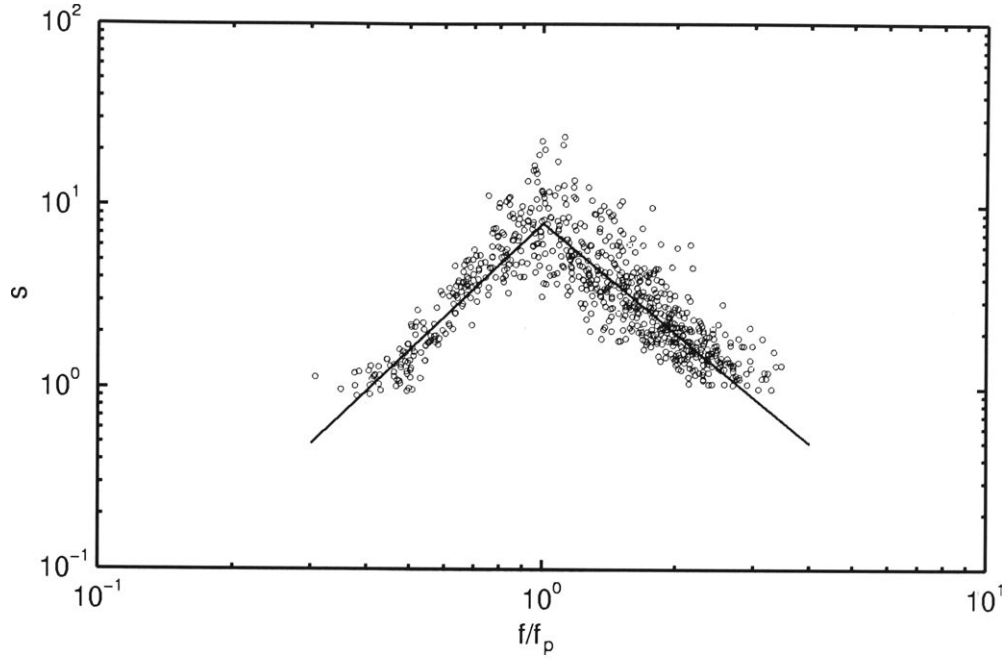

Figure 6.1 The directional parameter (s) as a function of the normalised frequency (f/f_p). Lines of the least square fit (with a break at $f/f_p = 1$) to the data are shown. Due to noise in the high frequencies the data that had an $\varepsilon > 0.01$ were disregarded.

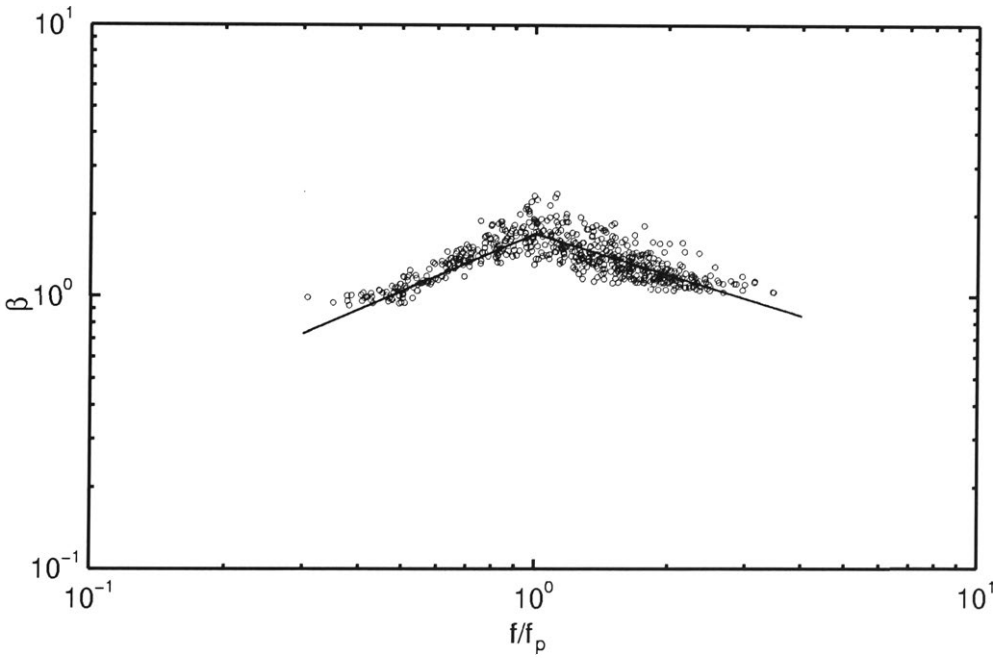

Figure 6.2 The directional parameter (β) as a function of the normalised frequency (f/f_p). Lines of the least square fit (with a break at $f/f_p = 1$) to the data are shown. Due to noise in the high frequencies the data that had an $\varepsilon > 0.01$ were disregarded.

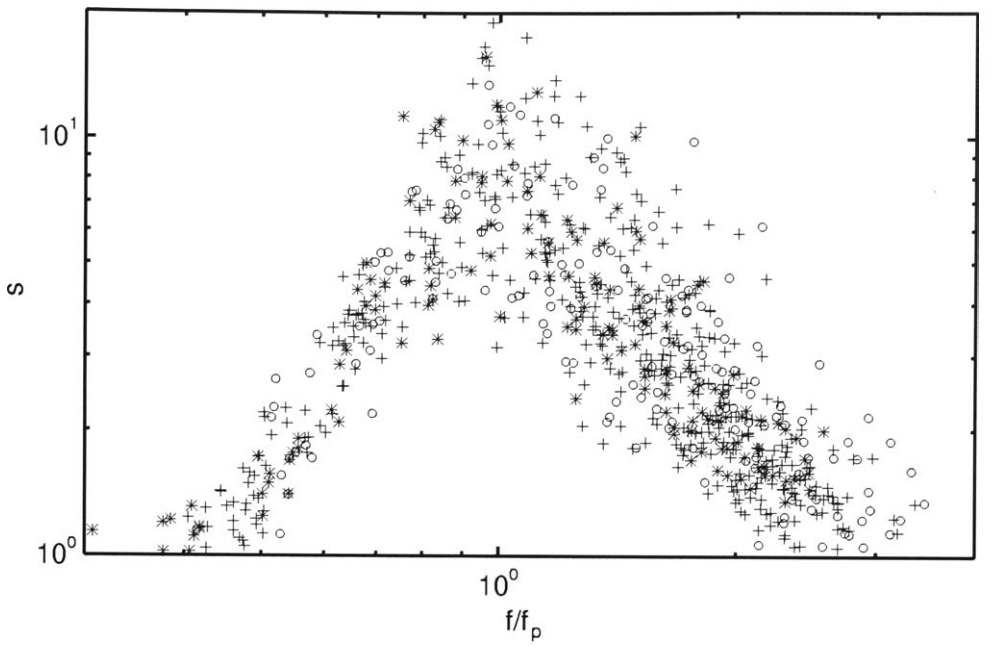

Figure 6.3 Values of the directional exponent (s) as a function of the normalised frequency (f/f_p). The data have been split into three groups of inverse wave age (U_{10}/C_p)

group 1	1	<	inverse wave age	≤	2	*
group 2	2	<	inverse wave age	≤	3	+
group 3	3	<	inverse wave age	≤	4	o

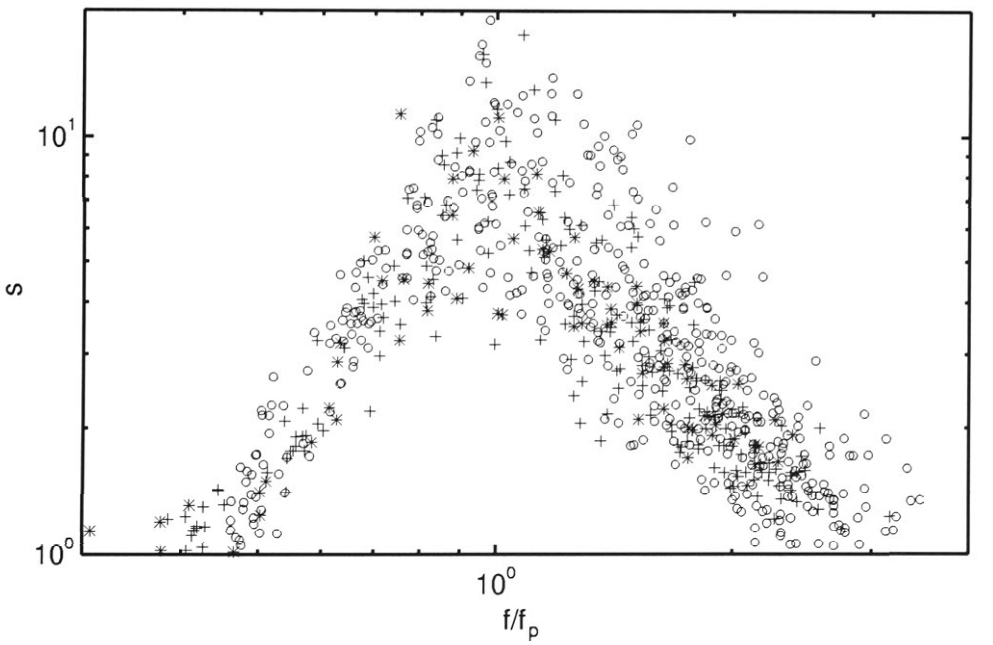

Figure 6.4 Values of the directional exponent (s) as a function of the normalized frequency (f/f_p). The data have been split into three groups of relative depth ($k_p\,d$)

group 1	1	<	$k_p\,d$	≤	1.5	o
group 2	1.5	<	$k_p\,d$	≤	2	+
group 3	2	<	$k_p\,d$			*

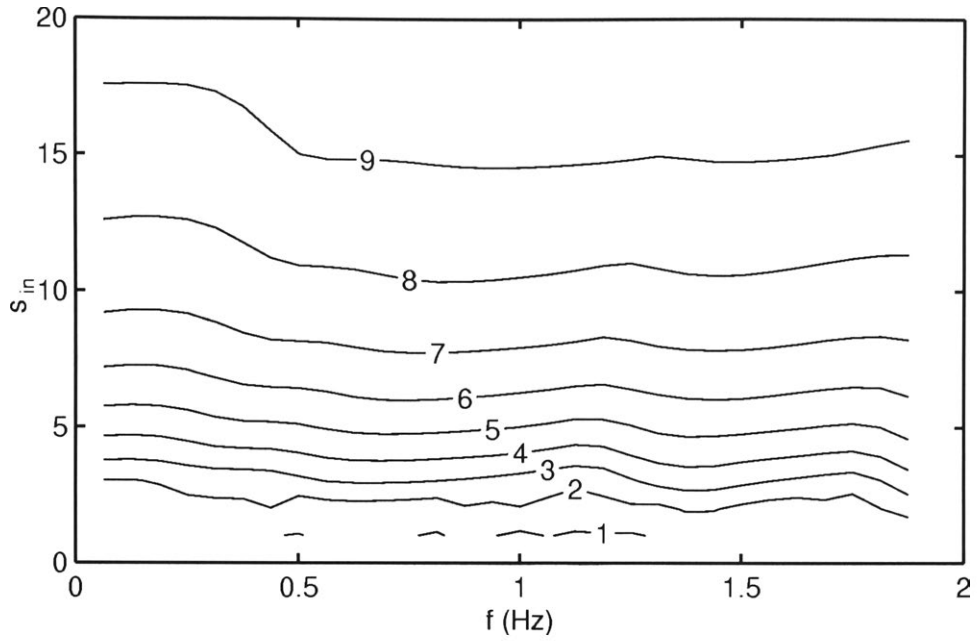

Figure 6.5 The input directional spreading (s_{in}) set against the frequency of the spectra. The result of the analyses is the output directional spread (s_{out}) which is shown in the graph. As can be seen the frequency does not influence the output directional spreading. However, the analysis does broaden the directional spreading significantly for the spectra that are narrowest.

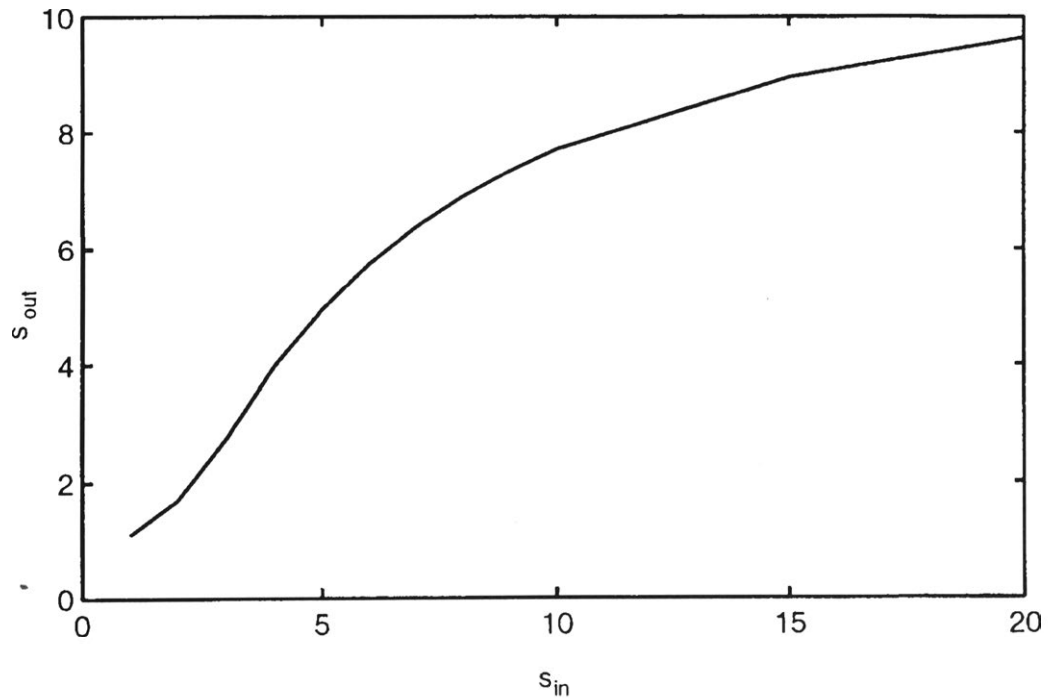

Figure 6.6 The "real" (in this case the generated directional spectra) directional spreading parameter (s_{in}) set out against the resulting directional spreading parameter (s_{out}) of the analysis. The difference in the narrower directional spectra are significant.

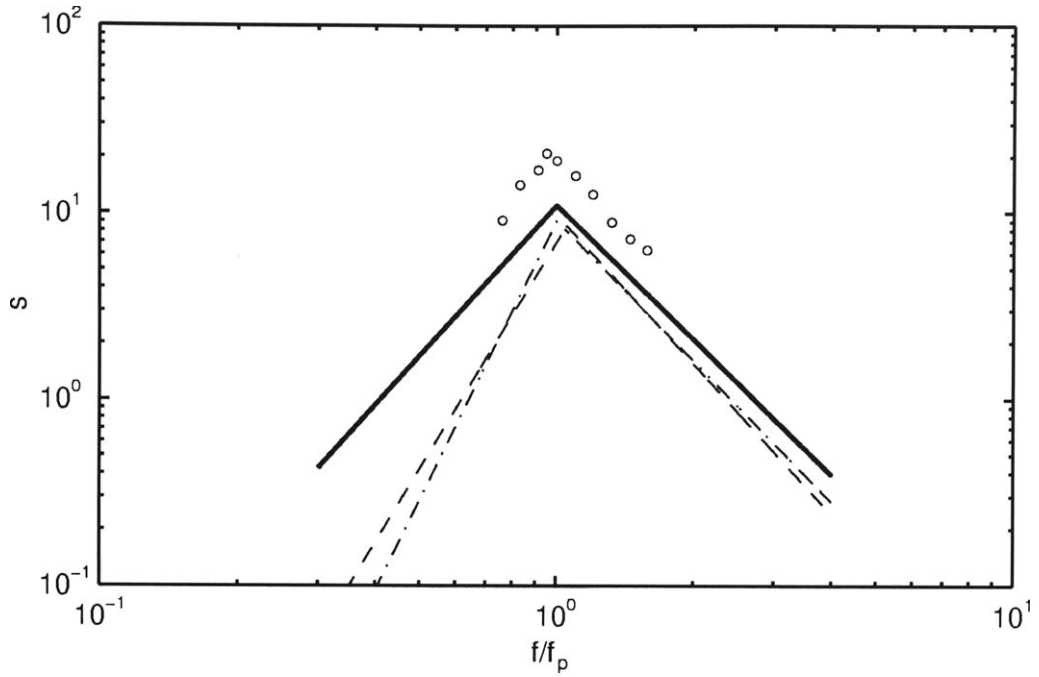

Figure 6.7 Directional spreading factor (s) from different deep water studies and Lake George.

Lake George	solid line
Mitsuyasu et al. (1975)	dash dot
Hasselman et al. (1980)	dash dash
Donelan et al. (1985)	open circles (digitized from their figure 30)

As can been seen the deep water data sets of Mitsuyasu et al. (1975) and Hasselman et al. (1980) are broader than the lake George Data set. However the Lake George data set is broader than Donelan et al. (1985) deep water data set.

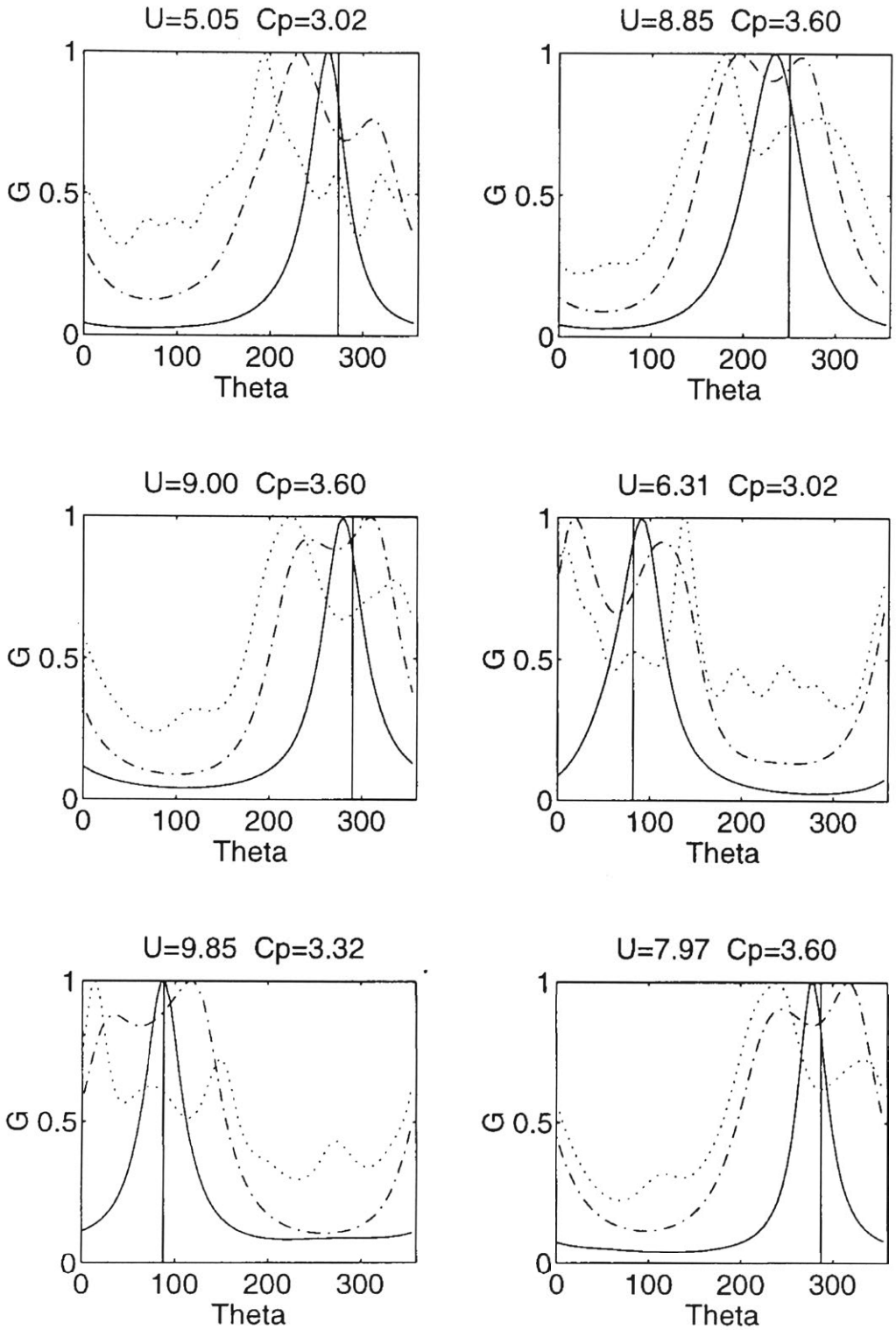

Figure 6.8 Several directional spreading factors $G(\omega,\theta)$ for different directional spectra. Note the bimodal modes for the spectra at the higher frequencies
$\omega/\omega_p = 1$ solid line
$\omega/\omega_p = 2$ dash dot line
$\omega/\omega_p = 3$ dotted line
The wind speeds and phase speed are given on top of the figures.

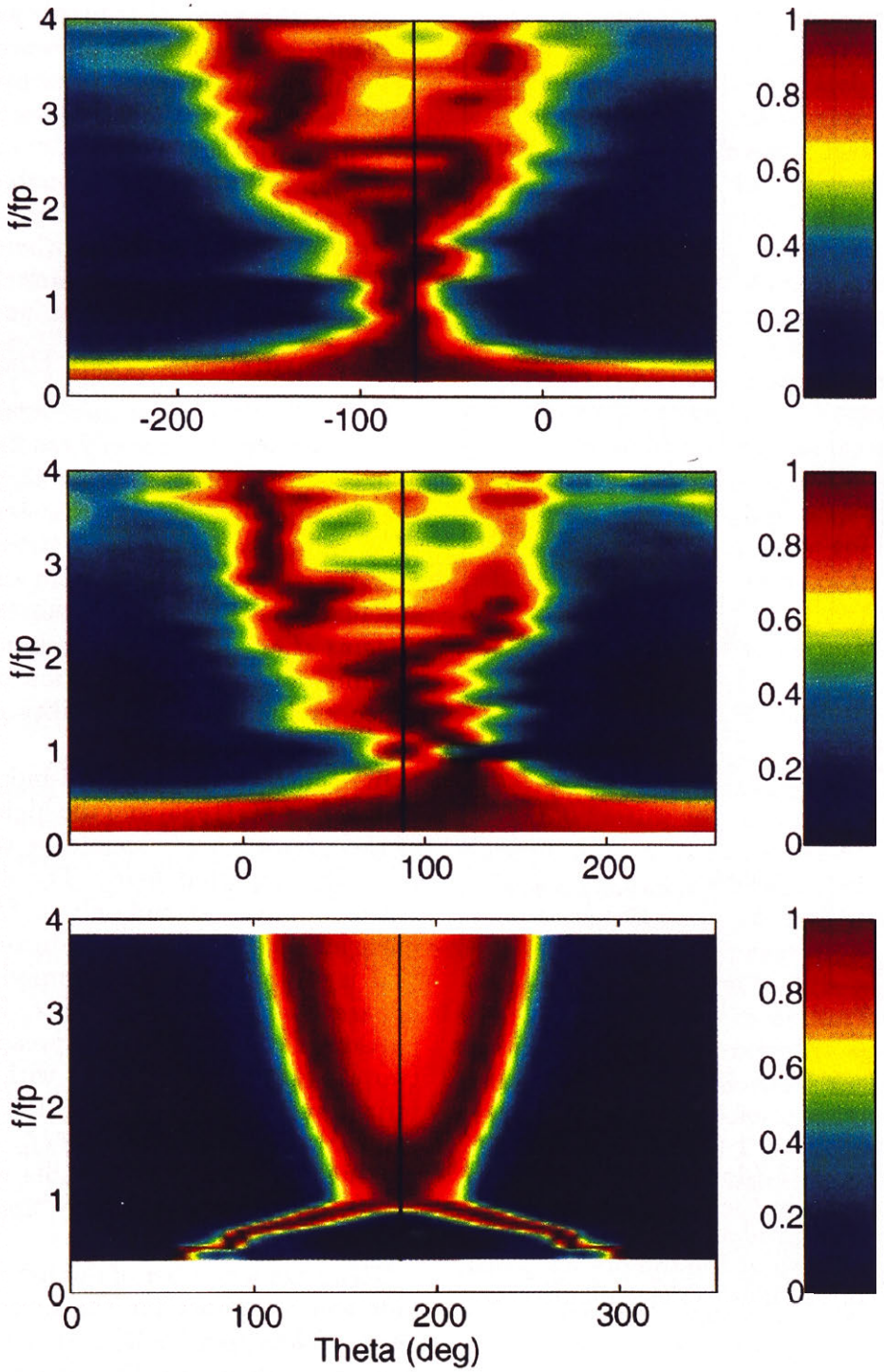

Figure 6.9 Examples of the directional spreading function recorded at Lake George (top and middle). Note the bimodal spreading at higher frequencies. Numerical results of Banner and Young (1994) are shown at the bottom. In all cases, the spectra are normalized to have a maximum of one, at each frequency.